PACIFIC EARTHQUAKE ENGINEERING RESEARCH CENTER

Modeling Viscous Damping in Nonlinear Response History Analysis of Steel Moment-Frame Buildings: Design-Plus Ground Motions

Xin Qian
John A. Martin and Associates

Anil K. Chopra
Department of Civil and Environmental Engineering
University of California, Berkeley

Frank McKenna
Pacific Earthquake Engineering Research Center
University of California, Berkeley

Revision 1.0

PEER Report No. 2020/01
Pacific Earthquake Engineering Research Center
Headquarters at the University of California, Berkeley

September 2020

PEER 2020/01
September 2020

Modeling Viscous Damping in Nonlinear Response History Analysis of Steel Moment-Frame Buildings: Design-Plus Ground Motions

Xin Qian
John A. Martin and Associates

Anil K. Chopra
Department of Civil and Environmental Engineering
University of California, Berkeley

Frank McKenna
Pacific Earthquake Engineering Research Center
University of California, Berkeley

Revision 1.0

PEER Report 2020-01
Pacific Earthquake Engineering Research Center
Headquarters at the University of California, Berkeley

September 2020

SUMMARY

This report investigates the question: can seismic demands on steel moment-frame buildings due to Maximum Considered Earthquake (MCE_R) design-level ground motions [2% probability of exceedance (PE) in 50 years] be estimated satisfactorily using linear viscous damping models or is a nonlinear model, such as capped damping, necessary? This investigation employs two models of a 20-story steel moment-frame building: a simple model and an enhanced model with several complex features. Considered are two linear viscous damping models: Rayleigh damping and constant modal damping; and one nonlinear model where damping forces are not allowed to exceed a pre-defined bound.

Presented are seismic demands on the building due to two sets of ground motions (GMs): MCE_R design-level GMs (2% PE in 50 years) and rarer excitations (1% PE in 50 years); and even more intense GMs. Based on these results, we conclude that linear damping models are adequate for estimating seismic demands on steel moment-frame buildings—designed to satisfy current story drift and plastic rotation limits due to MCE_R design-level GMs. Between the two linear damping models, constant modal damping is preferred; it is available in commercial computer codes for earthquake structural analysis.

ACKNOWLEDGMENTS

Dr. N. Simon Kwong developed the Uniform Hazard Spectrum for the site and the Conditional Mean Spectrum, and then selected and scaled ground motions consistent with the target spectrum. Professor John Hall's comments on an earlier draft led to an improved report.

Any opinions, findings, and conclusions or recommendations expressed in this material are those of the authors and do not necessarily reflect those of the Pacific Earthquake Engineering Research Center (PEER).

REVISION HISTORY

Two sections—Introduction and Conclusions—of the report, first issued in June 2020, were expanded in September 2020. These revisions were prompted by comments on a paper submitted to the journal *Earthquake Engineering and Structural Dynamics*. These comments came from two anonymous reviewers and Michael Constantinou, the editor.

The Conclusions now emphasize several results of interest to the profession: First, linear viscous damping models are adequate for estimating seismic demands on buildings—designed to satisfy current story drift and plastic rotation limits—due to MCE_R design-level ground motions (GMs). Second, between the two linear damping models—Rayleigh damping and constant modal damping—the latter is preferable for nonlinear RHA of buildings because it leads to modestly larger demands. This is a prudent choice in the absence of a benchmark or "exact" result. Third, we do not recommend the Rayleigh damping model in nonlinear RHA of buildings because it leads to smaller demands and, hence, could lead to the conclusion that design or evaluation criteria have been satisfied, when other linear damping models lead to the opposite conclusion. Furthermore, various problems and deficiencies have been identified with Rayleigh damping depending on how the yielding elements in the building are modeled. Fourth, if the goal is to arrive at conclusions valid for professional practice, research investigations on modeling damping in nonlinear RHA of buildings should be based on realistic, state-of-the-practice models of buildings subjected to an ensemble of GMs that correspond to the MCE_R and have been selected by modern methods. In contrast, earlier studies have questioned the validity of linear models, but they typically used simplistic models of buildings and/or extremely intense GMs.

CONTENTS

LIST OF TABLES

LIST OF FIGURES

1 Introduction

It is standard in earthquake dynamics of structures to model the various energy-dissipating mechanisms that exist at small amplitude (pre-yield) motions by linear viscous damping; i.e., damping forces $\mathbf{f}_D$ are a linear function of nodal velocities $\dot{\mathbf{u}}$: $\mathbf{f}_D = \mathbf{c}\dot{\mathbf{u}}$, where $\mathbf{c}$ is the damping matrix. The damping matrix should be consistent with modal damping ratios estimated by system identification methods applied to structural motions recorded during earthquakes. The data that are most useful but hard to come by are from structures shaken strongly but not deformed into the inelastic range. The damping ratios determined from smaller structural motions are usually not representative of the larger energy dissipation expected at higher amplitudes—say, just-below yield amplitudes—of structural motions. On the other hand, recorded motions of structures that have experienced yielding during an earthquake would provide damping ratios that also include the energy dissipation due to yielding of structural materials. These damping ratios would not be directly useful in dynamic analysis because the energy dissipation in yielding is usually modeled separately through nonlinear hysteretic force-deformation relations for structural elements.

The measured damping ratios represent the combined effect of energy dissipated in the structure and underlying soil, as well as energy radiated due to soil–structure interaction. It is impractical to separate the individual damping contributions of these mechanisms. Because soil–structure interaction is usually not modeled rigorously in dynamic analysis of buildings, the tradition is to use modal damping ratios estimated from available data directly for dynamic analysis of buildings on fixed base. This simplified approach would not be appropriate if soil–structure interaction effects are significant, as expected for nuclear containment structures and concrete dams, for example.

A large majority of the data for the "measured" damping ratios are for the first mode of vibration of buildings. Until recently, limited data that was available for higher mode damping ratios did not show any systematic variation with modal frequency. Thus, it has been common to assume the same damping ratio for all modes. However, this assumption may begin to change as more data becomes available for damping in higher modes [Cruz and Miranda 2017].

A damping matrix consistent with all specified modal damping ratios can be constructed by superposition of modal damping matrices [Wilson and Penzien 1972; Chopra 2017; Section 11.4.3]. However, this model leads to a full damping matrix. The storage and computational requirements to work with such a full matrix can be prohibitive. As a result, computer codes resort to numerical tricks to implement this damping model. For example, in PERFORM 3D [CSI 2011] and OpenSees, the full damping matrix is used on the right side of the equations to be solved in

Newmark's method [Chopra 2017: Section 16.3.3] but is reduced, so that only those terms that fit within the storage scheme of the stiffness matrix appear on the left side of the equations.

In contrast, Rayleigh damping is computationally attractive because such a damping matrix, which is a linear combination of the mass and stiffness matrices, does not require extra computer resources or tricks when solving the equations in Newmark's method. As a result, Rayleigh damping is perhaps the most commonly used model, although it leads to modal damping ratios that increase indefinitely with increasing frequency, thus leading to excessive damping in higher modes of vibration, and violating the experimental evidence cited earlier. Furthermore, several authors have identified problems associated with the use of Rayleigh damping, as will be described below.

Although the damping matrix is constructed to be consistent with damping ratios estimated from structural motions within the pre-yield range, it is customary to use the same linear viscous damping model for nonlinear response history analysis (RHA) of structures. This extension is based on the tacit assumption that the energy-dissipating mechanisms that exist at small-amplitude motions continue unchanged even after the structure has yielded. Unfortunately, experimental evidence is not available to support or refute this assumption.

Researchers have demonstrated that spurious damping forces may develop and damping forces may be unrealistically large if the Rayleigh damping model is used in nonlinear RHA of buildings [Chrisp 1980; Bernal 1994; Carr 1997; Hall 2006; Charney 2008; Zareian and Medina 2010; and Luco and Lanzi 2017]. This problem has been demonstrated in the context of Rayleigh damping, but it is expected to exist for other linear viscous damping models. It arises because yielding of structural elements limits their resisting forces, but no such mechanism exists for limiting the damping forces. They can increase without limit in proportion to velocities, which may become large because of yielding, especially as the structure approaches a state of collapse.

Several proposals exist to control the damping forces after the structure has yielded. One is to exclude stiffness-proportional damping from the hinge rotational springs in the Rayleigh damping matrix [Medina and Krawinkler 2014; Zareian and Medina 2010]. Another proposal is to replace the initial stiffness in Rayleigh damping by the tangent stiffness Charney [2008]; Leger et al 1992; and Jehel et al 2014]. Based on a shaking table test on a simple bridge pier [Petrini et al. 2008], it was concluded that a plastic-hinge model with viscous damping based on tangent stiffness provided good agreement. Unfortunately, experimental data on multistory buildings that is suitable for resolving issues related to modeling damping is lacking. In a new damping model [Luco and Lanzi 2017], the damping forces are proportional to the elastic component of velocity instead of total velocity. Although the model is based on initial properties of the structure, the resulting response is similar to that obtained by conventional viscous damping models but using tangent stiffness properties. However, as discussed elsewhere, defining Rayleigh damping based on tangent stiffness lacks a physical basis and is conceptually troubling; therefore, this damping scheme is not considered in this study [Chopra and McKenna 2016(a); 2016b; Hall 2018].

The most direct way of controlling the damping forces is to impose an upper bound on the magnitude of the damping forces, an idea motivated by the results of earthquake analysis of a 10-story shear building with 5% damping subjected to the ground motion (GM) recorded at the Olive View Hospital site during the 1994 Northridge, California, earthquake. This is a very intense pulse-like GM with peak ground acceleration (PGA) = 0.84g, peak ground velocity (PGV) = 129.3 cm/sec, peak-to-peak velocity = 186.1 cm/sec, and peak ground displacement = 32.1 cm. The computed value of the total damping force was 7.2% of the weight of the building or 60% of the yield strength of the building [Hall 2006]. Because no plausible damping mechanism could cause these unrealistically large damping forces, which would lead to unconservative estimates of seismic demands, it was concluded that a limit should be imposed on the magnitude of the damping forces; the term "capped damping" was introduced. However, the scope of the problem is not clear because the model analyzed was a shear building, which is not applicable to modern moment-resisting frames or modern coupled shear walls, structural systems that are common for tall buildings.

A comprehensive investigation of the performance of the conventional linear viscous damping models—including Rayleigh damping and superposition of modal damping matrices—as well as nonlinear viscous damping models—including tangent Rayleigh damping and capped damping—has been presented by Hall [2018]. He analyzed an enhanced model of the SAC 20-story steel-moment frame with 3% damping subjected to very intense, pulse-like ground motion, causing roof displacement of approximately 2% of the height of the building and plastic rotations of over 7% rad, which are beyond the acceptable limits in design guidelines.

The objective of this report is to answer the question: Can building response to Maximum Considered Earthquake (MCE_R) design-level GMs (2% probability of exceedance in 50 years or a return period of 2475 years) be estimated satisfactorily using linear viscous damping models or is a capped-damping model—which may be cumbersome to implement in commercial computer codes—necessary? Resolving this issue is important because, as mentioned above, researchers have questioned the validity of linear models, which are standard in professional practice. This issue should be investigated in the context of realistic, state-of-the-practice models of "actual" buildings subjected to an ensemble of ground motions that are consistent with the hazard defined by the MCE_R and are selected by modern methods. These two requirements are satisfied in this study, whereas they were not in most previous studies. Although the focus is on MCE_R design-level GMs, excitations associated with rarer events are also considered to explore the limits on validity of linear damping models.

2 Damping Models

Considered in this study are three damping models: Rayleigh damping based on initial stiffness; superposition of modal damping matrices with constant (or equal) damping ratios specified in all modes; and interstory dampers with an upper bound imposed on the damping forces.

2.1 RAYLEIGH DAMPING

In this linear viscous damping model, the damping matrix is a linear combination of the mass and stiffness matrices:

$$\mathbf{c} = a_0\mathbf{m} + a_1\mathbf{k} \tag{1}$$

In this study, the initial stiffness matrix is constructed for the structure with hinges modeled implicitly. Internal hinge rotations are eliminated by static condensation of the element stiffness matrix, thus structural elements appear as a single two-node element. This implementation of Rayleigh damping is similar to that in PERFORM-3D, a commercial software widely used in professional practice for nonlinear RHA of buildings.

The coefficients a_0 and a_1 were computed from modal damping ratios specified for the first and third vibration modes of the building. Beyond the third-mode frequency, the damping ratios increase with frequency without bound, leading to large values in higher modes, even exceeding critical damping.

2.2 CONSTANT MODAL DAMPING

In this linear viscous damping model, the classical damping matrix is defined as the superposition of modal damping matrices [Wilson and Penzien 1972]:

$$\mathbf{c} = \mathbf{m}\left(\sum_{n=1}^{N}\frac{2\zeta_n\omega_n}{M_n}\boldsymbol{\phi}_n\boldsymbol{\phi}_n^T\right)\mathbf{m} \tag{2}$$

The nth term in this summation is the contribution of the nth mode with its damping ratio ζ_n to the damping matrix; if this term is not included, the resulting **c** implies zero damping ratio in the nth mode. A common assumption is to specify the same damping ratio in every mode of vibration. We will refer to this model as *Constant Modal Damping*. In this study; damping in the first 20 modes was specified.

2.3 CAPPED DAMPING

In this nonlinear viscous damping model, a bound (or a cap) is imposed on the damping forces. Energy dissipation in the linear range of vibration is modeled by interstory viscous dampers, which develop lateral damping forces proportional to the relative velocity between the two floors of a story. The height-wise distribution of damping coefficients C_i (i denotes story number) is taken as proportional to the story stiffnesses K_i, i.e., $C_i = \alpha K_i$; thus the interstory damper model is akin to initial-stiffness-proportional damping. With this assumption, the constant α corresponding to a specified value of the first-mode damping ratio ζ_1, can be determined from

$$\zeta_1 = \alpha \frac{T_1 \sum_i K_i \left(\phi_{i,1} - \phi_{i,l-1}\right)^2}{4\pi \sum_i m_i \phi_{i,1}^2} \tag{3}$$

where m_i is the mass lumped at the ith floor, and $\phi_{i,1}$ is the lateral displacement of the ith floor in the fundamental vibration mode. Computation of story stiffnesses is described in Appendix A.

How should the bound on the damping force in each interstory damper be defined? Consider a linear single-degree-of-freedom (SDF) system with damping ratio ζ. The ratio of the damping force to stiffness force when the system is undergoing steady-state harmonic motion at its own natural frequency is 2ζ. This result is applicable also to an SDF system subjected to wide-frequency-band earthquake excitations because the response of the system is akin to harmonic motion (at its natural frequency), but with a slowly-varying amplitude [Crandall and Mark 1963]. This result is also valid for complex systems vibrating in a single mode of vibration at the modal frequency. Based on such considerations, we limit the damping force in a story to 2ζ times the story strength, an idea first proposed by Hall [2006]. Computation of story strengths is described in Appendix A.

Compared in Figure 1 are the characteristics of a linear viscous damper and the same damper with a bound (or cap) imposed on the magnitude of the damping force, both undergoing harmonic motion at frequency ω. The damping force-velocity and damping force-displacement relations for both dampers are plotted. At small amplitudes of motion ($u \le u_1$ or $\dot{u} \le \omega u_1$), the two dampers are identical; the damping force is a linear function of velocity, i.e., $f_D = c\dot{u}$, and the damping force-displacement plot is the familiar hysteresis loop of elliptical shape. At larger motions, ($u > u_1$ or $\dot{u} > \omega u_1$), $f_D = c\dot{u}$ remains valid for the linear viscous damper, but for the damper with bounded damping force, this relationship becomes bilinear, valid for both increasing and decreasing velocity; see Figure 1(a). At these larger motions, the elliptical hysteresis loop remains valid for the linear viscous damper, but the loop is truncated at the positive and negative bounds on the damping force in the case of the nonlinear damper with bounded force.

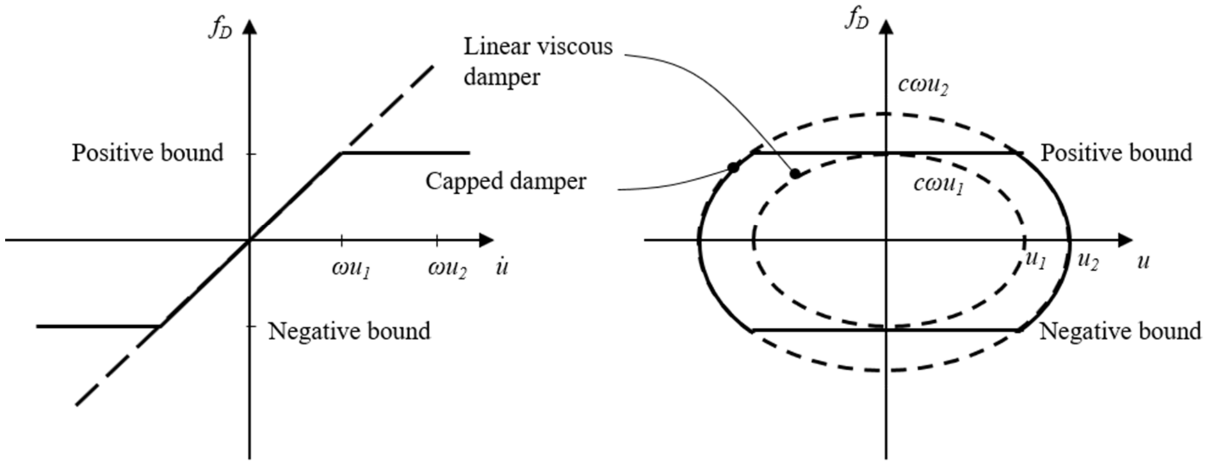

Figure 1 **Linear viscous damping and capped damping models: (a) damping force-velocity relation; and (b) damping force-deformation relation.**

3 Structural Systems

Analyzed is a 20-story steel moment-resisting frame building in Los Angeles that was designed as part of the SAC project for post-Northridge earthquake design criteria [Gupta and Krawinkler 1999; Krawinkler 2000]. The dimensions and section sizes were taken from Appendix B of the FEMA-356 SAC Steel report [FEMA 2000]. The subterranean part of the building was not modeled and the columns were fully constrained at the base.

A simple model of a perimeter frame of the building was based on centerline dimensions; beams were modeled between centerlines of columns without rigid offsets, panel zones, or top and bottom flange cover plates. The fundamental period of vibration is 3.81 sec. Two values of modal damping were considered: 2%. and 5%. This lower value is generally consistent with values estimated from motions of tall buildings recorded during earthquakes [Bernal et al. 2015] and also conforms to values recommended in design guidelines [PEER 2017]. The larger value was considered simply because it had been commonly assumed for decades.

An enhanced model of the 20-story steel moment-frame included several complex features: geometric nonlinearity; strain hardening and deterioration in plastic hinges; flexibility and yielding of panel zones; tri-element beams to model cover plated ends, and the interior gravity frames. The fundamental period of vibration of the enhanced model is 3.38 sec, and modal damping was assumed to be 3%. Implicit plastic hinges are employed for both building models. Details of these models are available in Appendix B.

This enhanced model is intended to be similar to the model for the same building developed by Hall [2018]. Vibration properties and earthquake responses of the two models are compared in Appendix C.

4 Ground Motions

Ground motions were selected for the Los Angeles City Hall site, the assumed location for the building, for earthquake events with 2% probability of exceedance (PE) in 50 years (i.e., return period of 2475 years). This corresponds to the MCE_R event defined in design codes and guidelines. Consistent with professional practice, the target spectrum was defined as the Conditional Mean Spectrum (CMS) [Baker 2011]. The CMS is constructed for a selected value of the conditioning period T^*, where the spectral acceleration is specified. As is common, T^* was selected as T_1, the fundamental vibration of the building, and $A(T^*)$ as the value that matches the Uniform Hazard Spectrum (UHS).

Shown in Figure 2 is the UHS for the selected site, and the CMS conditioned on $T^* = 3.81$ sec, the fundamental vibration period T_1 of the simple model of the 20-story frame. The spectral acceleration $A(T^*) = 0.195$g. Ground motions in the NGAWest-2 database were scaled to this $A(T^*)$, and those with scale factor (SF) greater than 5 were excluded from further consideration. From the database of scaled GM records, 11 GMs that most closely agree with (or "match," for brevity) the CMS in shape were selected. Shown in Figure 2 are the response spectra for these 11 GMs, all of which pass through $A(T^*)$ of the CMS, as enforced by the scaling criterion. Results of the nonlinear RHA of the 20-story frame to this set of GMs will be presented in Section 5.1.

The process of scaling and selecting GM records outlined above was repeated to select GMs appropriate for nonlinear RHA of the enhanced model of the 20-story building, with fundamental vibration period $T_1 = 3.38$ sec and $A(T^*) = 0.225$ g. The UHS for the site remains unchanged, of course, but the CMS is now conditioned on $T^* = 3.38$ sec. Presented in Figure 3 are the UHS, CMS, and the response spectra for the 11 GMs that were selected. Results of nonlinear RHA of the enhanced model of the 20-story building to this set of GMs will be presented in Section 5.2.

Ground motions from earthquake events rarer than MCE_R, those with 1% PE in 50 years (i.e., return period of 4975 years), were also selected for analysis of the enhanced model of the 20-story building. The UHS for the site is now more intense, of course, with a spectral acceleration $A(T_1 = 3.38 \text{ sec}) = 0.285$ g. Shown in Figure 4 are the UHS, the CMS conditioned on $T^* = 3.38$ sec, and the response spectra for the 11 GMs that were selected. Results of nonlinear RHA of the enhanced model of the 20-story building to this set of GMs will also be presented in Section 5.2.

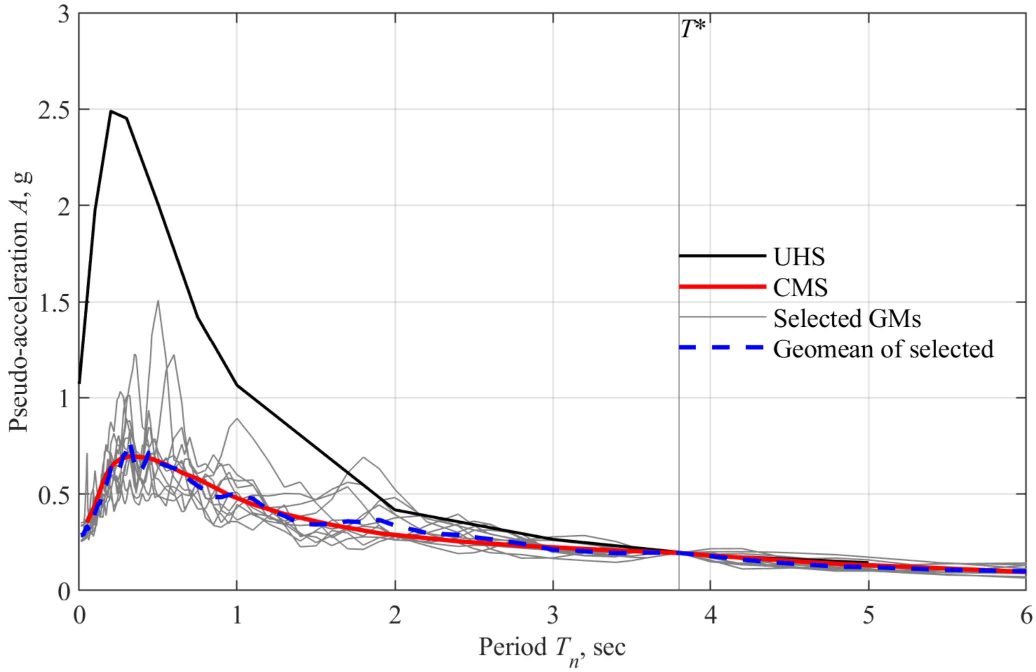

Figure 2 **Uniform Hazard Spectrum (UHS) for 2% PE in 50 years, Conditional Mean Spectrum (CMS) for *T** = 3.81 sec, response spectra for 11 scaled GMs selected for similarity to the CMS, and their geomean.**

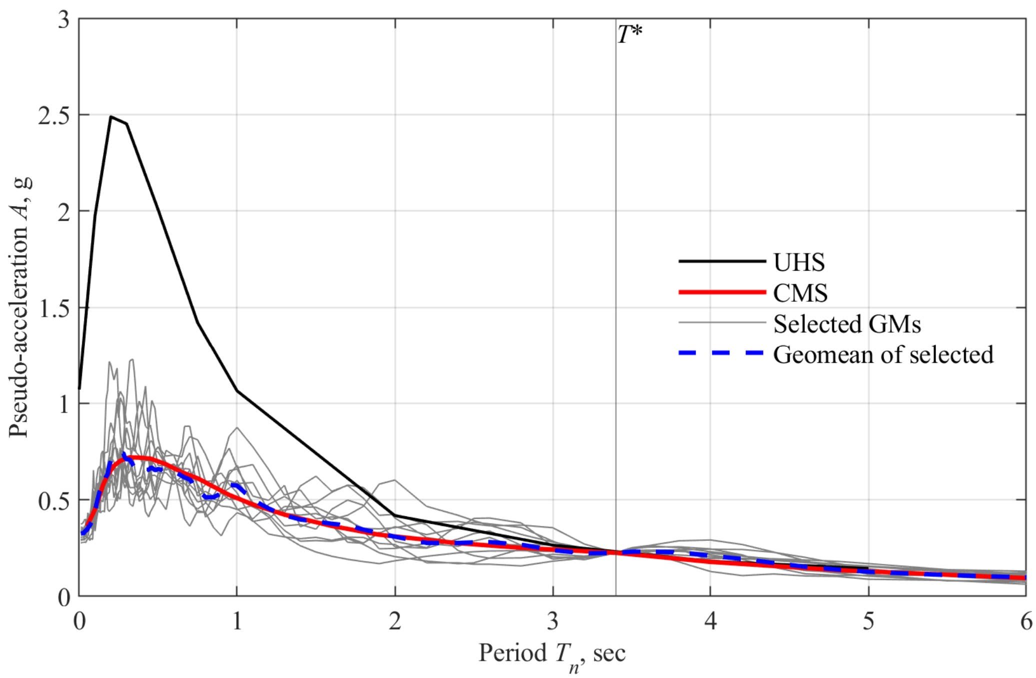

Figure 3 **Uniform Hazard Spectrum (UHS) for 2% PE in 50 years, Conditional Mean Spectrum (CMS) for *T** = 3.38 sec, response spectra for 11 scaled GMs selected for similarity to the CMS, and their geomean.**

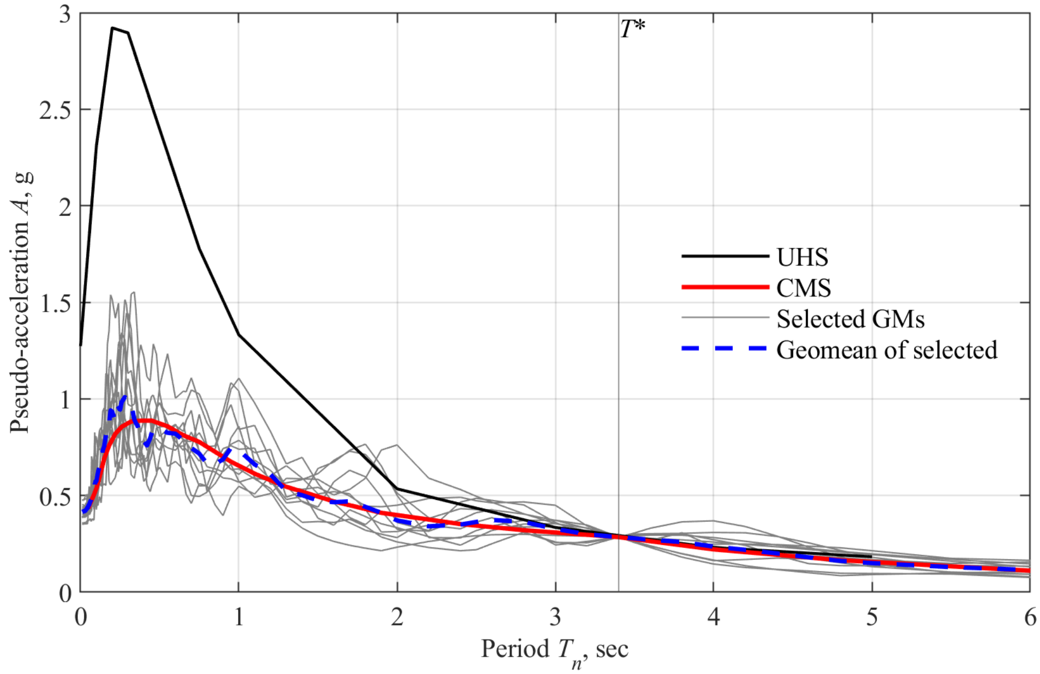

Figure 4 **Uniform Hazard Spectrum (UHS) for 1% PE in 50 years, Conditional Mean Spectrum (CMS) for *T** = 3.38 sec, response spectra for 11 scaled ground motions selected for similarity to the CMS, and their geomean.**

5 Structural Response for Three Damping Models

Nonlinear RHAs of the two structural systems (Section 3) subjected to the pertinent set of 11 GMs (Section 4) were performed using OpenSees [McKenna et al. 2000; McKenna 2011] for three different damping models (Section 2). These results were processed to determine: (1) the average value of demand over 11 GMs; and (2) the largest demand on the building among the 11 GMs. Both of these response data are of direct interest because some design codes and guidelines specify limits on one [ASCE 41-17 2017] or both [PEER 2017] response quantities.

Structural engineers evaluate story drifts, which are measures of global system behavior, as well as member and connection rotations, which are measures of local system behavior when implementing a performance-based seismic design. Acceptance criteria for plastic rotations vary by element type (e.g., moment-frame beams and connections, braced-frame beams and connections, and coupling beams in a wall building). For welded cover-plate flanges with connections designed by post-Northridge criteria, ASCE 41-17 [2017] limits plastic rotations to 2.33% and 3.1% rad for life safety and collapse prevention, respectively; however, generally applicable limits on global demands are not specified. For special building types—e.g., schools and hospitals—drift limits are specified in other codes or standards, e.g., the California Building Code (CBC) and California Existing Building Code (CEBC). Sometimes the drift limit is determined indirectly from performance requirements for non-structural components. In contrast, PEER's TBI Guidelines [2017] provide acceptance criteria for story drifts: the average value of peak-story drifts over 11 GMs should not exceed 3%, and the largest value over all GMs should not exceed 4.5%; limits on residual drifts are also specified.

There is no direct way of evaluating different damping models in the absence of a benchmark model for damping or the *exact* seismic demand on a structure due to a given GM. However, as cited earlier, researchers have argued that linear viscous damping models are unconservative because they underestimate seismic demands compared to nonlinear models, such as Rayleigh damping with tangent stiffness or the capped damping model. In this section, the results of nonlinear RHA will be presented and interpreted to determine if and when the underestimation by two linear viscous damping models—Rayleigh damping (with initial stiffness) and constant modal damping—relative to the capped damping model is small enough to be acceptable.

5.1 TWENTY-STORY FRAME: SIMPLE MODEL

Presented in Figure 5 and Table 1(a) are the average values of peak floor displacements, peak story drifts (expressed as percent of story height), and peak plastic rotations for the simple model with 2% damping; these structural responses are essentially identical for the two linear viscous damping models but both underestimate the demands relative to the capped damping model by less than 11%; see Table 2(a).

The response of the structure to the GM 1188, which imposes the largest demands among the 11 GMs, is plotted in the same format in Figure 7; in addition, the variation of roof displacement with time is presented in Figure 6. Observe that the response is, essentially, identical among the three damping models for the first 100 sec of the GM, but thereafter the results begin to diverge; see Figure 6. For this GM of very long duration, the peak demands occur near the end of the excitation. Interstory drifts of over 6% and plastic rotations just below 6% radian are significantly larger than the 4.5% allowed by design guidelines [PEER 2017; ASCE 2017]. At these large inelastic deformations [Table 1(a)], the constant modal damping model underestimates seismic demands by 18–21% relative to the capped damping model; greater underestimation of 23–26% is observed for the Rayleigh damping model; see Table 2(a).

Table 1 Seismic demands on a simple model of the 20-story frame for three damping models due to GMs with 2% PE in 50 years; damping = 2% and 5%.

Damping Model	(a) 2% damping				(b) 5% damping			
	Avg of 11 GMs		Max over 11 GMs		Avg of 11 GMs		Max over 11 GMs	
	Story drift %	Plastic rotations % radians	Story drift, %	Plastic rotations % radians	Story drift %	Plastic rotations, % radians	Story drift %	Plastic rotations % radians
Rayleigh	2.28	1.88	4.72	4.36	2.01	1.54	3.88	3.50
Constant modal	2.30	1.90	4.98	4.64	2.04	1.63	4.22	3.85
Capped	2.48	2.11	6.11	5.85	2.13	1.73	4.44	4.02

Table 2 Underestimate (%) in seismic demands on a simple model of the 20-story frame by linear viscous damping models relative to capped damping subjected to GMs with 2% PE in 50 years; damping = 2% and 5%.

Damping Model	(a) 2% damping				(b) 5% damping			
	Avg of 11 GMs		Max over 11 GMs		Avg of 11 GMs		Max over 11 GMs	
	Story drift %	Plastic rotations, % radians	Story drift %	Plastic rotations % radians	Story drift %	Plastic rotations, % radians	Story drift %	Plastic rotations, % radians
Rayleigh	8.1	10.9	22.8	25.4	5.6	11.0	12.5	13.0
Constant modal	7.3	10.0	18.5	20.7	4.2	5.8	4.9	4.2

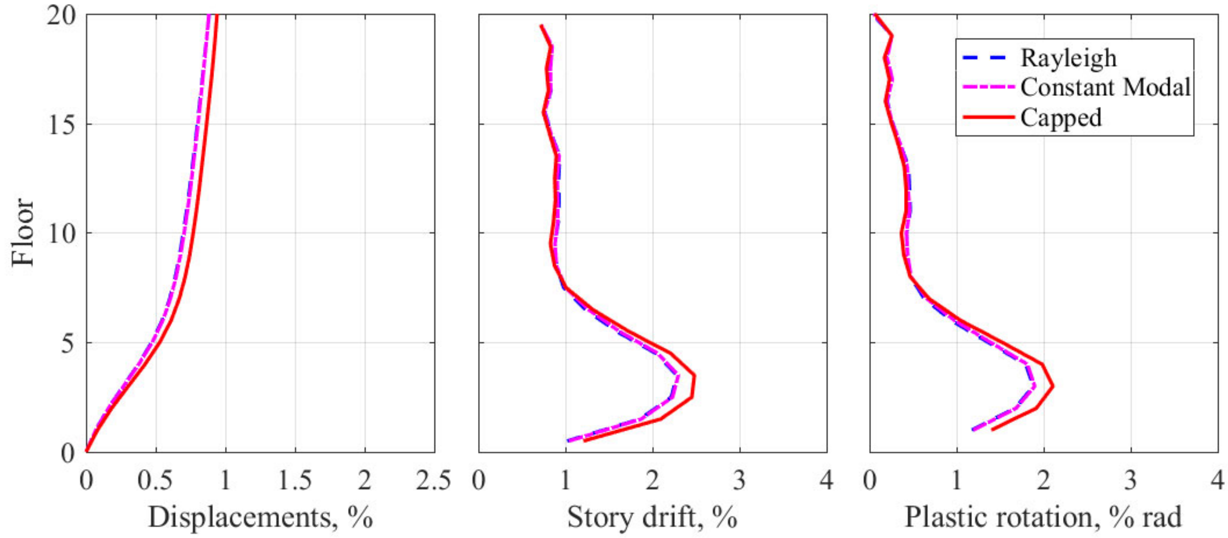

Figure 5 **Average (over 11 GMs) seismic demands on a simple model for the 20-story frame for three damping models due to GMs with 2% PE in 50 years; 2% damping: (a) peak floor displacements; (b) peak story drifts; and (c) peak plastic rotations.**

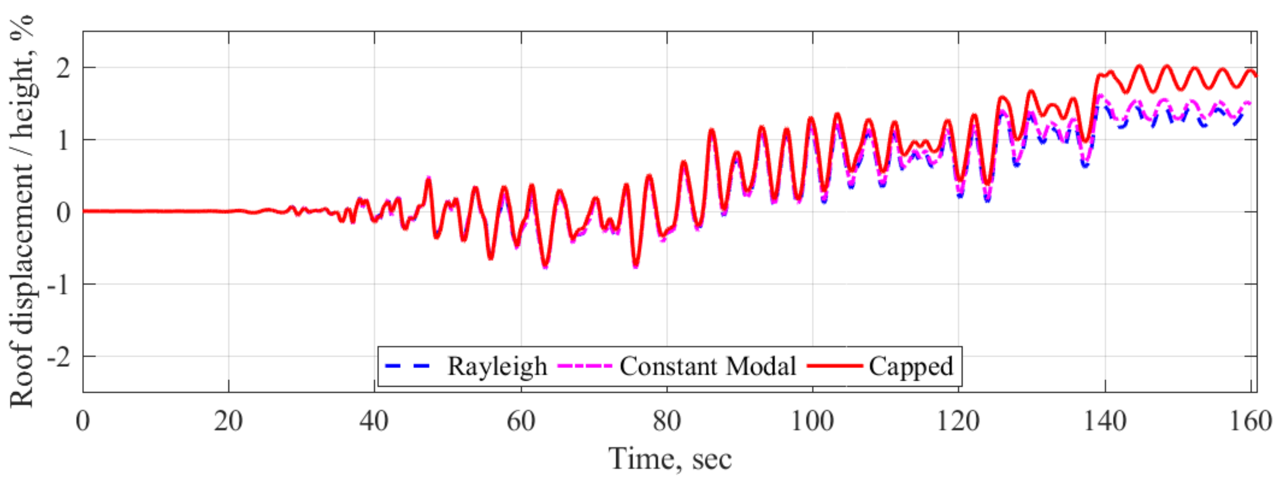

Figure 6 **Response history of roof displacement of a simple model for the 20-story frame for three damping models subjected to GM 1188 scaled corresponding to 2% PE in 50 years; 2% damping.**

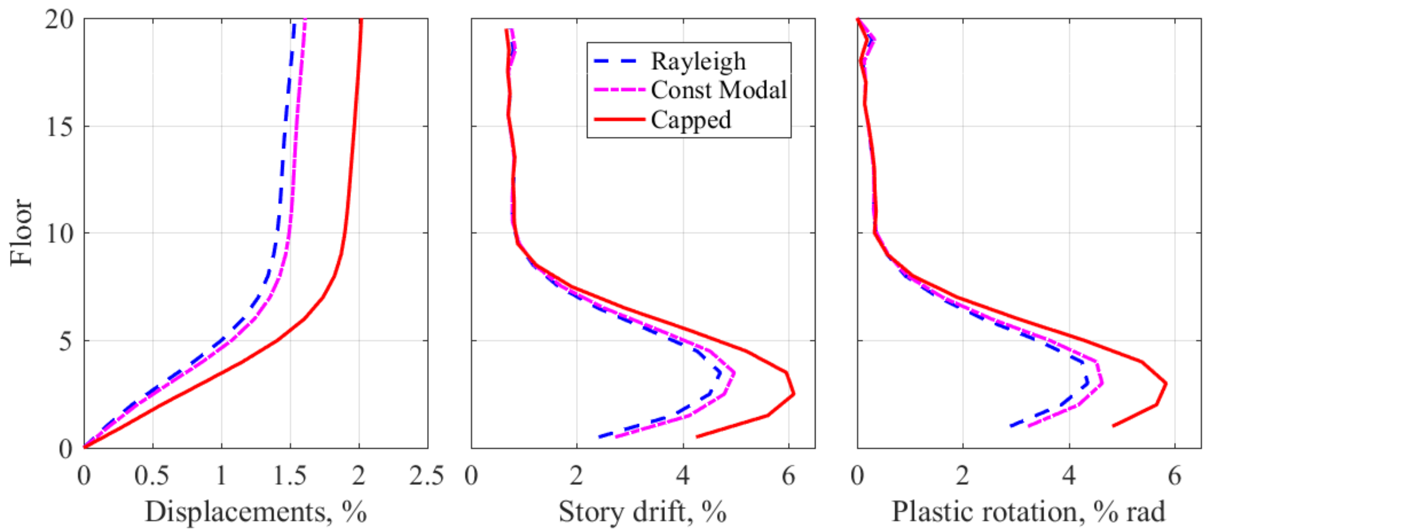

Figure 7 Maximum (over 11 GMs) seismic demands on a simple model for the 20-story frame for three damping models due to GMs with 2% PE in 50 years; 2% damping: (a) peak floor displacements; (b) peak story drifts; and (c) peak plastic rotations.

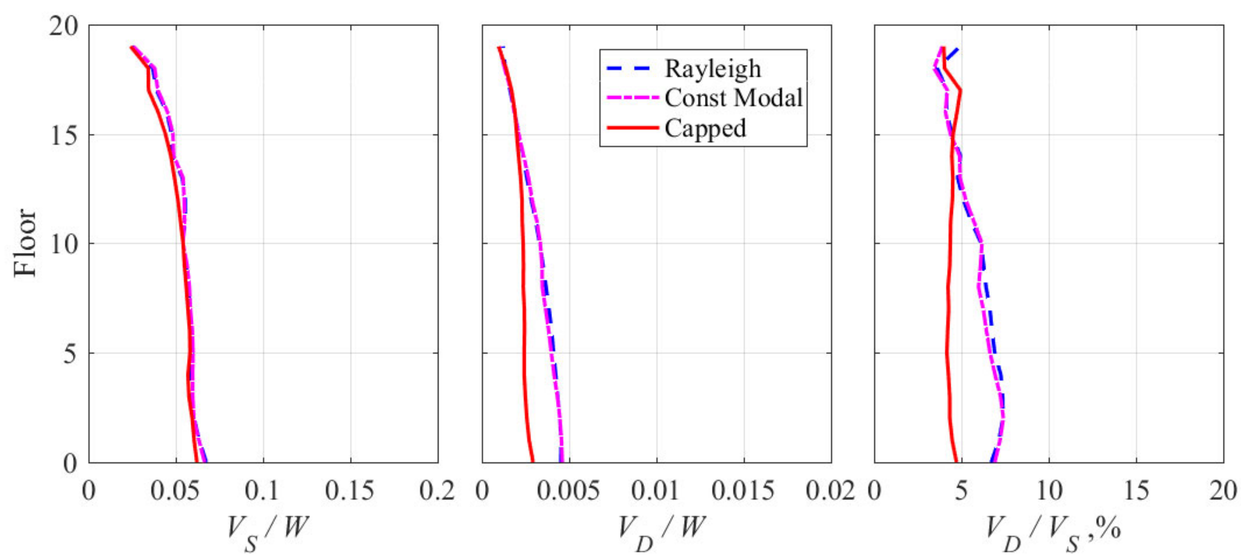

Figure 8 Maximum (over 11 GMs) forces in a simple model of the 20-story frame for three damping models due to GMs with 2% PE in 50 years; 2% damping: (a) peak shear force V_S; (b) peak damping force V_D; and (c) ratio V_D/V_S.

Presented in Figure 8 are the height-wise distribution of peak story shears, V_S, and peak story damping forces, V_D, both normalized relative to the total weight of the building and the ratio V_D / V_S; computation of V_D and V_S is described in Appendix E. Because all stories of the building yielded, the V_S/W plot is the same for all damping models; it is simply the height-wise distribution of the story strengths. The ratio V_D / V_S is close to 4%, the limit of 2ζ imposed in the capped damping model, but this ratio reaches approximately 7% (or 3.5ζ) for the linear damping models. Note that although larger than 2ζ; this ratio is nowhere close to the alarming value of 46% (approximately 9ζ) reported for a shear building with 5% damping [Hall 2006], even though story drifts and plastic rotations are quite large: approximately 6%.

Although 2% damping assumed in the preceding example is generally consistent with measured values for tall steel buildings [Bernal et al. 2015] and recommended values [PEER 2017], we examine if the preceding observations would remain valid if damping were 5%, a value that had been commonly assumed for several decades. Larger damping tends to increase damping forces, which would suggest larger differences between structural responses with linear and capped damping models. However, it also reduces the response, implying less yielding, which would suggest smaller differences between the two responses; after all, linear and capped damping models would give essentially identical response in the absence of yielding of the structure.

To explore the overall effect of the two competing factors, nonlinear RHAs of the 20-story frame with 5% damping subjected to the same 11 GMs were repeated. The average responses are shown in Figure 9, and the maximum demands (over 11 GMs) due to GM 1188 in Figure 10 and Figure 11. The story drifts and plastic rotations are now reduced, and the constant modal damping model is able to closely follow the roof displacement history determined using the capped damping model during the entire 160 sec duration of the GM. For this GM, the constant modal damping model predicts peak demands within 5% of those from the capped damping model; in contrast, the Rayleigh damping model underestimates demands by 13%; see Table 2 (b). At average (over 11 GMs) plastic rotations less than 2% rad [Table 1(b)], the linear damping models underestimate seismic demands to a lesser degree: see Table 2(b).

Compared to Rayleigh damping, the constant modal damping model consistently predicts seismic demands closer to the capped damping model. Rayleigh damping implies much higher damping in the higher modes of vibration compared to the latter model, thus underestimating the seismic demands to a greater degree; see Table 2.

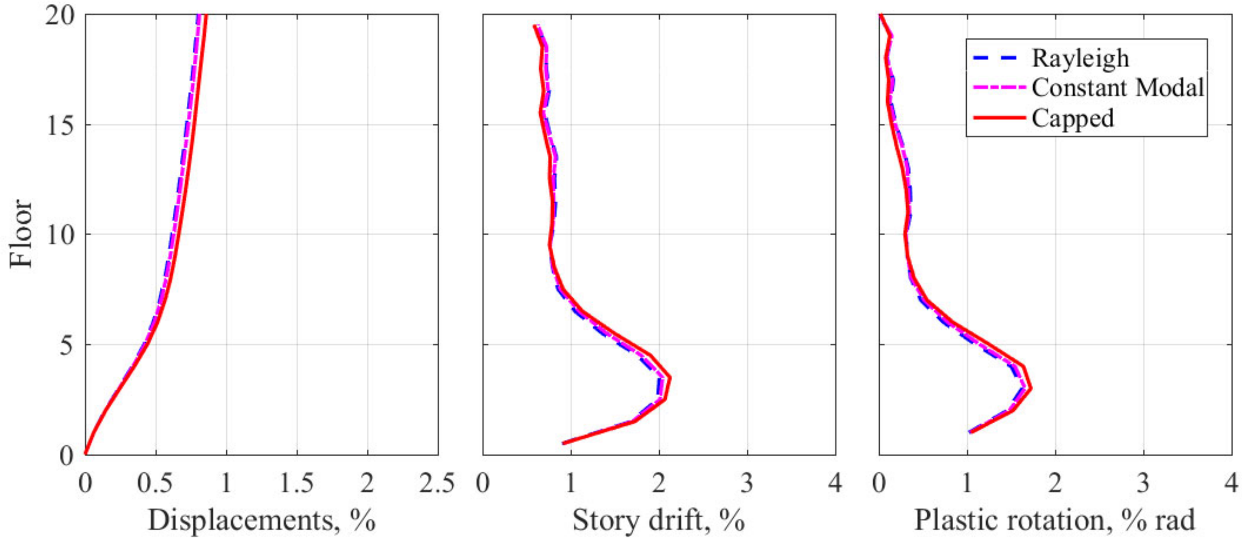

Figure 9 **Average (over 11 GMs) seismic demands on a simple model of the 20-story frame for three damping models due to GMs with 2% PE in 50 years; 5% damping: (a) peak shear drifts; (b) peak story drifts; and (c) peak plastic rotations.**

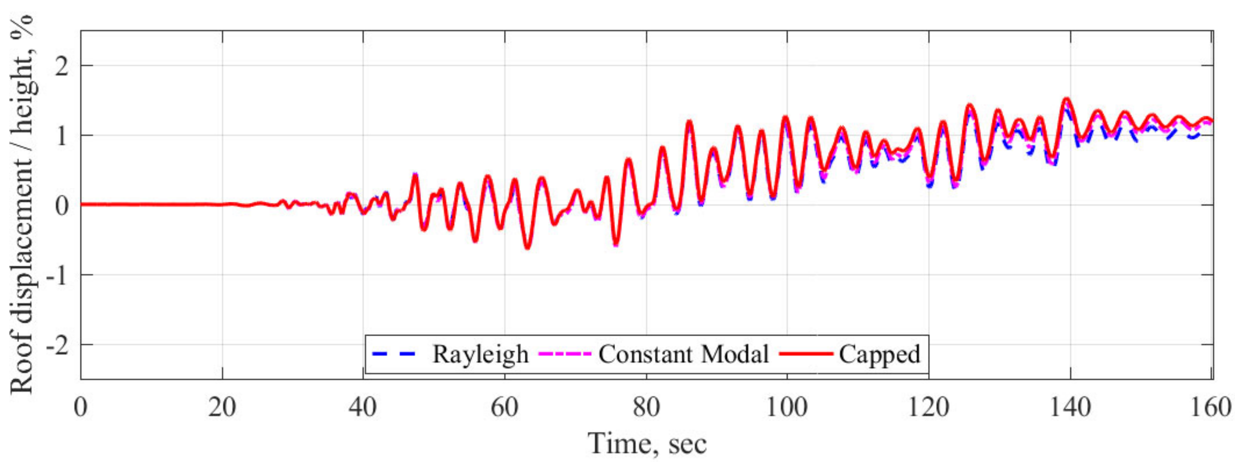

Figure 10 **Response history of roof displacement of a simple model of the 20-story frame for three damping models subjected to GM 1188 scaled corresponding to 2% PE in 50 years; 5% damping.**

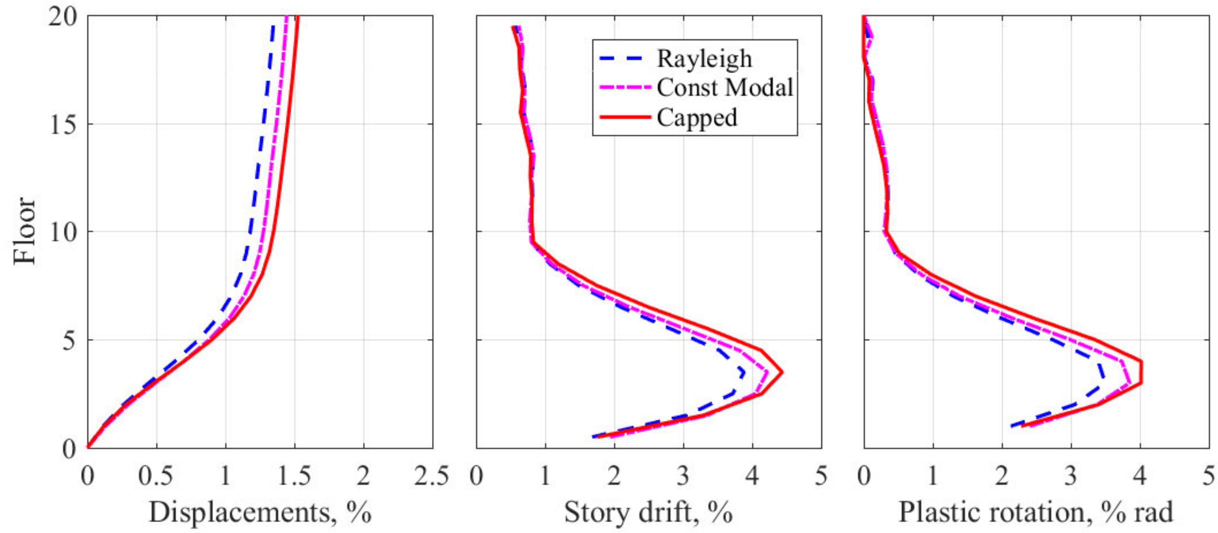

Figure 11 **Maximum (over 11 GMs) forces on a simple model of the 20-story frame for three damping models due to GMs with 2% PE in 50 years; 5% damping: (a) peak floor displacements; (b) peak story drifts; and (c) peak plastic rotations.**

5.2 TWENTY-STORY BUILDING: ENHANCED MODEL

Nonlinear response history analysis of the enhanced model of the 20-story building with 3% damping was implemented for 11 GMs corresponding to probability of exceedance (PE) of 2% in 50 years (average return period = 2475 years), which is the MCE_R event defined in design codes and guidelines. Presented in Figure 12 are average values (over 11 GMs) of peak floor displacements, peak story drifts, and peak plastic rotations. The seismic demands are similar for the two linear damping models, with the constant modal damping model resulting in slightly larger responses; see Table 3(a). It underestimates the demands relative to the capped damping model by 3–5%, whereas Rayleigh damping underestimates them by 5–6%; see Table 4(a).

Table 3 **Seismic demands on an enhanced model of the 20-story building for three damping models subjected to 11 GMs with: (a) 2% PE in 50 years; and (b) 1% PE in 50 years.**

Damping Model	(a) PE = 2% in 50 years				(b) PE = 1% in 50 years			
	Avg of 11 GMs		Max over 11 GMs		Avg of 11 GMs		Max over 11 GMs	
	Story drift %	Plastic rotations % radians	Story drift %	Plastic rotations % radians	Story drift %	Plastic rotations % radians	Story drift %	Plastic rotations % radians
Rayleigh	1.69	1.42	2.48	2.49	2.02	1.89	4.03	4.96
Constant modal	1.71	1.45	2.55	2.62	2.09	1.98	4.35	5.42
Capped	1.78	1.51	2.56	2.64	2.18	2.10	4.35	5.39

Table 4 **Underestimate (%) in seismic demands on an enhanced model of the 20-story building by linear viscous damping models relative to capped damping subjected to GMs with: (a) 2% PE in 50 years; and (b) 1% PE in 50 years.**

Damping Model	(a) 2% in 50 years				(b) 1% in 50 years			
	Avg of 11 GMs		Max over 11 GMs		Avg of 11 GMs		Max over 11 GMs	
	Story drift %	Plastic rotations % radians	Story drift %	Plastic rotations % radians	Story drift %	Plastic rotations % radians	Story drift %	Plastic rotations % radians
Rayleigh	4.8	6.2	3.2	5.7	7.3	9.8	7.4	8.0
Constant modal	3.5	4.4	0.2	0.9	4.2	5.7	0.1	-0.6

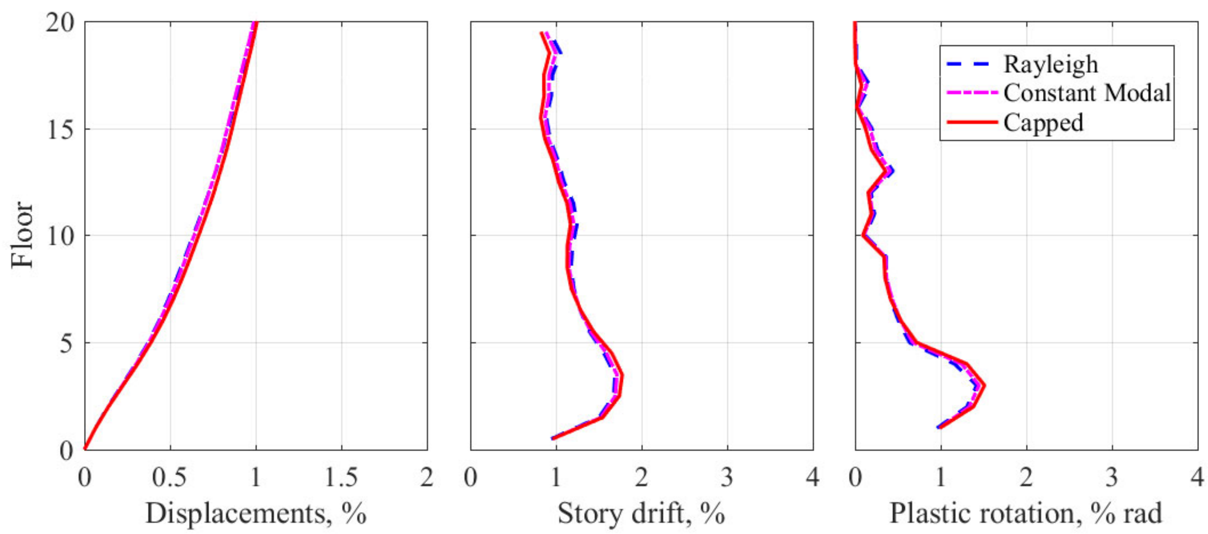

Figure 12 **Average (over 11 GMs) seismic demands on an enhanced model of the 20-story building for three damping models due to GMs with 2% PE in 50 years: (a) peak floor displacements; (b) peak story drifts; and (c) peak plastic rotations.**

The response of the enhanced model to GM 6953, which imposes the largest demands among the 11 GMS, are plotted in the same format in Figure 14; in addition, the variation of roof displacement with time is presented in Figure 13. Story drifts due to this ground motion exceed 4% and plastic rotations are large. Observe that the roof displacement is essentially unaffected by bounding the damping forces. At the moderate inelastic deformations, indicated by story drifts of approximately 2.5% and plastic rotations of 2.5% rad, the seismic demands on the frame with constant modal damping are essentially identical to those obtained with capped damping, whereas Rayleigh damping underestimates seismic demands by 3–6%; see Table 4(a).

Presented in Figure 15 are the height-wise distributions of the peak story shears, V_S, and peak story damping forces, V_D, normalized relative to the total weight of the building; and the ratio

V_D/V_S. Because all stories of the building yielded, the V_S/W plot is the same for all damping models; it is simply the height-wise distribution of the story strengths. The ratio V_D/V_S is approximately 6%, the limit of 2ζ imposed in the capped damping model, but this ratio at the base is close to 9% (or 3ζ) for the linear damping models. Because of this "excessive" damping force, the seismic demands are underestimated, but only slightly: less than 1% by the constant damping model and 3–6% by Rayleigh damping; see Table 4(a).

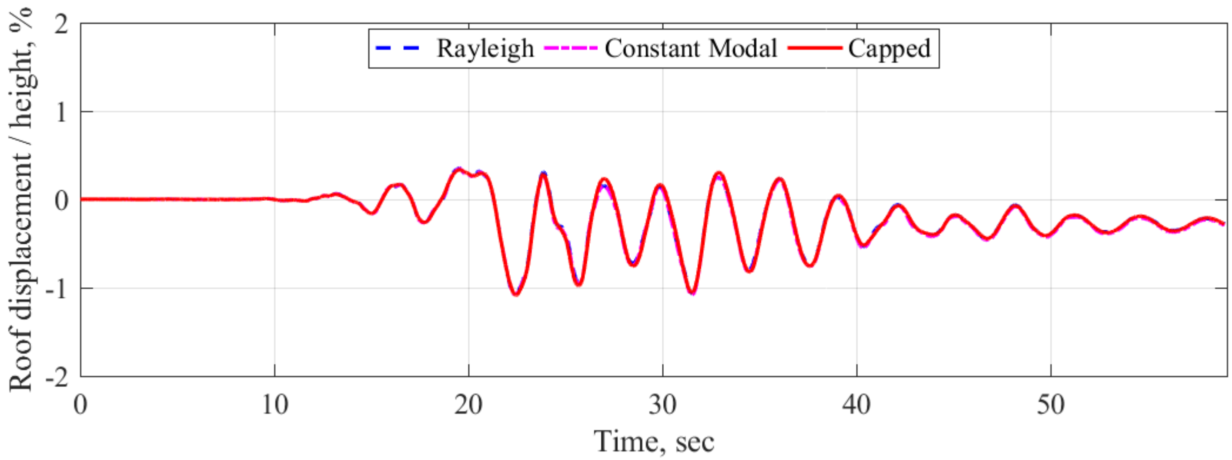

Figure 13 Response history of roof displacement of an enhanced model of the 20-story building for three damping models subjected to GM 6953 scaled corresponding to 2% PE in 50 years.

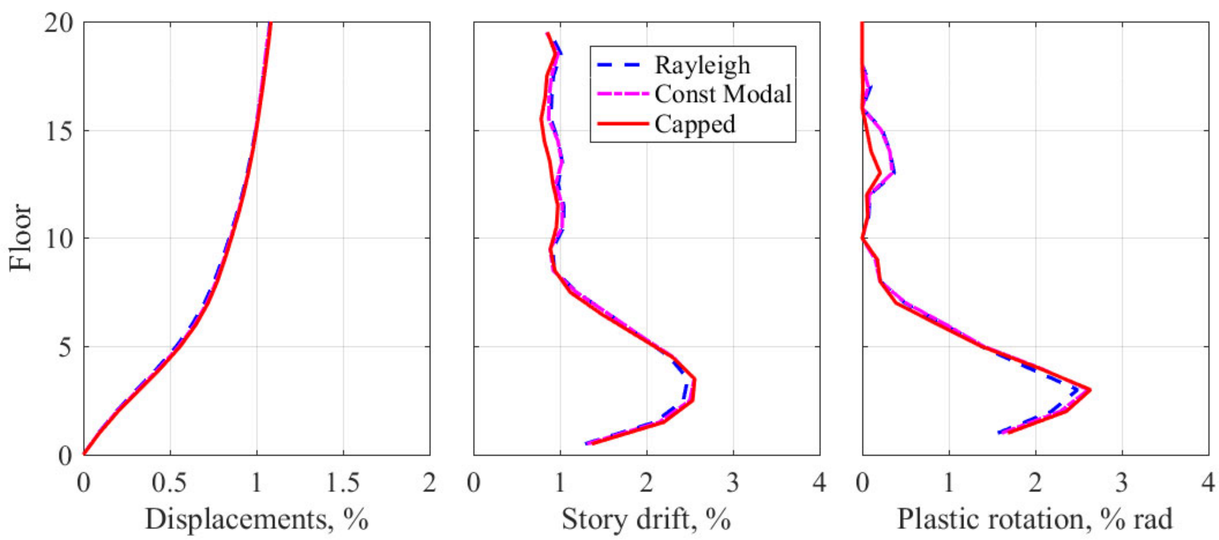

Figure 14 Maximum (over 11 GMs) seismic demands on an enhanced model of the 20-story building for three damping models due to GM 6953 scaled corresponding to 2% PE in 50 years: (a) peak floor displacements; (b) peak story drifts; and (c) peak plastic rotations.

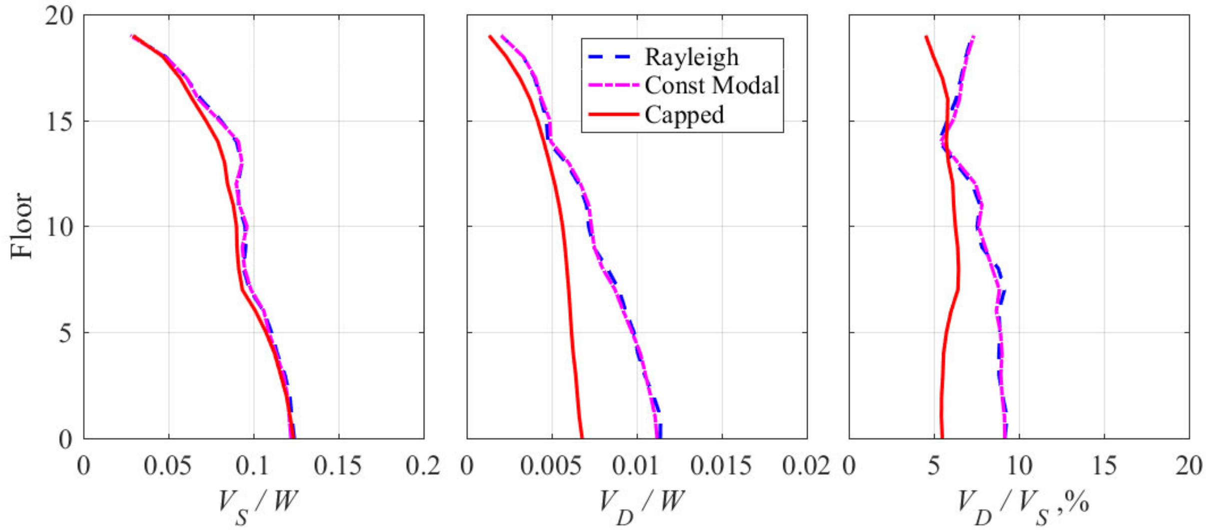

Figure 15 Maximum (over 11 GMs) forces on an enhanced model of the 20-story building for three damping models due to GM 6953 scaled corresponding to 2% PE in 50 years: (a) peak shear force V_S; (b) peak damping force V_D; and (c) ratio V_D/V_S.

Based on these results, it is reasonable to conclude for this building that the linear damping models considered here, Rayleigh damping and constant modal damping, are satisfactory for estimating seismic demands due to MCE_R design-level GMs. Between these two linear models, constant modal damping is recommended because it leads to larger demands that are closer to those obtained using the capped damping model. These results indicate that at MCE_R design-level GMs, the building with constant modal damping satisfies the story drift and plastic rotation limits of 4.5% and 3.1% rad, respectively, specified in design guidelines. Bounding the damping forces—such that V_D/V_S does not exceed 2ζ—does not increase the seismic demands significantly enough to reach a contradictory conclusion.

For more intense GMs causing larger inelastic deformations, the underestimation in response using linear damping models may increase. To explore whether linear damping models would then become unacceptable, we examine the response to 11 GMs associated with earthquake events with 1% PE in 50 years, i.e., average return period of 4975 years, which is twice that corresponding to the MCE_R event.

Presented in Figure 16 and Table 3(b) are the average (over 11 GMs) values of the peak floor displacements, peak story drifts, and peak plastic rotations; story drifts now exceed 2%, and plastic rotations are approximately 2% rad. At these inelastic deformations, the linear damping models underestimate average seismic demands relative to the capped damping model to a greater degree: 4–6% for constant modal damping and 7–10% in the case of Rayleigh damping; see Table 4(b).

The response of the enhanced model to GM 6953, which imposes the largest seismic demands among the 11 GMs, are presented next; the roof displacement history in Figure 17, and the height-wise distribution of peak values of floor displacements, story drifts, and plastic rotations in Figure 18. Story drifts due to this ground motion exceed 4%, and plastic rotations are larger than 5% rad. Observe that all three damping models give very similar roof displacement histories; more precisely, the peak values of roof displacement, story drifts, and plastic rotations are slightly underestimated by linear viscous damping models. The constant modal damping model underestimated seismic demands by less than 1% and the Rayleigh damping model by 7–8%; see Table 4(b). This underestimation results from the fact that "excessive" damping forces are developed in linear viscous damping models, as indicated by the V_D/V_S ratio in several stories of the building being close to 10% in contrast to the $2\zeta = 6\%$ in the capped damping model; see Figure 19. Observe by comparing data in Table 4(a) and Table 4(b) that, when viscous damping is represented by linear models, the underestimation of average seismic demands increases with the intensity of GMs.

Although larger than 2ζ, the V_D/V_S ratio is nowhere close to the alarming value of 46% (or 9ζ) reported for a shear building with 5% damping [Hall 2006]. Among the 22 cases* analyzed, the largest value of V_D/V_S was approximately 12% (or 4ζ), well below the 20% considered as dubious [Hall 2018].

Based on these results, it is reasonable to conclude for this building that the constant modal damping model is satisfactory for estimating seismic demands due to GMs with PE of 1% in 50 years, seismic demands are underestimated relative to the capped damping model by less than a few percent. Between the two linear models, the constant modal damping model is preferred because it leads to larger demands. This is a prudent choice in the absence of a benchmark result.

The degree to which seismic demands are underestimated by linear damping models varies with ground-motion characteristics. This is illustrated in Table 5 and Table 6 by comparing the responses computed for two excitations: GM 6953, which produced the largest demands (over 11 GMs) and GM 185. Recall that both (in fact, all 11) GMs have been scaled to match the spectral acceleration $A(T_1)$ of the UHS. When scaled to PE of 2% in 50 years, GMs 185 and 6953 cause story drifts of ~2% and ~2.5%, respectively; at PE of 1% in 50 years, the two GMs cause story drifts of ~2.5% and ~4% ; see Table 5. Although GM 185 causes significantly less yielding relative to GM 6953, contrary to expectation, linear damping models underestimate its seismic demands by a significantly larger degree. For example, at PE of 1% in 50 years, story drifts due to GM 185 were underestimated by 9.6% in the case of constant modal damping, but only by 0.1% when the excitation was GM 6953; see Table 6. This observation indicates that (1) the inelastic response of buildings depends in a complex manner on the detailed characteristics of GMs, and (2) spectral acceleration $A(T_1)$ is an inadequate intensity measure for selecting GMs to be used in nonlinear RHA of buildings. This is not surprising when we recall that $A(T_1)$ characterizes completely the response of a linear single-degree-of-freedom system, but not if the simple system is inelastic. It is even less appropriate a GM intensity measure for inelastic response of buildings.

The influence of increasing intensity of GMs on seismic demands and their underestimation by linear damping models is investigated further by considering a wider range of intensities. The peak seismic demands—story drifts and plastic rotations—due to GM 6953 scaled to five intensities, including the two corresponding to PEs 2% in 50 years and 1% in 50 years, are presented in Figure 20; also included is the percent underestimation of demand by linear damping models relative to capped damping. With increasing intensity of the GM, as expected, the seismic demands increase. The percent underestimation of demands also increases but not necessarily

* Two sets of 11 GMs corresponding to PEs of 2% and 1% in 50 years.

monotonically, which is yet another indication of the complexity of dynamics of buildings deforming far into the inelastic range.

The most intense GM considered—which was 50% more intense than 2% PE in 50 years and approximately 20% more intense than 1% PE in 50 years—caused story drift exceeding 15% and plastic rotation of 22% radian. Seismic demands were underestimated by less than 10% when constant modal damping was used, but by almost 30% in the case of Rayleigh damping. Clearly, the latter model is unacceptable.

As noted earlier, the seismic demands on the building with the capped damping model are expected to be larger relative to linear damping models. This is what has been observed in most of the 22 cases analyzed; however, there were occasional exceptions. One of these is identified in Table 6(b) where the capped damping model led to 0.6% smaller plastic rotation relative to constant modal damping.

Table 5 **Seismic demands on an enhanced model of the 20-story building for three damping models due to GMs 6953 and 185 scaled to (a) 2% PE in 50 years and (b) 1% PE in 50 years.**

Damping Model	(a) PE = 2% in 50 years				(b) PE = 1% in 50 years			
	GM 6953		GM 185		GM 6953		GM 185	
	Story drift %	Plastic rotations % radians	Story drift %	Plastic rotations % radians	Story drift %	Plastic rotations % radians	Story drift %	Plastic rotations % radians
Rayleigh	2.48	2.49	2.05	1.81	4.03	4.96	2.32	2.22
Constant Modal	2.55	2.62	2.13	1.91	4.35	5.42	2.41	2.32
Capped	2.56	2.64	2.26	2.10	4.35	5.39	2.66	2.77

Table 6 **Underestimate (%) in seismic demands on an enhanced model of the 20-story building by linear viscous damping models relative to capped damping subjected to GMs 6953 and 185 scaled to (a) 2% PE in 50 years and (b) 1% PE in 50 years.**

Damping Model	(a) PE = 2% in 50 years				(b) PE = 1% in 50 years			
	GM 6953		GM 185		GM 6953		GM 185	
	Story drift %	Plastic rotations % radians	Story drift %	Plastic rotations % radians	Story drift %	Plastic rotations % radians	Story drift %	Plastic rotations % radians
Rayleigh	3.2	5.7	9.3	14.0	7.4	8.0	12.8	19.9
Constant Modal	0.2	0.9	5.7	9.2	0.1	-0.6	9.6	16.3

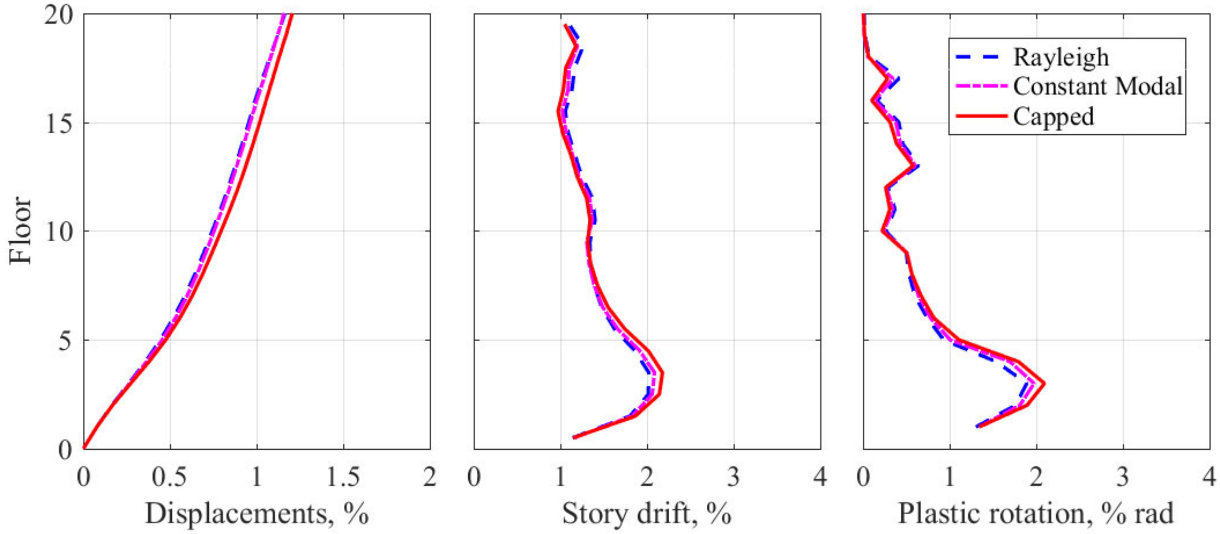

Figure 16 **Average (over 11 GMs) seismic demands on an enhanced model of the 20-story building for three damping models due to GMs with 1% PE in 50 years: (a) peak floor displacements; (b) peak story drifts; and (c) peak plastic rotations.**

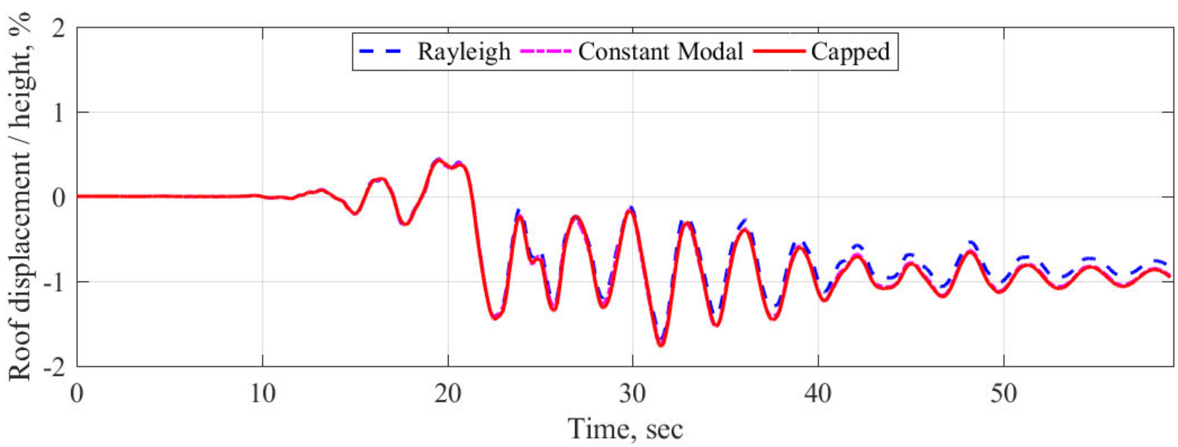

Figure 17 **Response history of roof displacement of an enhanced model of the 20-story building for three damping models due to GM 6953 scaled corresponding to 1% PE in 50 years.**

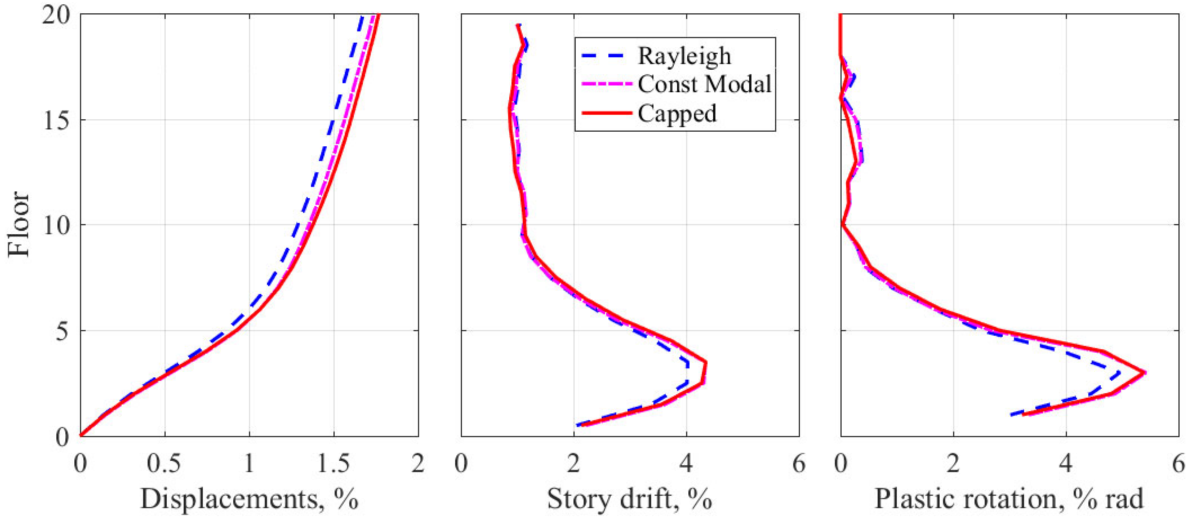

Figure 18 **Maximum (over 11 GMs) seismic demands on an enhanced model of the 20-story building for three damping models due to GM 6953 scaled corresponding to 1% PE in 50 years: (a) peak floor displacements; (b) peak story drifts; and (c) peak plastic rotations.**

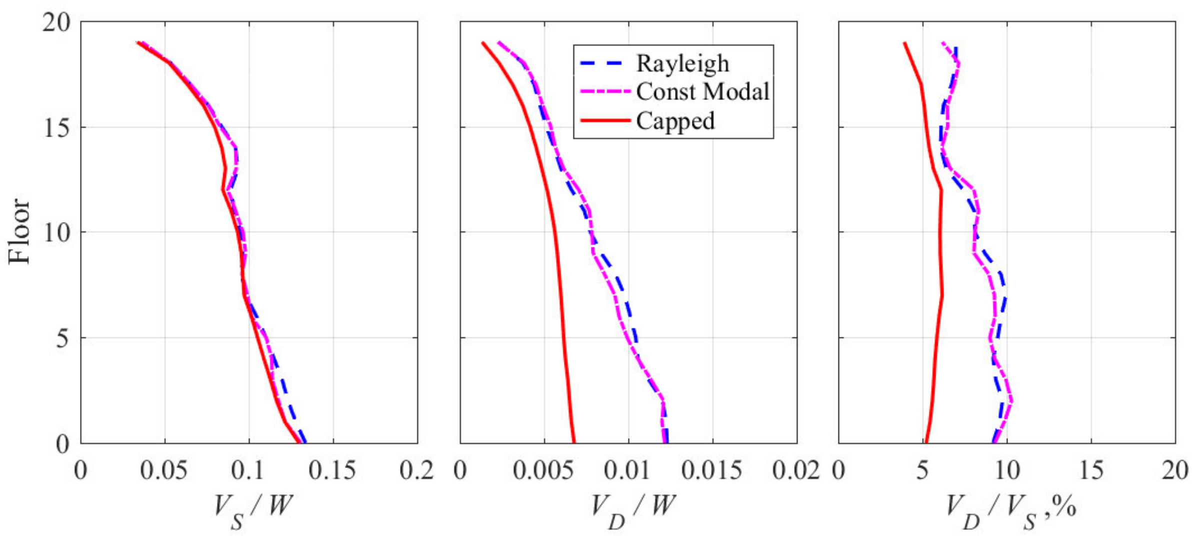

Figure 19 **Maximum (over 11 GMs) story forces on an enhanced model of the 20-story building for three damping models due to due to GM 6953 with 1% PE in 50 years: (a) peak shear force V_S; (b) peak damping force V_D; and (c) ratio V_D/V_S.**

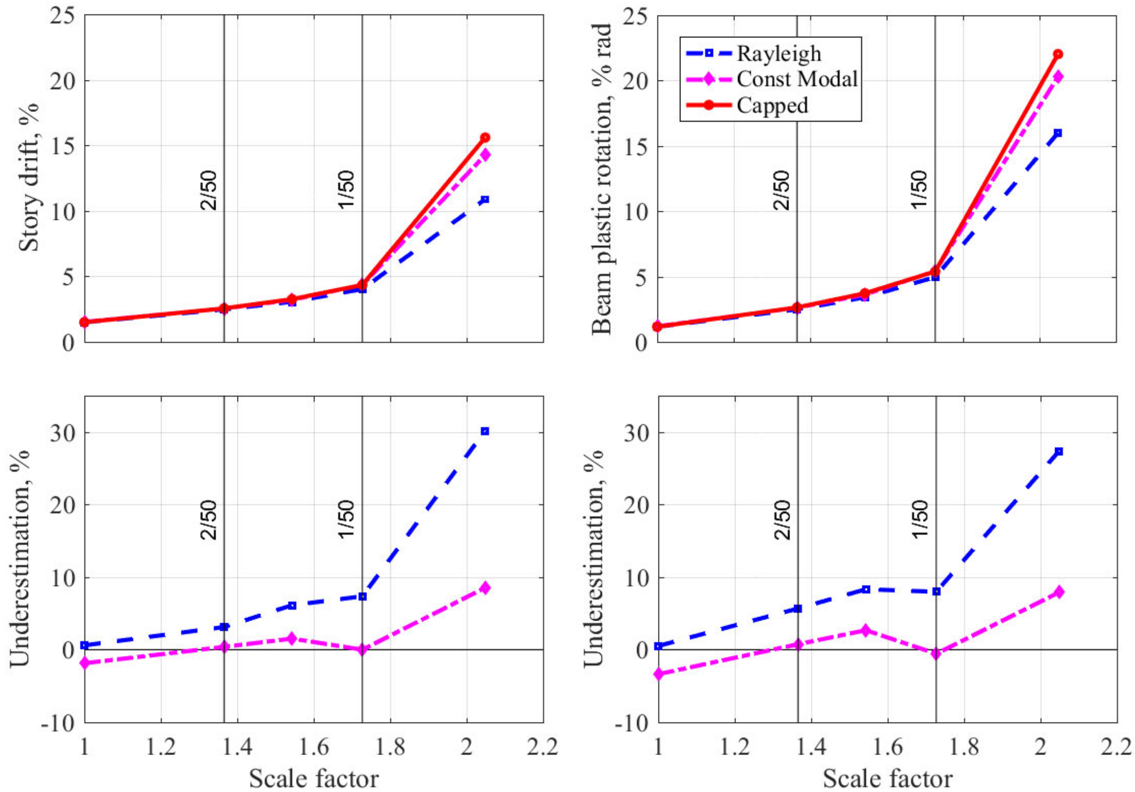

Figure 20 **Response of an enhanced model of the 20-story building for three damping models due to GM 6953 scaled to five different intensities, including the two corresponding to PE 2% and 1% in 50 years: Top two panels: seismic demands; and bottom two panels: underestimate by linear damping models.**

Finally, we return to the GM that imposed the largest demands on either model of the building, combined with the most underestimation of demand by linear damping models. This occurred for the combination of GM 1188 with scale factor of 3.61 (Table D.1) and the simple model; results were presented in Table 1 and Figure 6 and Figure 7. The response spectrum for this scaled GM is plotted in Figure 21, together with the UHS for 2% PE in 50 years and the CMS with conditioning period $T^* = 3.38$ sec., the fundamental vibration period of the enhanced model. Observe that $A(T_1 = 3.38$ sec) for this GM exceeds the CMS value, and the spectral shape is generally consistent with the CMS, indicating that this GM is an acceptable choice for analysis of the enhanced model for seismic hazard defined by 2% PE in 50 years.

The response of the enhanced model to this GM is presented in Figure 22 and Figure 23. Comparison of Figure 22 and Figure 23 versus Figure 6 and Figure 7 indicates that the large residual displacement of the simple model is absent in the case of the enhanced model, and the seismic demands on the enhanced model are approximately one-third compared to the simple model. Most importantly, constant modal damping underestimates seismic demands on the enhanced model by only 4% compared to the unacceptably large underestimate of 21% (see Table 2) in the case of the simple model. These disparities demonstrate the importance of realistic modeling of buildings and selection of ground motions.

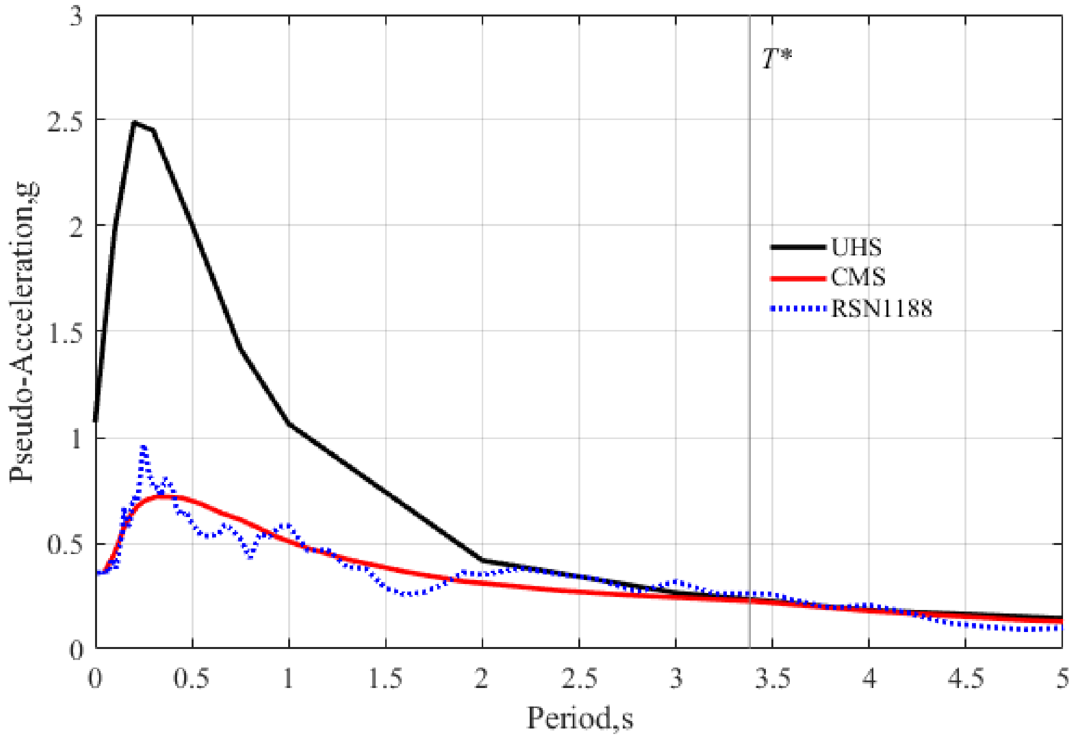

Figure 21 **Uniform Hazard Spectrum (UHS) for 2% PE in 50 years, Conditional Mean Spectrum (CMS) for *T** = 3.38 sec, and the response spectrum for scaled GM 1188.**

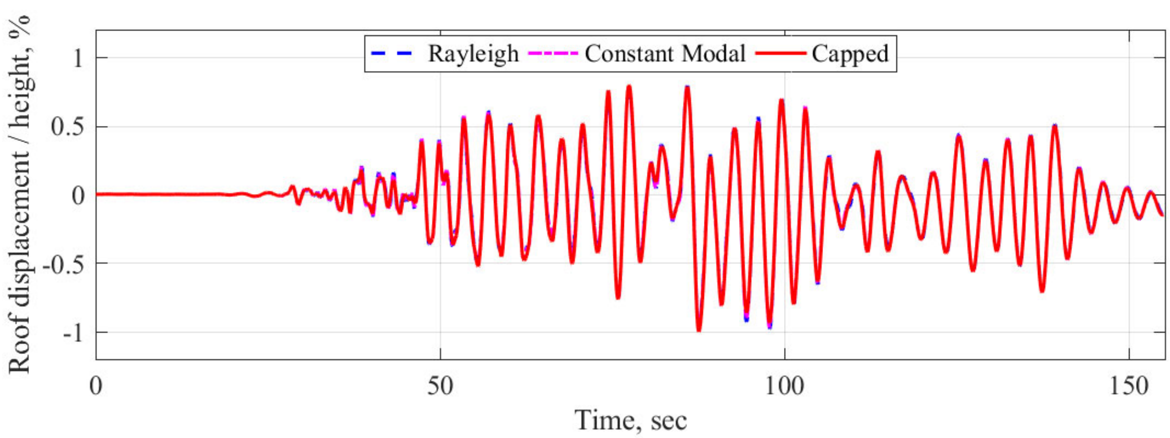

Figure 22 **Response history of roof displacement of an enhanced model of the 20-story building for three damping models due to scaled GM 1188.**

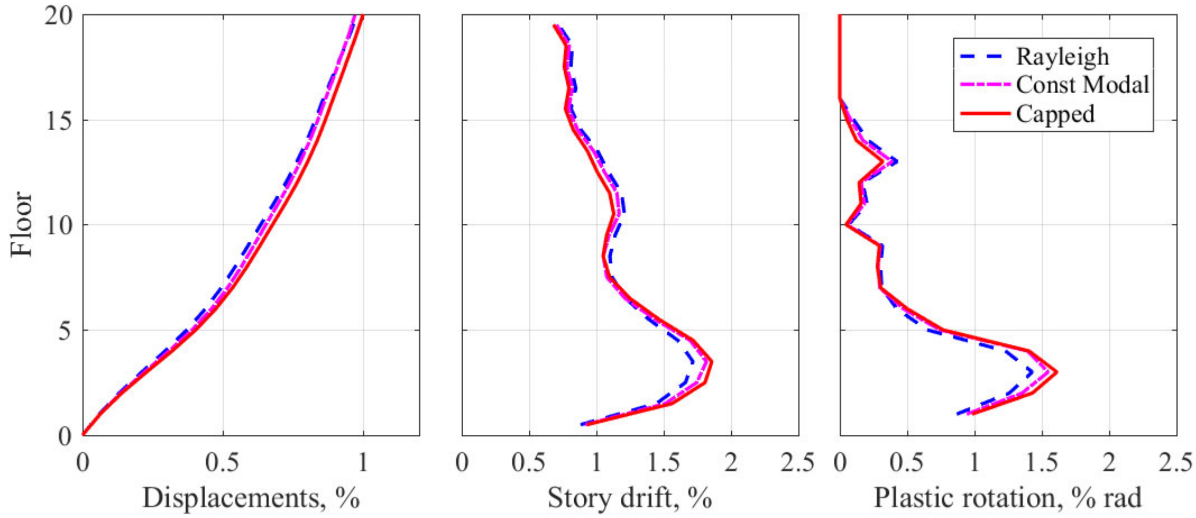

Figure 23 **Seismic demands on an enhanced model of the 20-story building for three damping models due to scaled GM 1188: (a) peak floor displacements; (b) peak story drifts; and (c) peak plastic rotations.**

6 Conclusions

This report has investigated the question: Can building response to MCE_R design-level ground motions (2% PE in 50 years) be estimated satisfactorily using linear viscous damping models or is a nonlinear model, such as capped damping, necessary? This question is pertinent for two reasons: First, nonlinear models have been recommended to limit damping forces in order to avoid underestimation of response; second, the capped damping model cannot be implemented readily in commercial computer codes, and it requires initial runs to define the lateral stiffness and lateral strength of each story.

This question was examined in the context of two models of a 20-story steel moment frame building: a simple centerline model and an enhanced model; the latter included several complex features to create a realistic model. The principal conclusions based primarily on the results for the enhanced model are as follows:

1. Linear viscous damping models are adequate for estimating seismic demands on buildings—designed to satisfy current story drift and plastic rotation limits—due to MCE_R design-level GMs. In contrast, earlier studies have questioned the validity of linear models, but they typically used simplistic models of buildings and/or extremely intense GM.
2. Between the two linear damping models—Rayleigh damping and constant modal damping—the latter is preferable for nonlinear RHA of buildings because it leads to modestly larger demands. This is a prudent choice in the absence of a benchmark or "exact" result.
3. We do not recommend the Rayleigh damping model in nonlinear RHA of buildings because it leads to smaller demands and hence could lead to the conclusion that design or evaluation criteria have been satisfied, when other linear damping models lead to the opposite conclusion. Furthermore, as mentioned in the Introduction, several researchers have identified various problems and deficiencies with Rayleigh damping depending on how the yielding elements in the building are modeled
4. Although constant modal damping is a satisfactory model for estimating seismic demands to MCE_R design-level ground motions—and even for 50% more intense GMs—it may not be appropriate for extreme motions that deform the structure close to collapse.

5. If the goal is to arrive at conclusions valid for professional practice, research investigations on modeling damping in nonlinear RHA of buildings should be based on realistic, state-of-the-practice models of buildings subjected to an ensemble of GMs that correspond to the MCE_R and have been selected by modern methods. The conclusions drawn here are from an investigation of an "actual" steel moment-frame building pushed close to the limit of 4.5% story drift [see Table 1(b)] imposed in modern design guidelines. Thus, these conclusions are expected to be valid for other MRF buildings designed to satisfy these criteria. However, such studies should be conducted on a variety of structural systems and materials to arrive at broadly applicable conclusions.

REFERENCES

ASCE (2017). *Seismic Evaluation and Retrofit of Existing Buildings, 41-17*, American Society of Civil Engineers, Reston, VA, 550 pgs.

Baker J.W. (2011). Conditional mean spectrum: Tool for ground-motion selection, ASCE*, J. Struct. Eng.*, 137: 322–331.

Bernal D. (1994). Viscous damping in inelastic structural response, ASCE*, J. Struct. Eng.*, 120(4): 1240–1254.

Bernal D., Döher M., Mozaffari K., Kwan K., Liu Y. (2015). First mode damping ratios for buildings, *Earth. Spectra*, 31(1): 367–381.

Carr A.J. (1997). Damping models for inelastic analysis, *Proceedings, Asia-Pacific Vibration Conference*, Kyonju, Korea.

Charney F.A. (2008). Unintended consequences of modeling damping in structures, ASCE*, J. Struct. Eng.*, 134(4): 581–592.

Chopra A.K. (2017). *Dynamics of Structures, Theory and Applications to Earthquake Engineering*, 5th edition, Pearson Education, Hoboken, NJ, 960 pgs.

Chopra A.K., McKenna F. (2016a). Modeling viscous damping in nonlinear response history analysis of buildings for earthquake excitation, *Earthq. Eng. Struct. Dyn.,* 45: 193–211.

Chopra A.K., McKenna F. (2016b). Author's reply to John Hall's discussion to Chopra and McKenna's Paper, Modeling viscous damping in nonlinear response history analysis of buildings for earthquake excitation, *Earthq. Eng. Struct. Dyn.,* 45(13): 2235–2238.

Chrisp D. (1980). *Damping Models for Inelastics*, Master's Thesis, University of Canterbury, Christchurch, New Zealand.

Computers & Structures (2006). *Components and Elements for Perform-3D and Perform-Collapse*, Version 4, Computers and Structures Inc., Walnut Creek, CA.

Computers & Structures (2011). *PERFORM-3D User's Guides, Version 5*, Computers & Structures, Inc., Walnut Creek, CA.

Crandall S.H., Mark W.D. (1963). *Random Vibration in Mechanical Systems,* Academic Press, Cambridge, MA.

Cruz C, Miranda E. (2017). Evaluation of Rayleigh damping model for buildings, *Eng. Struct*., 138: 324–336.

FEMA (2000). *Prestandard and Commentary for the Seismic Rehabilitation of Buildings*, *FEMA-256,* Federal Emergency Management Agency, Washington, D.C.

Gupta A., Krawinkler H. (1999). Seismic demands for the performance evaluation of steel moment resisting frame structures, *John A. Blume Earthquake Engineering Center Report No. 132*, Stanford University, Stanford, CA.

Hall J.F. (2006). Problems encountered from the use (or misuse) of Rayleigh damping, *Earthq. Eng. Struct. Dyn.*, 35: 525–545.

Hall J.F. (2018). Performance of viscous damping in inelastic seismic analysis of moment-frame buildings, *Earthq. Eng. Struct. Dyn.*, 47(14): 2756–2776.

Ibarra L.F., Krawinkler H. (2005). Global collapse of frame structures under seismic excitations, *John A. Blume Earthquake Engineering Center Technical Report 152*, Stanford Digital Repository, Stanford University, Stanford, CA.

Jehel P., Leger P., Ibrahibegovic A. (2014). Initial versus tangent-stiffness based Rayleigh damping in inelastic time history analysis, *Earthq. Eng. Struct. Dyn.*, 43: 476–484.

Krawinkler H. (2000). *State of the Art Report on Systems Performance of Steel Moment Frames Subject to Earthquake Ground Shaking*, *FEMA-355C*, Federal Emergency Management Agency, Washington, D.C.

Leger P., Dussault S. (1992). Seismic-energy dissipation in MDOF structures, ASCE, *J. Struct. Eng.,* 118(6): 1251−1267.

Lignos D.G., Krawinkler H. (2010). A steel database for component deterioration of tubular hollow square steel columns under varying axial load for collapse assessment of steel structures under earthquakes, Proceedings*, 7th International Conference on Urban Earthquake Engineering*, Tokyo Institute of Technology, Tokyo, Japan.

Lignos D.G., Krawinkler H. (2011). Deterioration modeling of steel components in support of collapse prediction of steel moment frames under earthquake loading, ASCE, *J. Struct. Eng*., 137(11): 1291–1302.

Luco J.E., Lanzi A. (2017). A new inherent damping model for inelastic time-history analyses, *Earthq. Eng. Struct. Dyn.*, 46: 1919−1939.

McKenna F., Fenves G.L., Scott M.H. (2000). *Open System for Earthquake Engineering Simulation*, Pacific Earthquake Engineering Research Center, University of California, Berkeley, CA.

McKenna F. (2011). OpenSees: a framework for earthquake engineering simulation, *Comp. Sci. Eng.,* 13: 58–66.

Medina R., Krawinkler H. (2004). Seismic demands for non-deteriorating frame structures and their dependence on ground motions, John A. Blume Earthquake Engineering Center, Department of Civil and Environmental Engineering, *Final Report on PEER Project 3011999*, Stanford University, Stanford, CA.

Petrini L., Maggi C., Priestley N., Calvi M. (2008). Experimental verification of viscous damping modeling for inelastic time history analyses, *J. Earthq. Eng.*, 12(1):125−145.

PEER (2010). Modeling and acceptance criteria for seismic design and analysis of tall buildings, *Technical Report PEER 2010/111 or PEER/ATC-72*, Pacific Earthquake Engineering Research Center, University of California, Berkeley, CA.

PEER (2017). Guidelines for performance-based seismic design of tall buildings, *PEER Report No. 2017/06*, Pacific Earthquake Engineering Research Center, University of California, Berkeley, CA.

Wilson E., Penzien J. (1972). Evaluation of orthogonal damping matrices, *Int. J. Num. Methods Eng.,* 4(1): 5–10.

Zareian F., Medina R.A. (2010). A practical method for proper modeling of structural damping in inelastic plane structural systems, *Comp. Struct.*, 88: 45−53.

Appendix A Capped Damping Model

A.1 STORY DAMPER COEFFICIENTS

Energy dissipation in the linear range of vibration is modeled by interstory viscous dampers, which develop lateral damping forces proportional to the relative velocity between the two floors of a story. As shown in Figure A.1, these dampers were placed in the middle bay of the 5-bay frame; however, other placements of the dampers would be equivalent because horizontal translational DOFs of all nodes on a floor are constrained.

For the purposes of defining the height-wise distributions of C_i, and only for this purpose, lateral stiffnesses of stories were estimated by various indirect methods: linear static analysis with three different lateral force distribution—first mode, code equivalent lateral forces, and uniform [Chopra 2017, Section 23.4.1]— and a trial linear RHA of the building with constant modal damping. From the results of these analyses, the lateral stiffness of a story was determined as the ratio of story shear to story drift. Although valid for results of static analysis, this approach may be reasonable for RHA results only if the peak values of story shear and drift occur at the same time instant; and this was confirmed in the results of linear RHA selected to compute story stiffness. The height-wise distribution of lateral story stiffnesses of the simple model of the 20-story frame determined by all four methods is presented in Figure A.2. Observe that the results from linear RHAs for two values of the damping ratio—2% and 5%—are almost identical. Story stiffness distributions determined by the three static analyses are very close in the lower 10 stories but differ in the upper stories because of differences in the three force distributions. The mean story stiffness distributions determined from linear RHA of the building subjected to 11 GMs are essentially the same as those determined from static analyses in the lower 10 stories, but are larger in the upper stories, perhaps because of the complex dynamics of the 20-story frame.

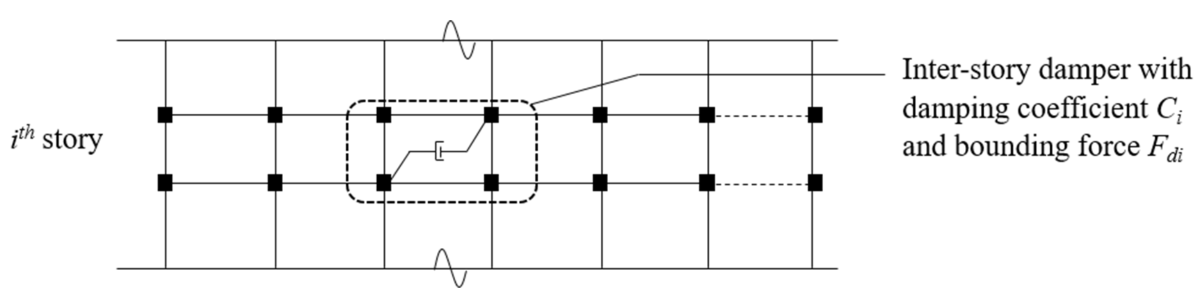

Figure A.1 Interstory viscous damper in the middle bay of the *i*th story; representative of all stories.

In this study, the height-wise distribution of the C_i's was assumed to be the same as the story stiffness distribution, determined from RHAs of the building. Note that the estimated values of story stiffness are not used in any part of the analyses other than to define the height-wise distribution of the C_i values required to determine their numerical values from Equation (3).

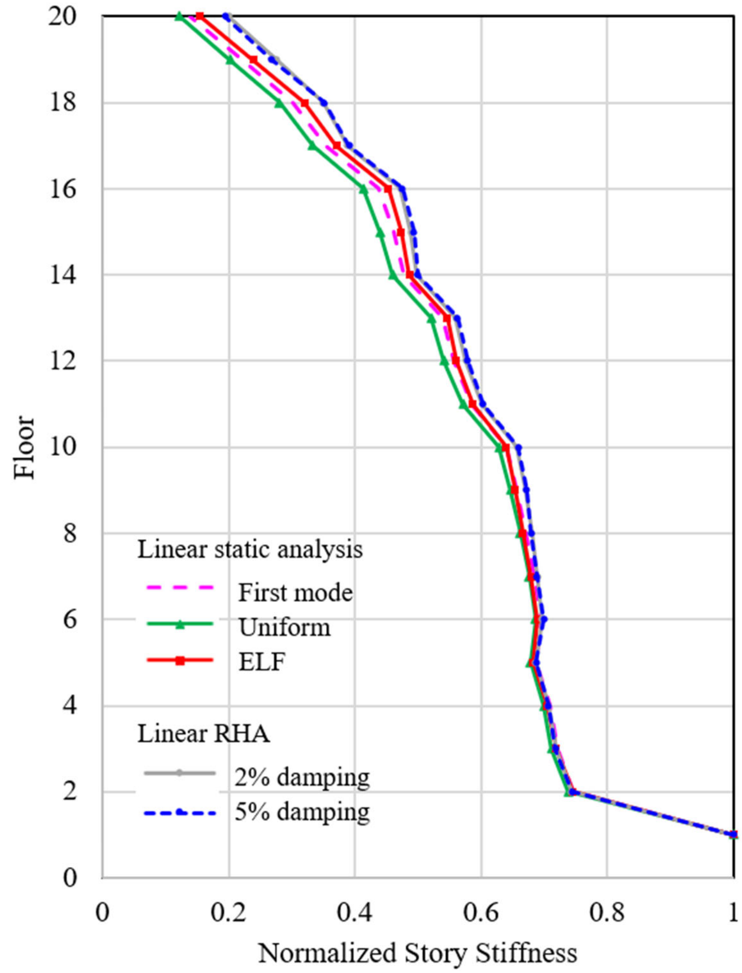

Figure A.2 **Story stiffness distribution estimated by linear static analyses with three different force distributions and by linear RHA with two values of constant model damping.**

A.2 BOUND ON STORY DAMPER FORCE

The bound on the damping force in each story is defined as 2ζ times the lateral strength of the story. The story strengths may be estimated by pushover analysis of the building. Nonlinear static analysis of the building subjected to gradually increasing lateral forces with a specified height-wise distribution leads to the pushover curve and the story shears when, ideally, all the stories have just yielded; however, inelastic deformation tends to be concentrated in the lower stories, which yield first; thereafter, further yielding tends to continue in those stories without additional deformation of the upper stories, making it often impractical to push the upper stories to yield. The computed story shears provide an estimate of the story strengths shown for the simple model in

Figure A.3 for two lateral force distributions: first mode and code-specified equivalent lateral forces [Chopra 2017; Section 23.4.1].

The story strengths may also be estimated by nonlinear RHA of the building subjected to a GM strong enough to cause yielding of all stories. These are given by the peak values of story shears determined by such an analysis. Used in this study are the average story strengths determined by nonlinear RHAs of the building (with 2% constant modal damping) subjected to 11 GMs presented in Figure A.3.

Note that these estimated values of story strengths are used only for establishing a bound on the story damper force, and not in any other part of the dynamic analyses.

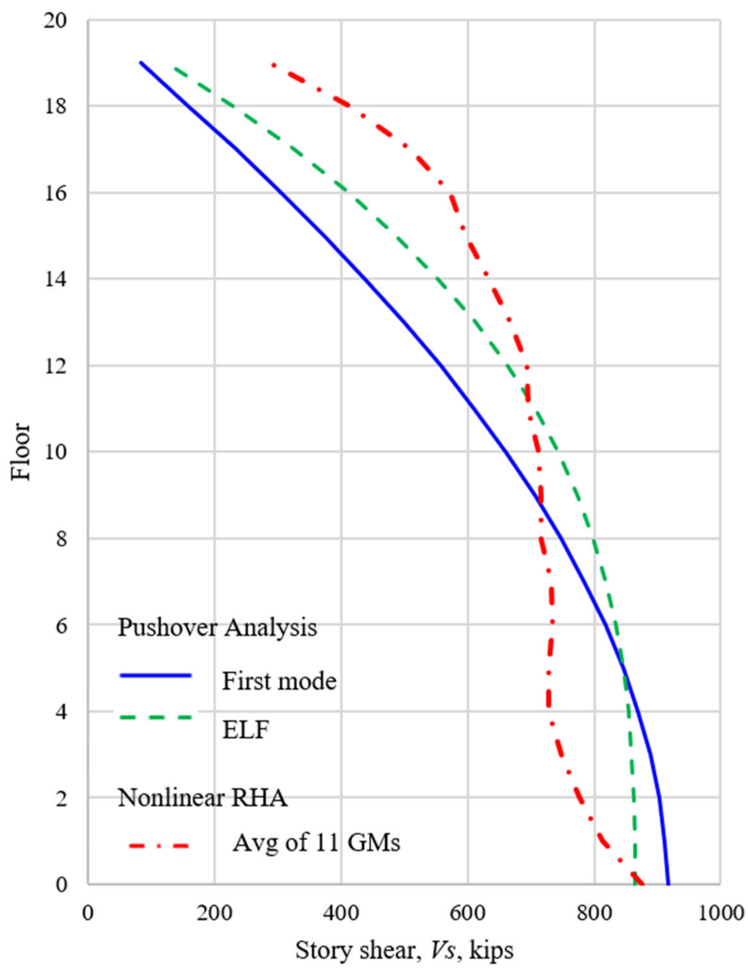

Figure A.3 **Story strengths estimated by pushover analyses with two different force distributions and nonlinear RHAs for 11 GMs.**

A.3 IMPLEMENTATION OF CAPPED DAMPING IN OPENSEES

An interstory damper is implemented as a zero-length element connected to the horizontal DOFs at the two floors of a story, with its force-velocity relationship defined by a uniaxial material model in OpenSees. The damping force-velocity relationship is bilinear, where the linear branch—defined by the damping coefficient C_i—is valid until the damping force reaches the bounding value; at larger velocities, the damping force remains constant at the bounding value.

Presented in Figure A.4 are the results from nonlinear RHA of the simple model of the 20-story building subjected to one of the 11 GMs for two models of interstory dampers: linear viscous damping and capped damping. For the damper in the third story of the building model, evolution of the damping force versus interstory relative velocity is shown in Figure A.4(a), and versus interstory drift in Figure A.4(b). At small amplitudes of motion—the two damping models are identical—the damping force is a linear function of velocity, and the damping force versus deformation plot is the familiar hysteresis loop of elliptical shape. At larger motions of the nonlinear damper with bounded force, the damping force-velocity relation is bilinear, and the hysteresis loop is truncated at positive and negative bounds on the damping force.

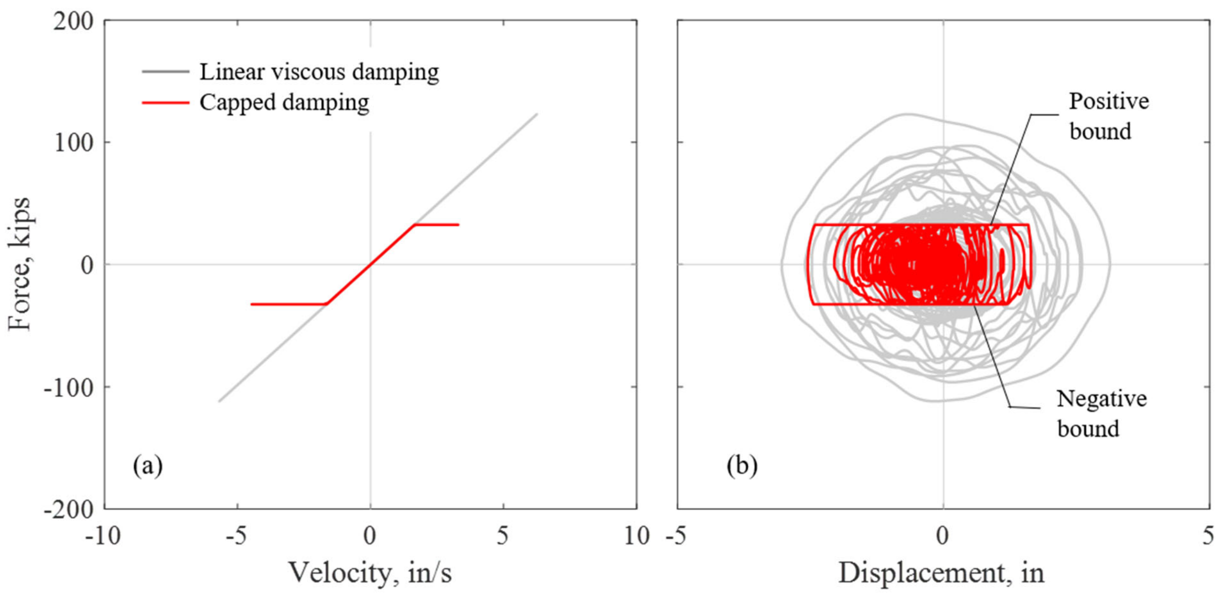

Figure A.4 **Plots of force in the third-story damper versus (a) interstory relative velocity and (b) interstory drift determined by RHA of a simple model of the 20-story frame.**

Appendix B Structural Models

The building considered is a 20-story steel moment-resisting frame building in Los Angeles that was designed according to the 1994 Uniform Building Code (UBC) as part of the SAC project for post-Northridge earthquake design criteria [Gupta and Krawinkler 1999; Krawinkler 2000]. The plan of the building and elevation of the moment-resisting perimeter frame, which is analyzed in this work, are presented in Figure B.1; the interior frames are gravity frames. Two planar models of an east–west, 5-bay perimeter frame of the building were developed: simple model and enhanced model. In both models the subterranean part of the building was ignored and the columns were fully clamped at the ground level.

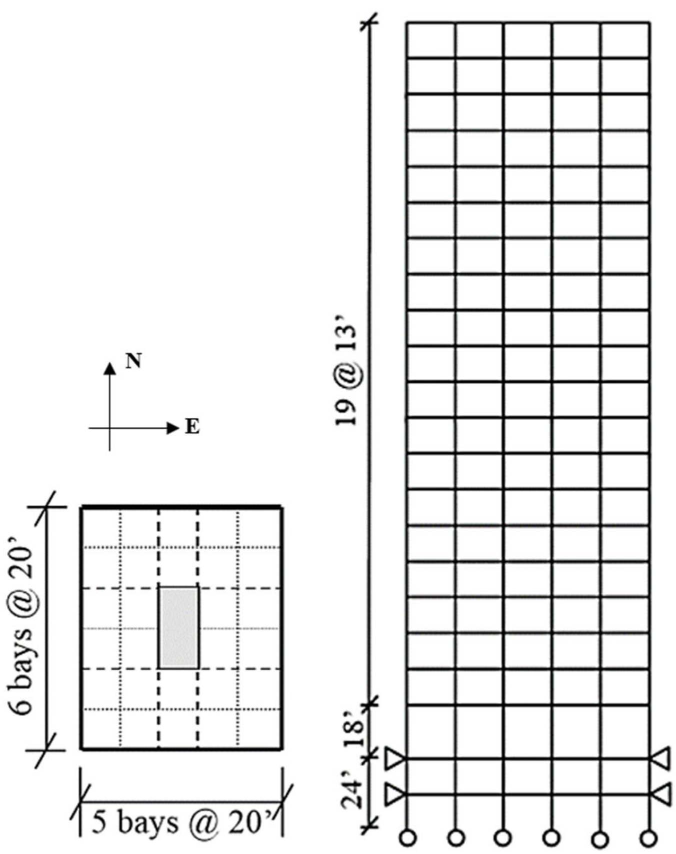

Figure B.1 **Plan and elevation of SAC 20-story building designed for Los Angeles [Gupta and Krawinkler 1999].**

The seismic masses were computed from the design dead and live loads, resulting in 40 kips-sec/ft at the 20th floor and 38 kips-sec/ft at floors 1–19 [Gupta and Krawinkler 1999, Appendix B].

B.1 SIMPLE MODEL

Presented in Figure B.2 is a simple model of the perimeter frame, based on centerline dimensions; beams were modeled between centerlines of columns without rigid offsets; deformations in panel zones and the contribution of the top and bottom cover plates to stiffness and strength were not considered. The first three natural periods of vibration of the model are T_1 = 3.81 sec, T_2 = 1.33 sec, and T_3 = 0.77 sec.

Each beam-and-column element was modeled as three elements in series: implicit zero-length rotational springs at the ends and an elastic element in between the hinges [Figure B.3(a)]. The unwanted internal rotational DOFs were condensed out. This approach was preferred over modeling hinges explicitly with damping omitted, because the latter approach leads to a damping model similar to tangent stiffness damping [Hall 2018], which is discarded for reasons mentioned in Chopra and McKenna [2016] and [Hall 2018].

The moment-rotation relation for plastic hinges is idealized by the multilinear backbone curve shown in Figure B.4(a), where M_y is the yield moment, M_c is the capping moment or peak moment, θ_p is the pre-peak plastic rotation, and θ_{pc} is the post-peak plastic rotation. For wide flange (WF) sections, definition of the backbone curve is based on Section 3.2.2 of the PEER/ATC-72 report [2010] for non-RBS (reduced-beam section) moment connections. In this reference, the modeling parameters were developed by multivariate regression analysis of a database of moment connection tests [Ibarra et al. 2005; Lignos and Krawinkler 2011]; modifications proposed by Ribeiro et al. [2017] were included in this study. The modeling parameters depend mainly on the geometry and section properties, including the depth-to-thickness ratio (h/t_w), flange width-to-thickness ratio ($b_f/2t_f$), ratio of unbraced-length to weak-axis radius of gyration (L_b/r_y), span-to-depth ratio (L/d), and yield strength (F_y).

For tubular Hollow Square Steel (HSS) columns, the backbone curve is based on Lignos and Krawinkler [2010]. The moment-rotation relationships were developed based on multivariate regression analysis of a database of tests on more than 120 HSS columns under constant axial load and cyclic moments. The component deterioration parameters depend strongly on the column depth-to-thickness ratio (D/t), axial load to strength ratio (N/N_y), and yield strength (F_y). Required in establishing these parameters is the axial force on the column under gravity loads. The moment-rotation relation shown in Figure B.4(b) is modeled without cyclic deterioration by a multilinear material in OpenSees.

In the simple model of the frame, material strengths were defined by their nominal values, i.e., yield strength of beams, F_{yb} = 36 ksi and yield strength of columns, F_{yc} =50 ksi. For both WF beams and HSS sections, the capping moment to yield moment ratio was assumed to be 1.05.

The initial stiffness of the hinge is typically modified to ensure that the natural periods of vibration in the linear range of the model remain unchanged. In this study, the initial stiffness of the hinge was multiplied by 1000. This is the default mode in PERFORM-3D [2011; Powell 2015] but not in OpenSees. The influence of this choice is described in Appendix B of Ibarra and Krawinkler [2013].

Each column element was assigned a P-delta transformation to account for gravity load effects. A gravity column, as shown in Figure B.2, was also added to model the P-delta effects of the gravity loads on the interior frames. Mass was distributed to the nodes based on the tributary area, and all horizontal DOFs at a floor were laterally constrained.

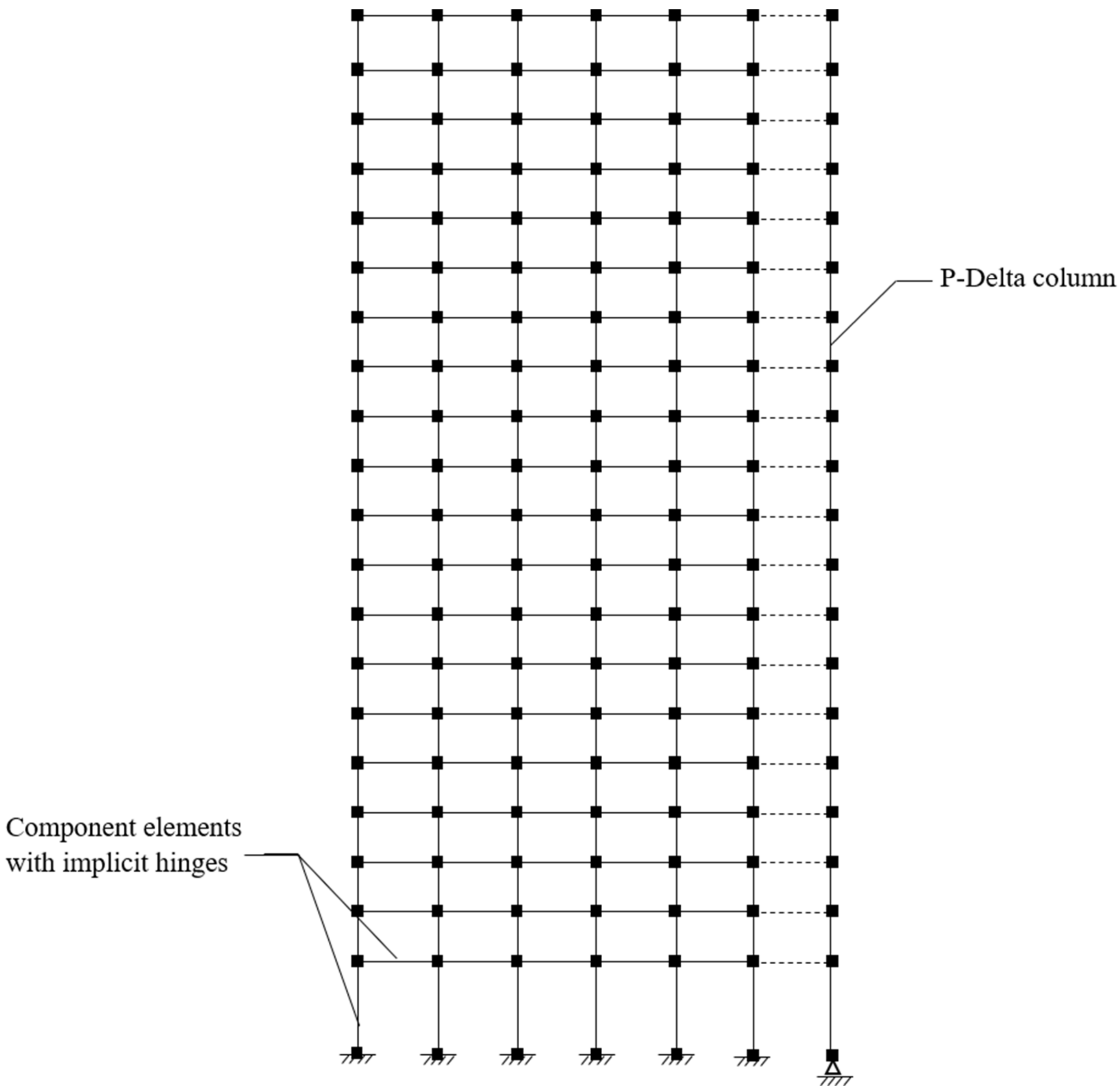

Figure B.2 Simple model of the 20-story frame.

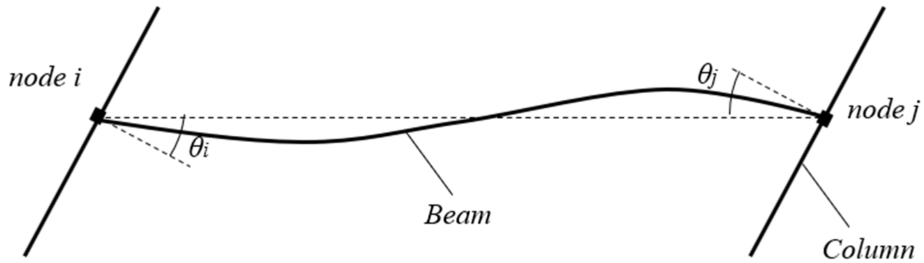

(a)

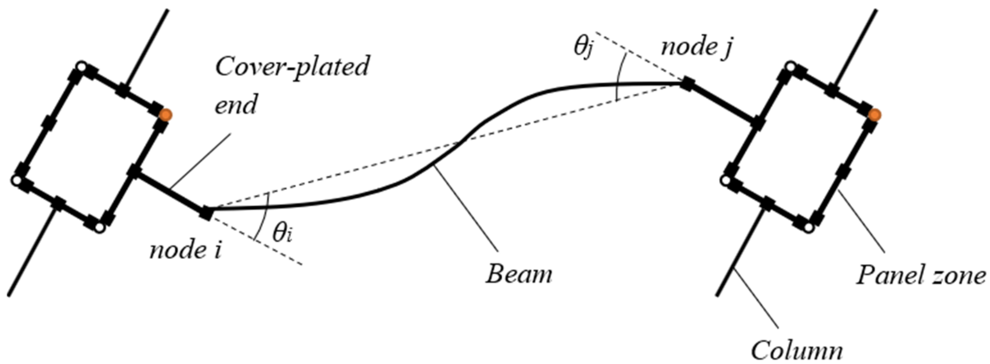

(b)

Figure B.3 Beam models: (a) single beam element in simple model; and (b) cover-plated beam elements connected rigidly to the panel zones and by plastic hinges to the main beam element in the enhanced model; plastic hinges form at nodes *i* and *j*.

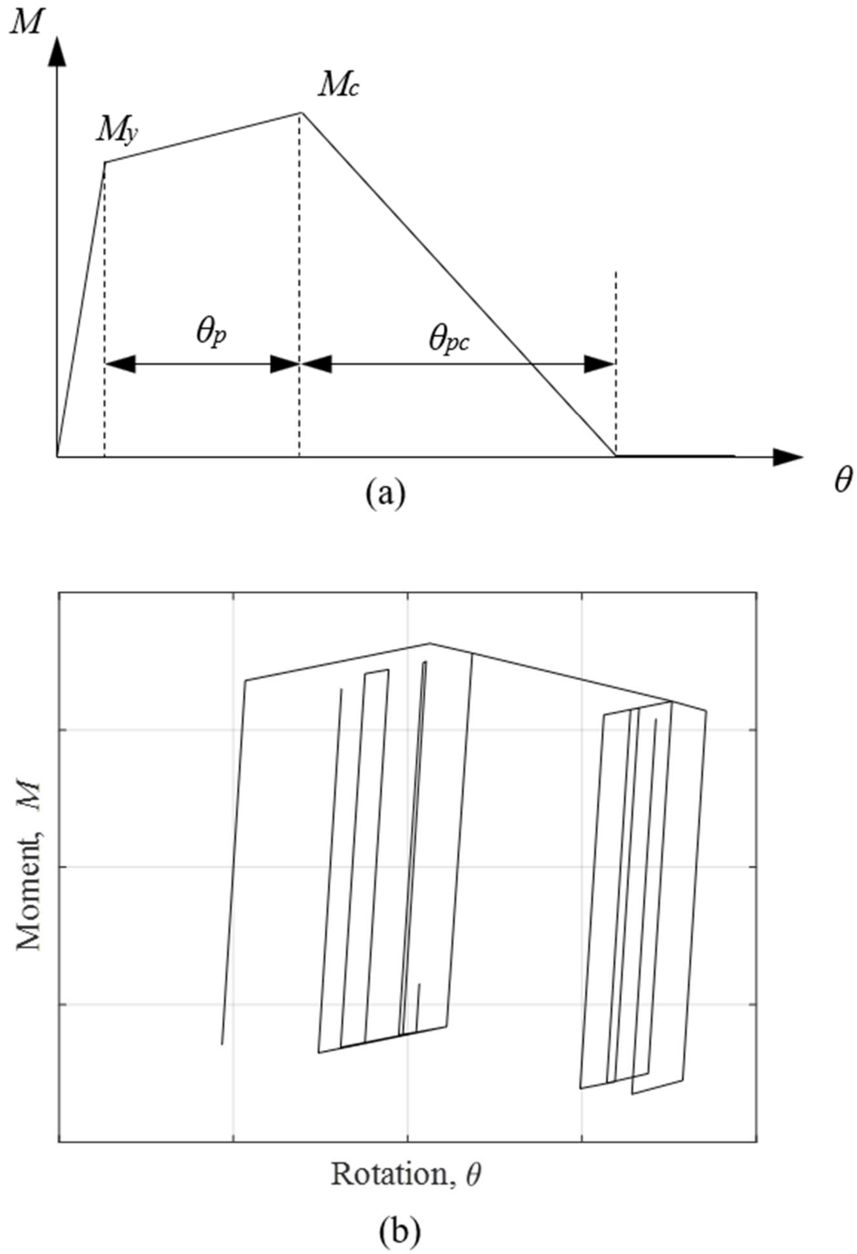

Figure B.4 **(a) Multilinear moment-rotation backbone curve for beam and column hinges; and (b) typical cyclic behavior.**

B.2 ENHANCED MODEL

An enhanced model of the 20-story steel moment-frame included several complex features: geometric nonlinearity; strain hardening and deterioration of plastic hinges; flexibility and yielding of panel zones, tri-element beams to model cover plated ends, and the interior gravity frames. The first three natural vibration periods of this model are T_1 = 3.38 sec, T_2 = 1.17 sec, and T_3 = 0.68 sec

The same approach was employed for modeling plastic hinges in the enhanced model, but it was modified (to the extent practical) to match Hall's model of the building [2018]. Instead of the nominal values, the yield strengths of the beams and the columns were defined as 46 ksi and 54 ksi, respectively. In defining the plastic hinges in beams, the capping-to-yield moment ratio was assumed to be 1.2. For columns, there seemed to be no good reason to increase the capping-to-yield moment ratio. Therefore, M_c/M_y was left unchanged at 1.05, consistent with the recommendation in Lignos and Krawinkler [2010], which differs from 1.2 in Hall [2018].

Following Gupta and Krawinkler [1999], the panel zone is modeled as a rectangular-shaped assembly of eight very stiff elastic beam-column elements and one zero-length rotational spring element that models the shear deformations in the panel zone; see Figure B.5. The other three corners of the rectangular assembly are pinned joints with the two connecting nodes constrained to move together, horizontally and vertically, without any resistance to shear distortion of the panel-zone assembly. This rectangular assembly of very stiff beam–column elements[+], rotational spring, and hinges will distort into a parallelogram under lateral deformation. The parameters defining the trilinear backbone curve for the rotational spring [Figure B.6(a)] depend on the depth, thickness, and yield strength of the panel zone, as well as the width and thickness of the column flange and the depth of the beam. Definition of these parameters followed the recommendations in Gupta and Krawinkler [1999], except that strain hardening ratio, α, was modified to 10% to match Hall's model [2018]. The rotational spring is modeled by a hysteretic material in OpenSees; see Figure B.6(b). Pinching or deterioration of the hysteresis loop is not modeled, as suggested by experimental evidence that deterioration in the shear force versus shear distortion relationship for panel zones is limited. The thickness of the panel zone is taken as the combined thicknesses of the column web and doubler plates where specified.

Figure B.3(b) describes schematically the model for a cover-plated beam that includes elastic beam–column elements for the cover plated ends, connected rigidly to the panel zone and by a plastic hinge to the main beam element. The design of the building specified different sizes for the top and bottom cover plates, with thickness that varies with the beam sections in different parts of the building. Instead of explicitly modeling all these different sizes, a simplified approach was adopted. For all beams, the area and moment of inertia of the cover-plated ends were defined to be 40% and 70% larger than for the main beam section, respectively.

Following Hall [2018], one planar gravity frame is included in the model to represent the interior gravity frames in the east–west direction. The gravity frame, modeled by elastic beams and columns connected at their centerlines, is intended to represent the contribution of half of the five gravity frames. Thus, the stiffnesses of one of the frames were multiplied by 2.5. However, it was assumed that the pinned connections in gravity frames can develop only 10% of the beam stiffness. Thus, the sectional area and moment of inertia of the structural elements in a gravity frame were multiplied by a factor of 0.25.

The gravity frame shown in Figure B.5 accounts for the P-delta effects of the vertical loads acting on the interior frames. The moment-frame columns include P-delta transformation to account for the gravity load effect on the perimeter frame. The node at the floor level on the right side of the panel zone is assigned the tributary mass (highlighted in Figure B.5). Horizontal DOFs

[+] An area of 1000 in^2 and moment of inertia of 100,000 in^4 were assigned to the stiff beam–column elements.

of all nodes on the same floor, i.e., nodes with tributary mass in the moment frame and all nodes in the gravity frame, were constrained to undergo the same horizontal displacement.

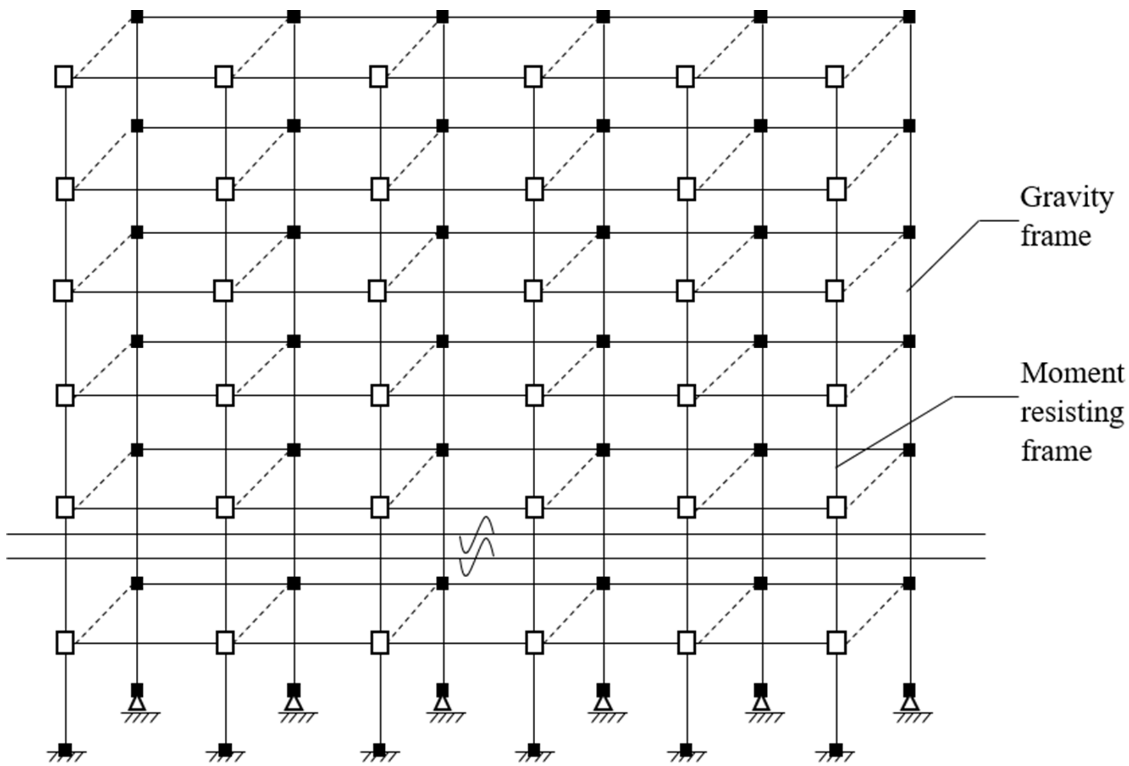

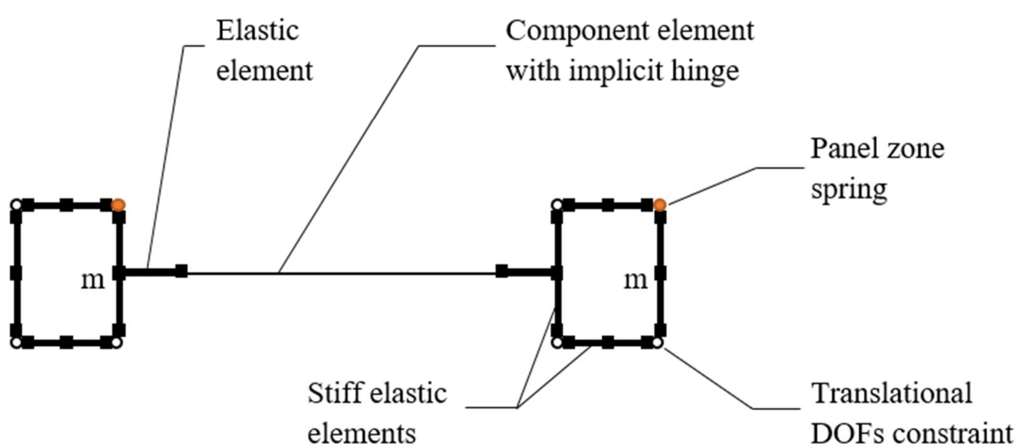

Figure B.5 Enhanced model of the 20-story building; modeling details for beams and panel zone are shown.

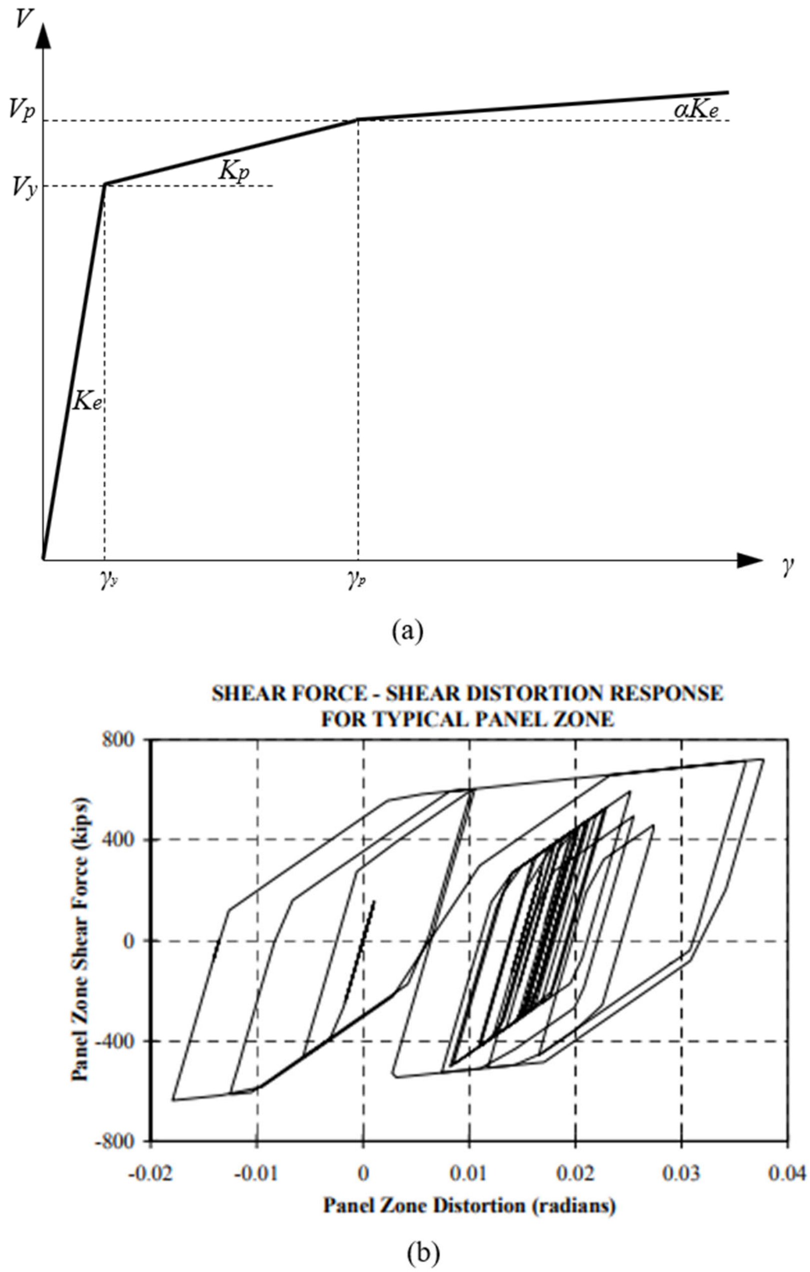

Figure B.6 **Shear force–shear distortion relation for panel zone: (a) backbone curve; and (b) typical cyclic behavior (from [Gupta and Krawinkler [1999]).**

B.3 COMPUTATION TIMES

Computation times for response history analysis of the enhanced model for 60 sec duration of GM 6953 with PE 2% in 50 years on a computer with a processor of Intel® Core™ i5-3570 CPU @3.40 GHz and an 8GB RAM were 1923, 3456, and 2295 seconds for Rayleigh, constant modal, and capped damping, respectively.

References

Chopra A.K., McKenna F. (2016). Author's reply to John Hall's discussion to Chopra and McKenna's Paper, Modeling viscous damping in nonlinear response history analysis of buildings for earthquake excitation, *Earthq. Eng. Struct. Dyn.,* 45(13): 2235–2238.

Computers & Structures (2006). *Components and Elements for Perform-3D and Perform-Collapse*, Version 4, Computers and Structures Inc., Walnut Creek, CA.

Computers & Structures (2011). *PERFORM-3D User's Guides, Version 5*, Computers & Structures, Inc., Walnut Creek, CA.

Gupta A., Krawinkler (1999). Seismic demands for performance evaluation of steel moment resisting frame structures, *John A. Blume Earthquake Engineering Center Technical Report 132*, Department of Civil and Environmental Engineering, Stanford University, Stanford, CA.

Hall J.F. (2016). Discussion of modeling viscous damping in nonlinear response history analysis of buildings for earthquake excitation by Anil K. Chopra and F. McKenna, *Earthq. Eng. Struct. Dyn*., 45(13): 2229–2233.

Ibarra L.F., Krawinkler H. (2005). Global collapse of frame structures under seismic excitations, *John A. Blume Earthquake Engineering Center Technical Report 152*, Stanford Digital Repository, Stanford University, Stanford, CA.

Ibarra L.F., Medina R.A., Krawinkler H. (2005). Hysteretic models that incorporate strength and stiffness deterioration, *Earthq. Eng. Struct. Dyn*., 34(12):1489-1511.

Lignos D.G., Krawinkler H. (2010), A steel database for component deterioration of tubular hollow square steel columns under varying axial load for collapse assessment of steel structures under earthquakes, Proceedings, 7th World Conference on Urban Earthquake Engineering, Center for Urban Earthquake Engineering, Tokyo Institute of Technology, Tokyo, Japan.

Lignos D.G, Krawinkler H. (2011). Deterioration modeling of steel components in support of collapse prediction of steel moment frames under earthquake loading, ASCE, *J. Struct. Eng*., 137(11): 1291–1302.

PEER (2010). Modeling and acceptance criteria for seismic design and analysis of tall buildings, *Technical Report PEER 2010/111 or PEER/ATC-72*, Pacific Earthquake Engineering Research Center, University of California, Berkeley, CA.

Ribeiro F.L.A., Neves L.A.C., Barbosa A.R. [2017]. Implementation and calibration of finite-length plastic hinge elements for use in seismic structural collapse analysis, *J. Earthq. Eng*., 21(8): 1197–1219.

Powell G.H. (2015). *Personal Communication*.

Appendix C Comparison with Hall's Model [2018]

The enhanced model developed here was intended to be similar to the model of the SAC building developed by Hall [2018]. The various modifications and features described in Section B.2 were intended to achieve this goal. However, the two models are not identical; the principal differences are listed below:

1. The building is restrained at the ground level to prevent lateral motion, and the columns are continuous into the basement in Hall [2018]. In contrast, in this work the columns were fully restrained at the ground level.
2. The panel zone was modeled by a shear element in Hall [2018] in contrast to an assemblage of rigid elements with a rotational spring in this work.
3. Capped damping was modeled by a viscous panel element and the bound on the damping force by a limit on the shear stress for the material in Hall [2018]. In contrast, in this work capped damping was modeled by interstory dampers with a bound (or cap) imposed on the damping forces.

However, the Rayleigh (R) and Wilson–Penzien (WP) damping models in Hall [2018] are essentially the same as Rayleigh (with implicit hinges) and Constant Modal Damping models in this study.

Results from nonlinear RHA of the two models of the 20-story building subjected to the LA35/36 GM described in Hall [2018] scaled by 0.5, are compared in Figures C.1, C.2, and C.3 The roof displacements histories are in good agreement for each of the three damping models; see Figure C.1. The height-wise distributions of the story damping forces are also in good agreement for each of the three damping models; see Figure C.2. However, the height-wise distribution of the plastic hinge rotations in the two models is significantly different—see Figure C.3—with the largest plastic rotation occurring in different stories: the third story in the OpenSees model developed in this study in contrast to the fifth story in Hall's model. Furthermore, the plastic hinge rotations are concentrated in the lowest three stories of the OpenSees model, whereas they are distributed over a larger number of stories in Hall's model. Finally, the OpenSees model predicts a larger value for the maximum (over the building height) plastic-hinge rotation compared to Hall's model.

These discrepancies in estimating local response by the two models arise, most likely, because the subterranean part of the structure included in Hall's model allows rotation at the base of the first-story columns, which tends to distribute the plastic rotations over several stories and reduces the magnitude of plastic rotations. Results from the OpenSees model are generally consistent with those reported by Goel and Chopra [2004], who also ignored the basement and fixed first-story columns at their base. They also reported largest plastic rotations in the third story of the building (Figure C.4).

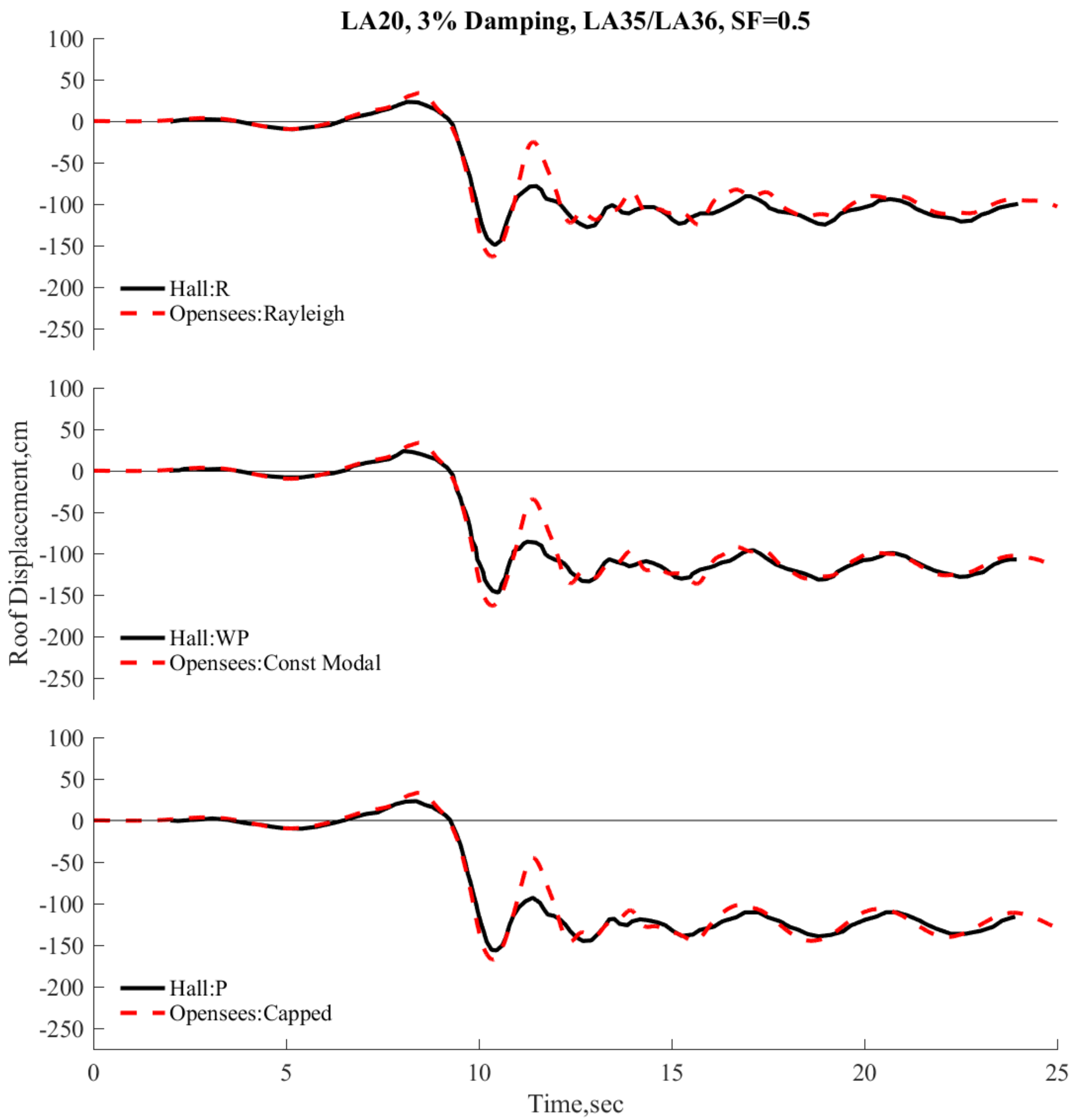

Figure C.1 Roof-displacement history for an enhanced model of the 20-story building for three damping models due to LA 35/36 ground motion.

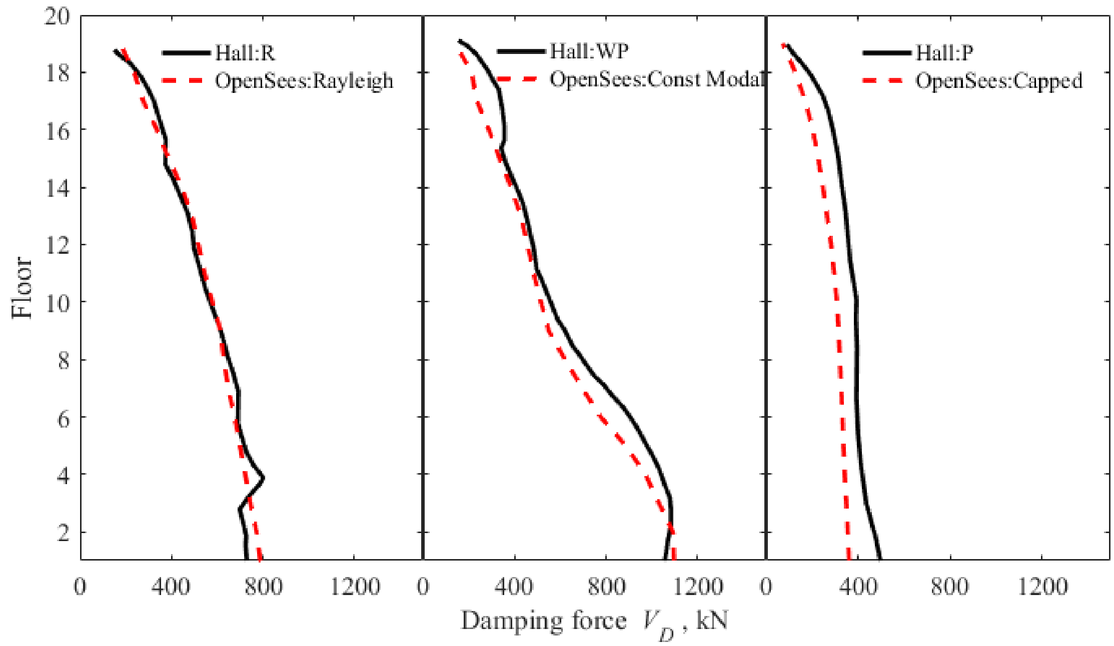

Figure C.2 **Story damping forces in an enhanced model of the 20-story building for three damping models due to LA 35/36 ground motion.**

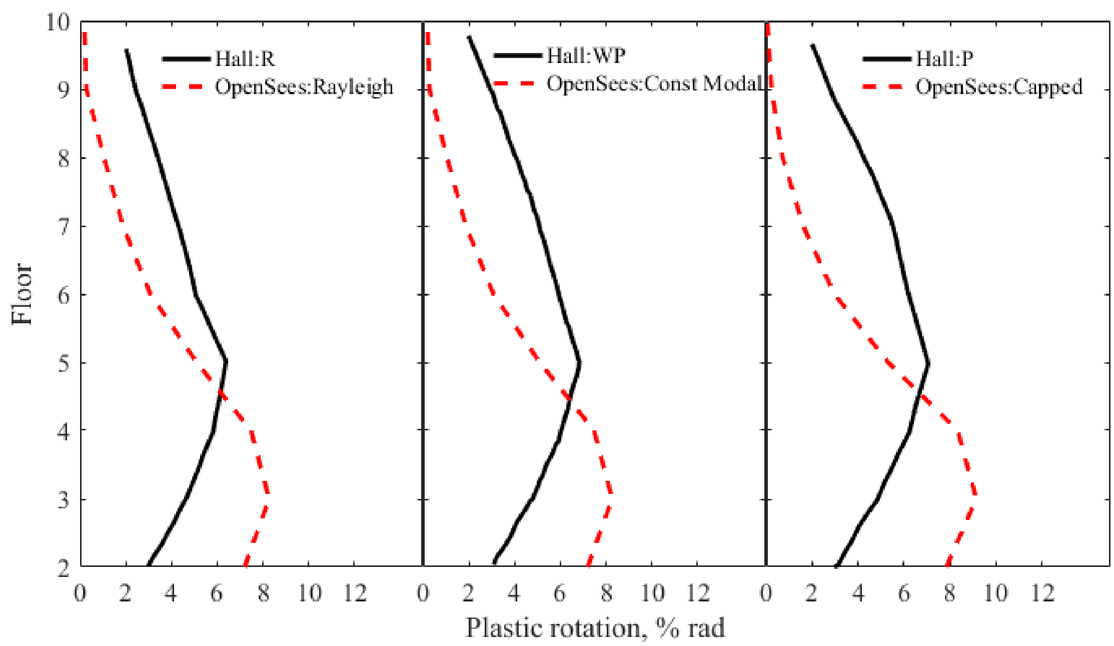

Figure C.3 **Beam plastic rotations in an enhanced model of the 20-story building for three damping models due to LA 35/36 ground motion.**

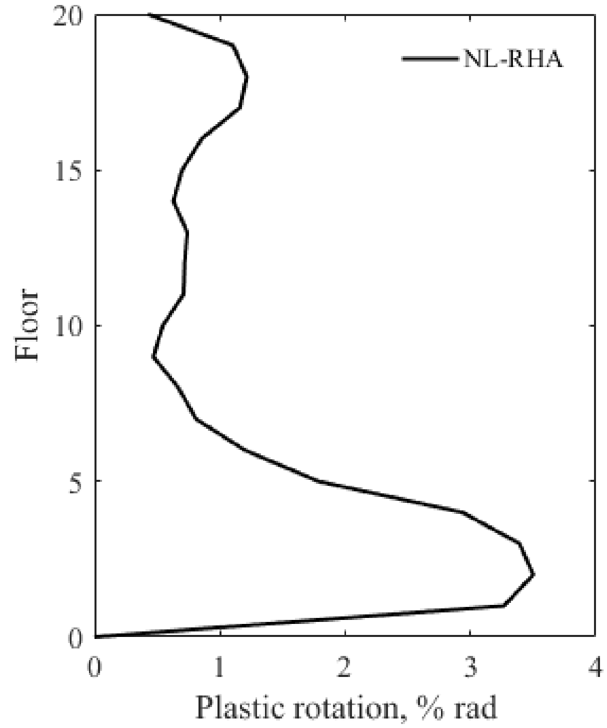

Figure C.4 Beam plastic rotations (Goel and Chopra [2004]).

References

Hall J.F. (2018). Performance of viscous damping in inelastic seismic analysis of moment-frame buildings, *Report No. EERL 2018-01*, Earthquake Engineering Research Laboratory, California Institute of Technology, Pasadena, CA.

Goel R, Chopra A.K. (2004). Evaluation of modal and FEMA pushover analyses: SAC buildings," *Earthq. Spectra*, 20(1): 225–254.

Appendix D Ground Motions

Listed in this Appendix are the selected ground-motion records and the scale factor for each record. These data are tabulated as follows:

Table D.1 Selected GM records, components, and scale factors for 2% PE in 50 years; *T = 3.81 sec.**

NGA Record Sequence Number (RSN)	Earthquake name	Station name	Component number	Scale factor	AT2 Filename
1183	1999 Chi-Chi Taiwan	CHY008	1	2.1855	RSN1183_CHICHI_CHY008-N.AT2
1188	1999 Chi-Chi Taiwan	CHY016	2	3.6098	RSN1188_CHICHI_CHY016-W.AT2
1213	1999 Chi-Chi Taiwan	CHY055	1	2.6423	RSN1213_CHICHI_CHY055-W.AT2
1237	1999 Chi-Chi Taiwan	CHY090	1	3.6167	RSN1237_CHICHI_CHY090-E.AT2
1261	1999 Chi-Chi Taiwan	HWA009	1	4.0660	RSN1261_CHICHI_HWA009-E.AT2
1436	1999 Chi-Chi Taiwan	TAP052	2	2.5945	RSN1436_CHICHI_TAP052-N.AT2
1471	1999 Chi-Chi Taiwan	TCU015	2	2.2389	RSN1471_CHICHI_TCU015-N.AT2
1490	1999 Chi-Chi Taiwan	TCU050	1	1.9079	RSN1490_CHICHI_TCU050-E.AT2
1545	1999 Chi-Chi Taiwan	TCU120	1	1.1193	RSN1545_CHICHI_TCU120-E.AT2
3747	1992 Cape Mendocino	College of the Redwoods	1	2.3645	RSN3747_CAPEMEND_CRW270.AT2
5825	2010 El Mayor-Cucapah	CERRO PRIETO GEOTHERMAL	2	0.8880	RSN5825_SIERRA.MEX_GEO090.AT2

Table D.2 Selected GM records, components, and scale factors for 2% PE in 50 years; T^* = 3.38 sec.

NGA Record Sequence Number (RSN)	Earthquake name	Station name	Component number	Scale factor	AT2 Filename
185	1979 Imperial Valley-06	Holtville Post Office	1	1.3112	RSN185_IMPVALL.H_H-HVP225.AT2
838	1992 Landers	Barstow	2	2.6455	RSN838_LANDERS_BRS090.AT2
1193	1999 Chi-Chi Taiwan	CHY024	1	1.3329	RSN1193_CHICHI_CHY024-E.AT2
1213	1999 Chi-Chi Taiwan	CHY055	1	3.4161	RSN1213_CHICHI_CHY055-W.AT2
1223	1999 Chi-Chi Taiwan	CHY067	2	4.9494	RSN1223_CHICHI_CHY067-W.AT2
1430	1999 Chi-Chi Taiwan	TAP042	2	3.5776	RSN1430_CHICHI_TAP042-N.AT2
1436	1999 Chi-Chi Taiwan	TAP052	2	2.6670	RSN1436_CHICHI_TAP052-N.AT2
1541	1999 Chi-Chi Taiwan	TCU116	1	1.4691	RSN1541_CHICHI_TCU116-E.AT2
1545	1999 Chi-Chi Taiwan	TCU120	1	1.3983	RSN1545_CHICHI_TCU120-E.AT2
1551	1999 Chi-Chi Taiwan	TCU138	2	1.4237	RSN1551_CHICHI_TCU138-W.AT2
6953	2010 Darfield New Zealand	Pages Road Pumping Station	2	1.3658	RSN6953_DARFIELD_PRPCS.AT2

Table D.3 Selected GM records, components, and scale factors for 1% PE in 50 years; T^* = 3.38 sec.

NGA Record Sequence Number (RSN)	Earthquake name	Station name	Component number	Scale factor	AT2 Filename
185	1979 Imperial Valley-06	Holtville Post Office	1	1.6582	RSN185_IMPVALL.H_H-HVP225.AT2
736	1989 Loma Prieta	APEEL 9 - Crystal Springs Res	2	3.6838	RSN736_LOMAP_A09227.AT2
838	1992 Landers	Barstow	2	3.3457	RSN838_LANDERS_BRS090.AT2
1193	1999 Chi-Chi Taiwan	CHY024	1	1.6857	RSN1193_CHICHI_CHY024-E.AT2
1277	1999 Chi-Chi Taiwan	HWA028	2	4.1181	RSN1277_CHICHI_HWA028-N.AT2
1430	1999 Chi-Chi Taiwan	TAP042	2	4.5244	RSN1430_CHICHI_TAP042-N.AT2
1436	1999 Chi-Chi Taiwan	TAP052	2	3.3729	RSN1436_CHICHI_TAP052-N.AT2
1541	1999 Chi-Chi Taiwan	TCU116	1	1.8579	RSN1541_CHICHI_TCU116-E.AT2
1545	1999 Chi-Chi Taiwan	TCU120	1	1.7683	RSN1545_CHICHI_TCU120-E.AT2
2655	1999 Chi-Chi Taiwan-03	TCU122	2	2.3702	RSN2655_CHICHI.03_TCU122E.AT2
6953	2010 Darfield New Zealand	Pages Road Pumping Station	2	1.7273	RSN6953_DARFIELD_PRPCS.AT2

Appendix E Computation of Story Shears and Story Damping Forces

A procedure to compute the horizontal shear forces and horizontal damping forces in all stories of the building are presented in this Appendix.

Consider a planar frame subjected to horizontal ground acceleration $\ddot{u}_g(t)$. Numerical solution of the equations governing the inelastic response of the frame provides the displacements $\mathbf{u}$, velocities $\dot{\mathbf{u}}$, and acceleration $\ddot{\mathbf{u}}$ at all nodes; these are motions relative to the ground.

The horizontal shear force V_{Si} and horizontal damping force V_{Di} at a section cut at the bottom of the ith story and the inertia forces associated with masses lumped at the floor levels above that section are in equilibrium, i.e.,

$$\sum_{j=i}^{N} f_{Ij} + V_{Di} + V_{Si} = 0 \tag{E.1}$$

The inertia force f_{Ij} associated with masses lumped at the jth floor is

$$f_{Ij} = \sum_{k} m_{kj}\ddot{u}_{kj}^{t} \tag{E.2}$$

where the summation is over all the nodes on the jth floor, m_{kj} is the mass at the kth node, and $\ddot{u}_{kj}^{t}$ is the total horizontal acceleration of that node. This total acceleration is equal to the acceleration $\ddot{u}_{kj}$ of the node relative to the ground plus the ground acceleration.

The horizontal shear force V_{Si} at the bottom of the ith story is the sum of the horizontal shears in the k columns in that story,

$$V_{Si} = \sum_{k} V_{Sik} \tag{E.3}$$

The horizontal damping force V_{Di} at the bottom of the ith story is given by rewriting Equation (E.1)

$$V_{Di} = -V_{Si} - \sum_{j=i}^{N} f_{Ij} \tag{E.4}$$

In OpenSees, V_{Si} are computed by recording the element forces that enter into Equation (E.3) and f_{Ij} by recording the nodal accelerations plus ground acceleration that enter into Equation (E.2); with these two terms known, V_{Di} is computed from Equation (E.4).

Appendix F Complete Set of Results

Table F.1 Response of a simple model of the 20-story frame to 11 GMs corresponding to 2% PE in 50 years; 2% damping.

GM#	Story drift, %			Plastic rotations, % radian			V_D/V_S at base,%		
	Rayleigh	Constant modal	Capped	Rayleigh	Constant modal	Capped	Rayleigh	Constant modal	Capped
1183	2.11	1.94	2.00	1.74	1.57	1.63	6.6	6.4	4.8
1188	4.72	4.98	6.11	4.36	4.63	5.85	6.7	6.9	4.7
1213	1.66	1.64	1.75	1.27	1.23	1.35	6.2	6.8	4.9
1237	2.42	2.51	2.81	2.00	2.10	2.39	7.0	7.2	4.3
1261	2.19	2.22	2.09	1.79	1.83	1.66	6.0	6.6	3.9
1436	1.60	1.50	1.70	1.23	1.13	1.30	6.8	6.7	4.7
1471	1.66	1.71	1.64	1.27	1.29	1.24	4.8	5.3	4.0
1490	2.44	2.45	2.57	2.04	2.04	2.16	6.0	6.6	4.1
1545	2.90	2.90	3.21	2.48	2.50	2.82	7.4	7.5	4.3
3747	2.10	2.09	2.36	1.72	1.71	1.99	7.1	7.2	4.3
5825	1.53	1.56	1.61	1.15	1.15	1.20	5.0	5.2	4.3

Response of a simple model of the 20-story frame to 11 GMs corresponding to 2% PE in 50 years; 2% damping.

Figures F.1–F.11

Results for 11 GMs listed in Table F.1 are presented in Figures F.1–F.11. Each figure is organized as follows:

Top row	Roof displacement history
Middle row	Peak values of floor displacement, story drifts, and plastic rotations
Bottom row	Peak story shears, V_S, peak story damping forces, V_D, and ratio V_D / V_S

Figure F.1 GM1183

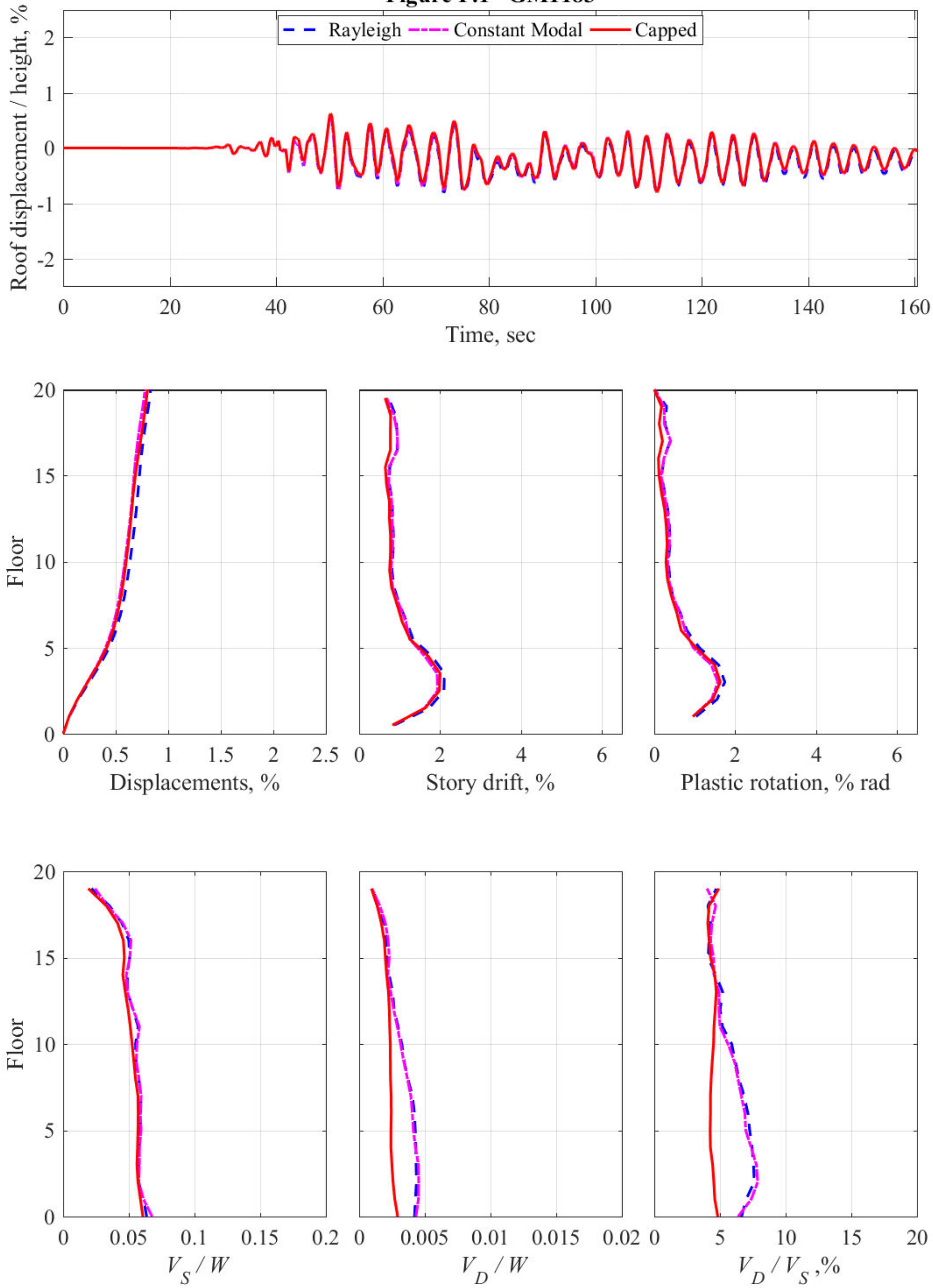

Figure F.2 GM1188

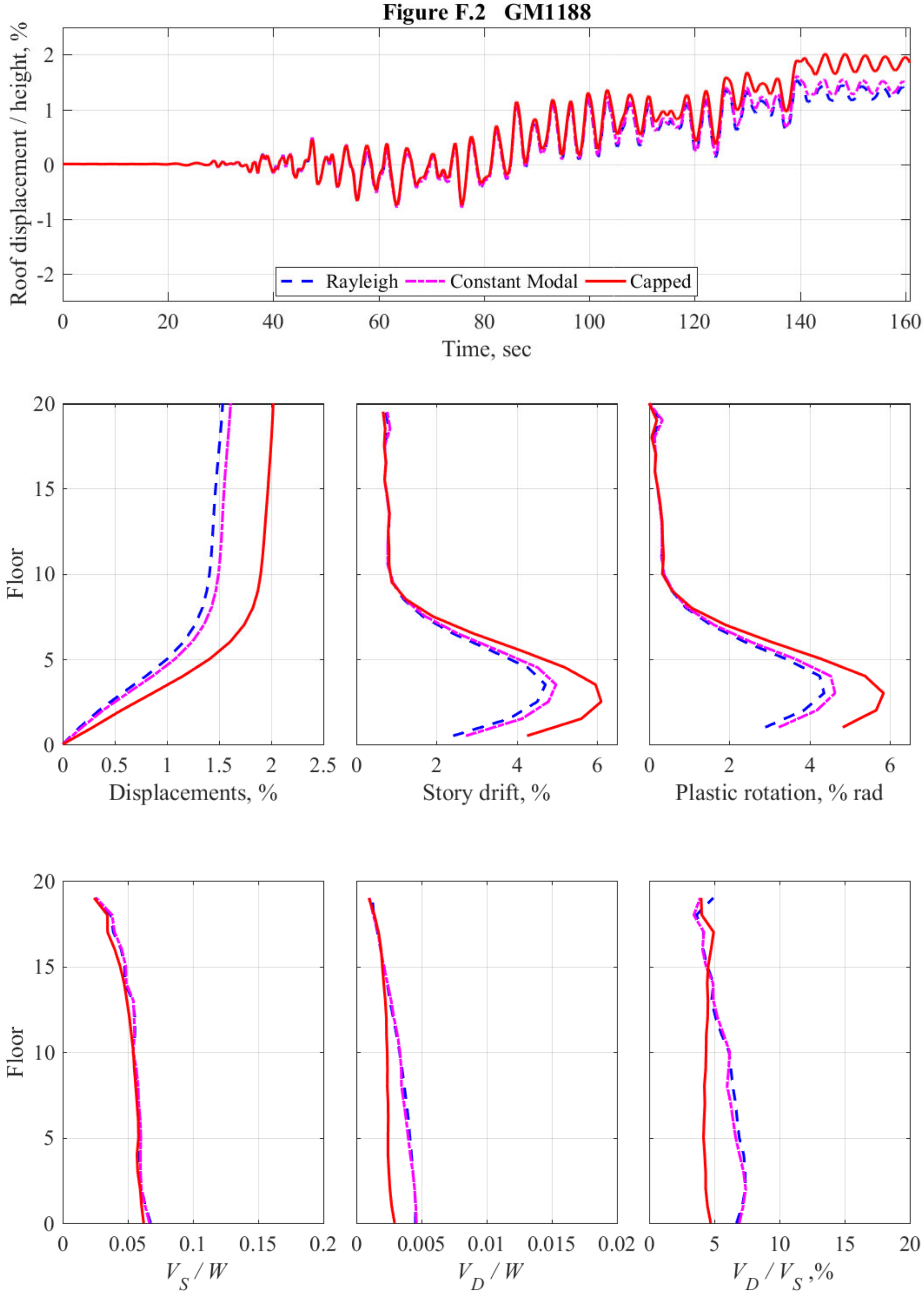

Figure F.3 GM1213

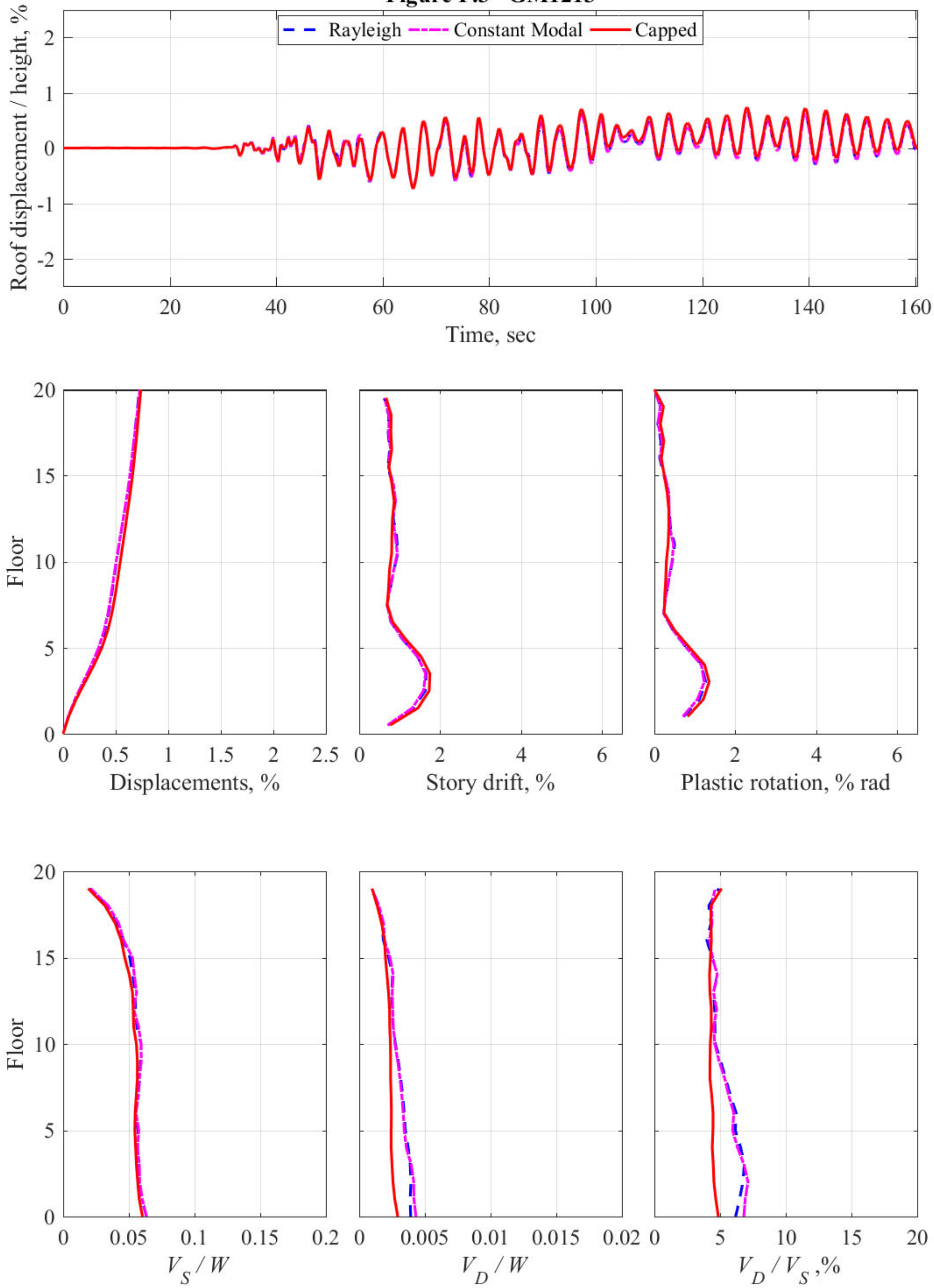

Figure F.4 GM1237

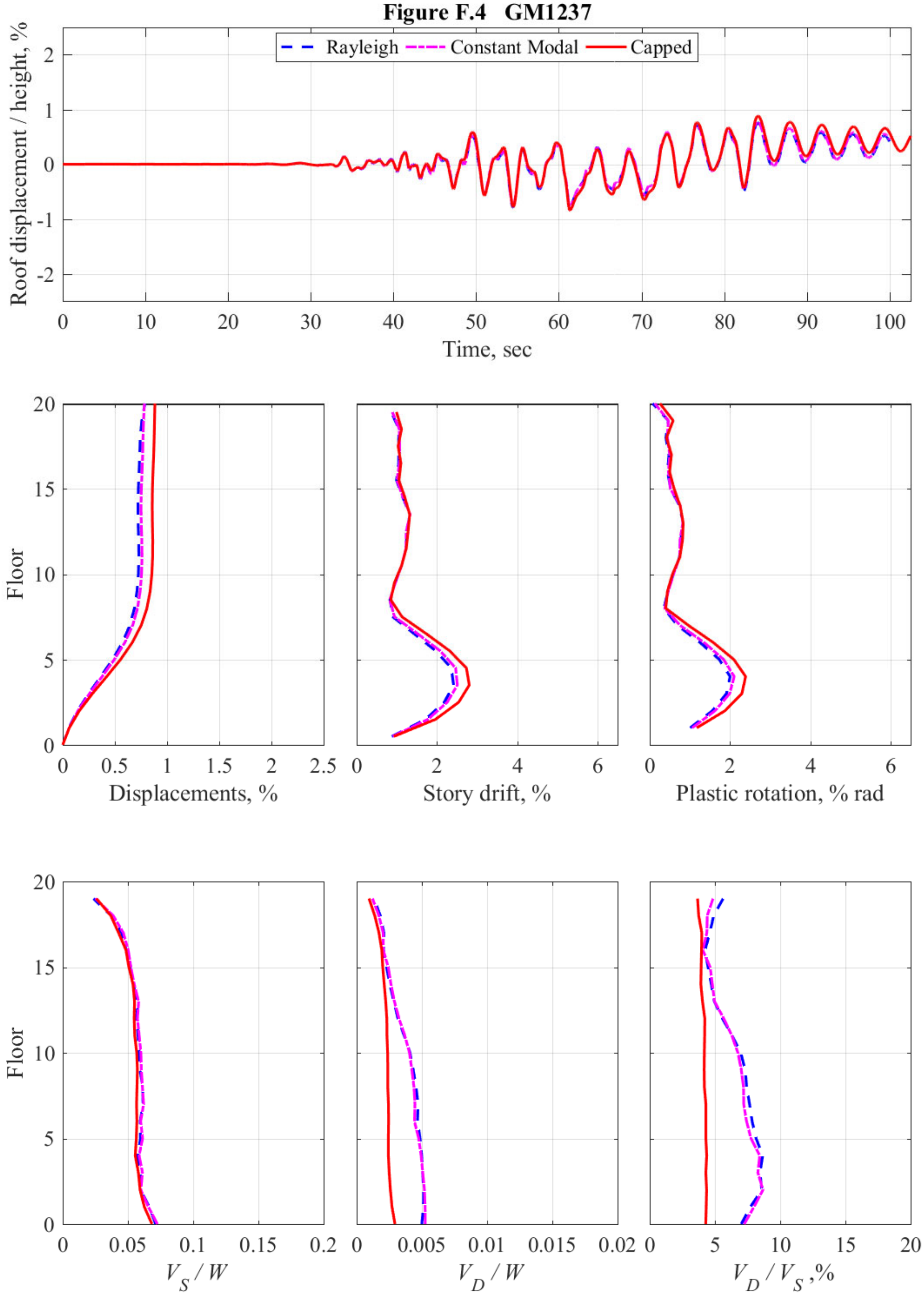

Figure F.5 GM1261

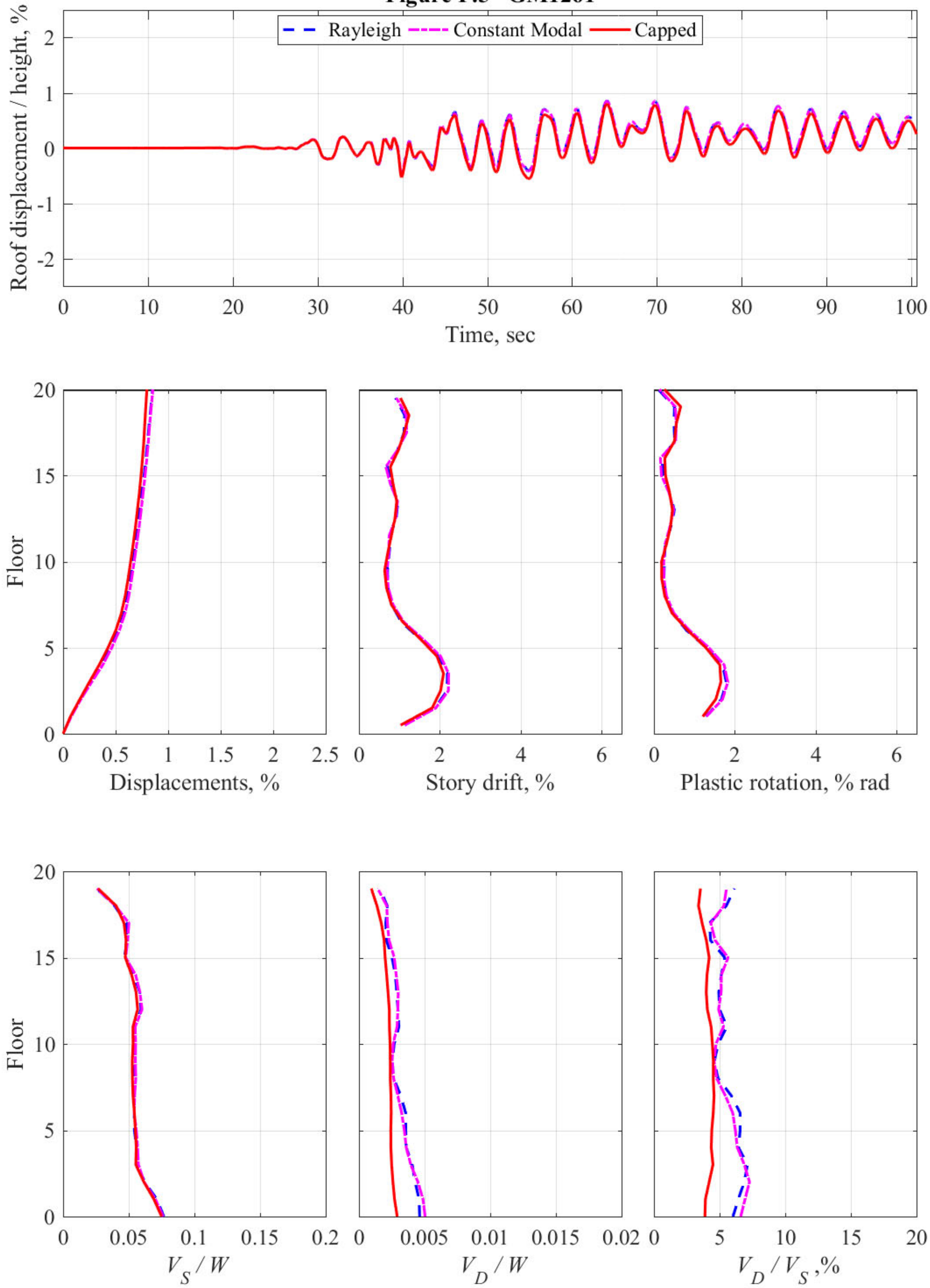

Figure F.6 GM1436

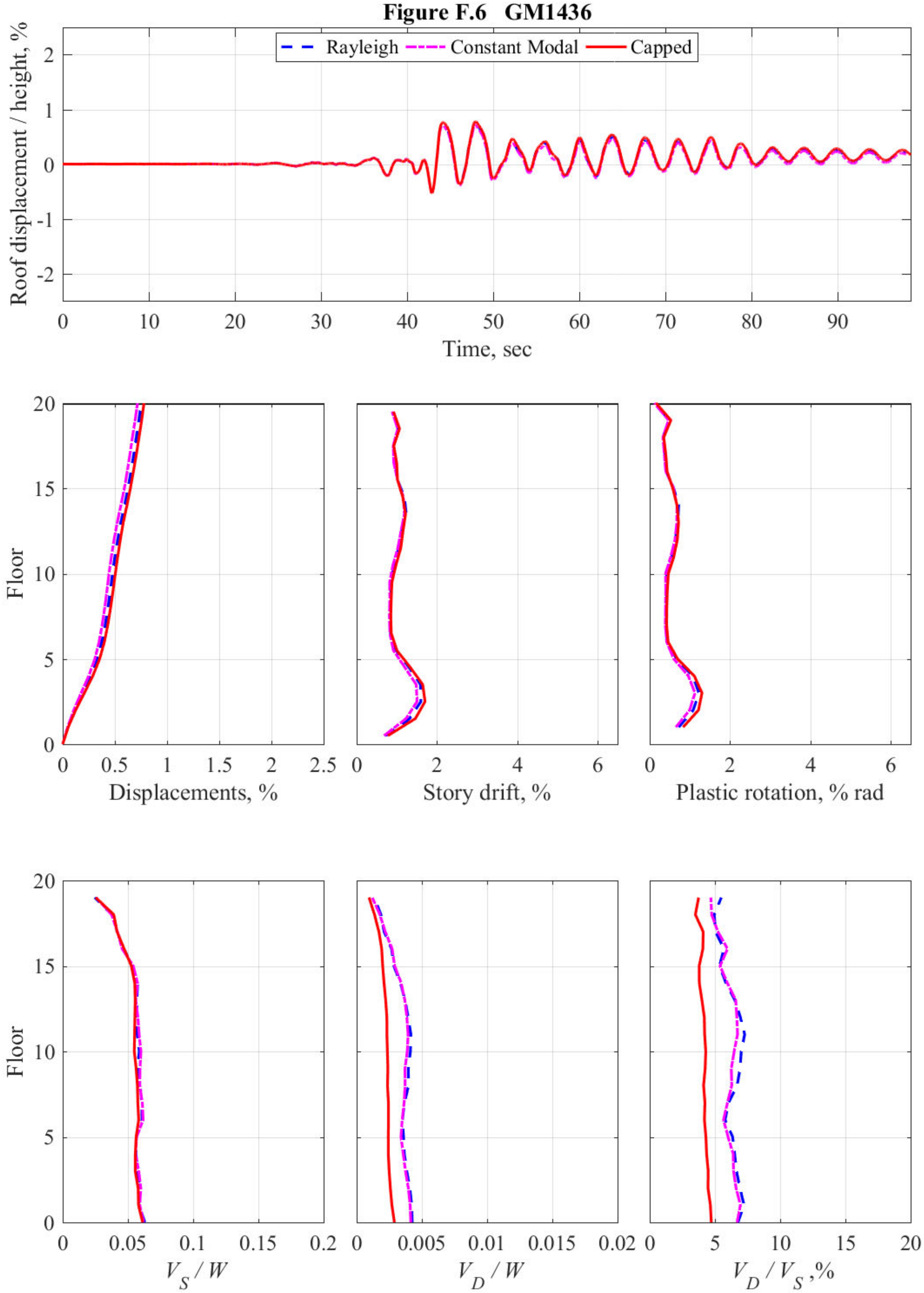

Figure F.7 GM1471

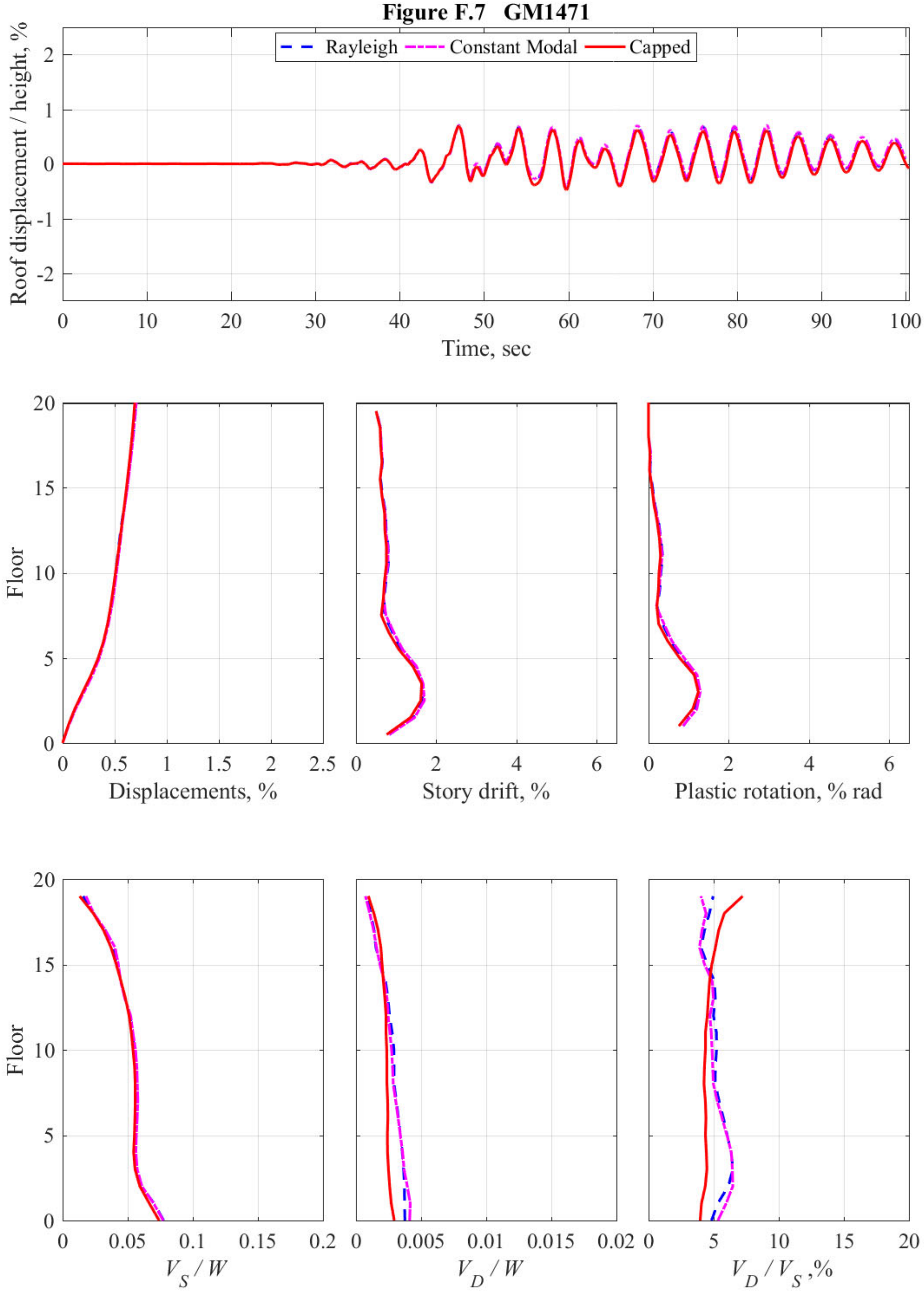

Figure F.8 GM1490

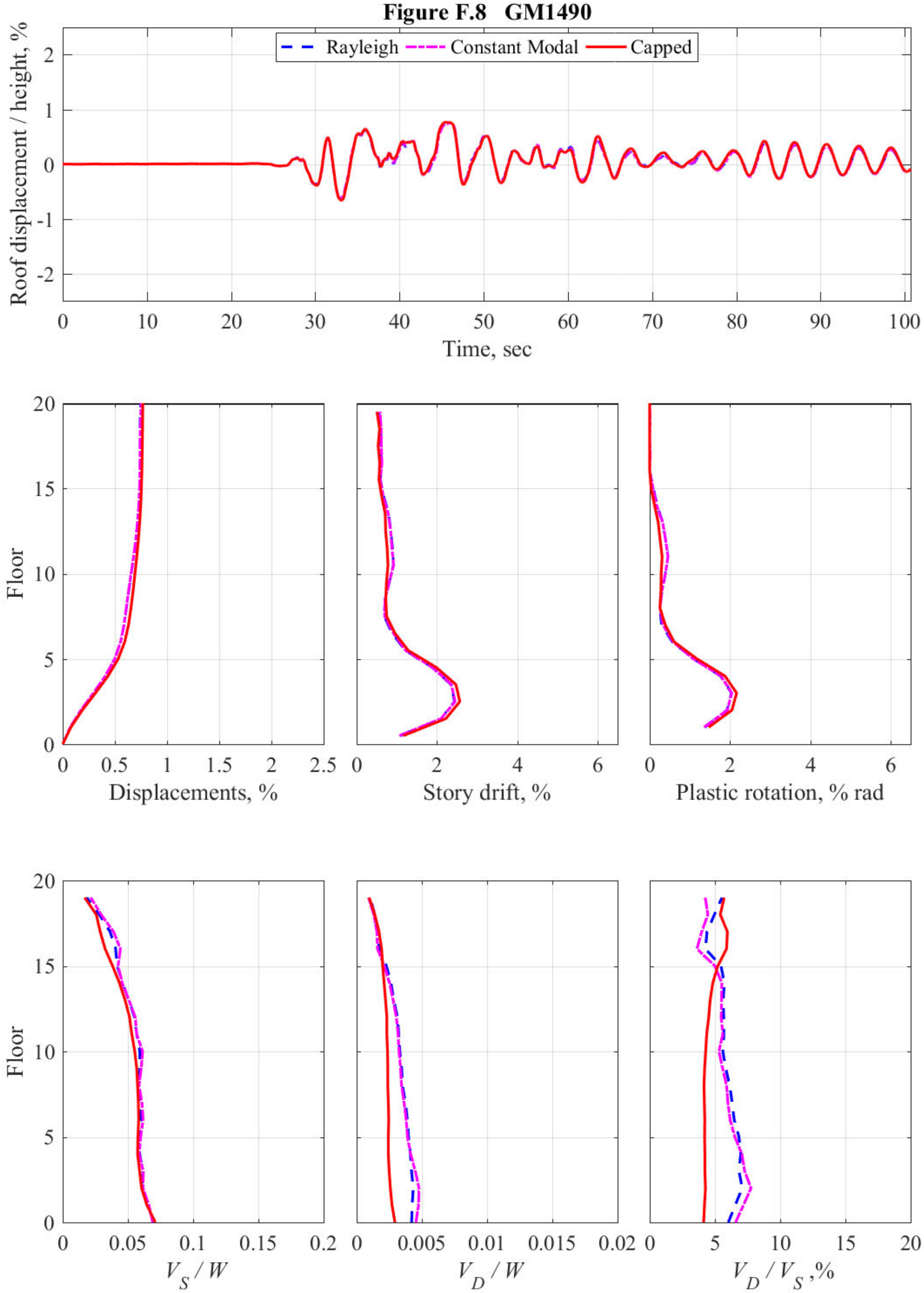

Figure F.9 GM1545

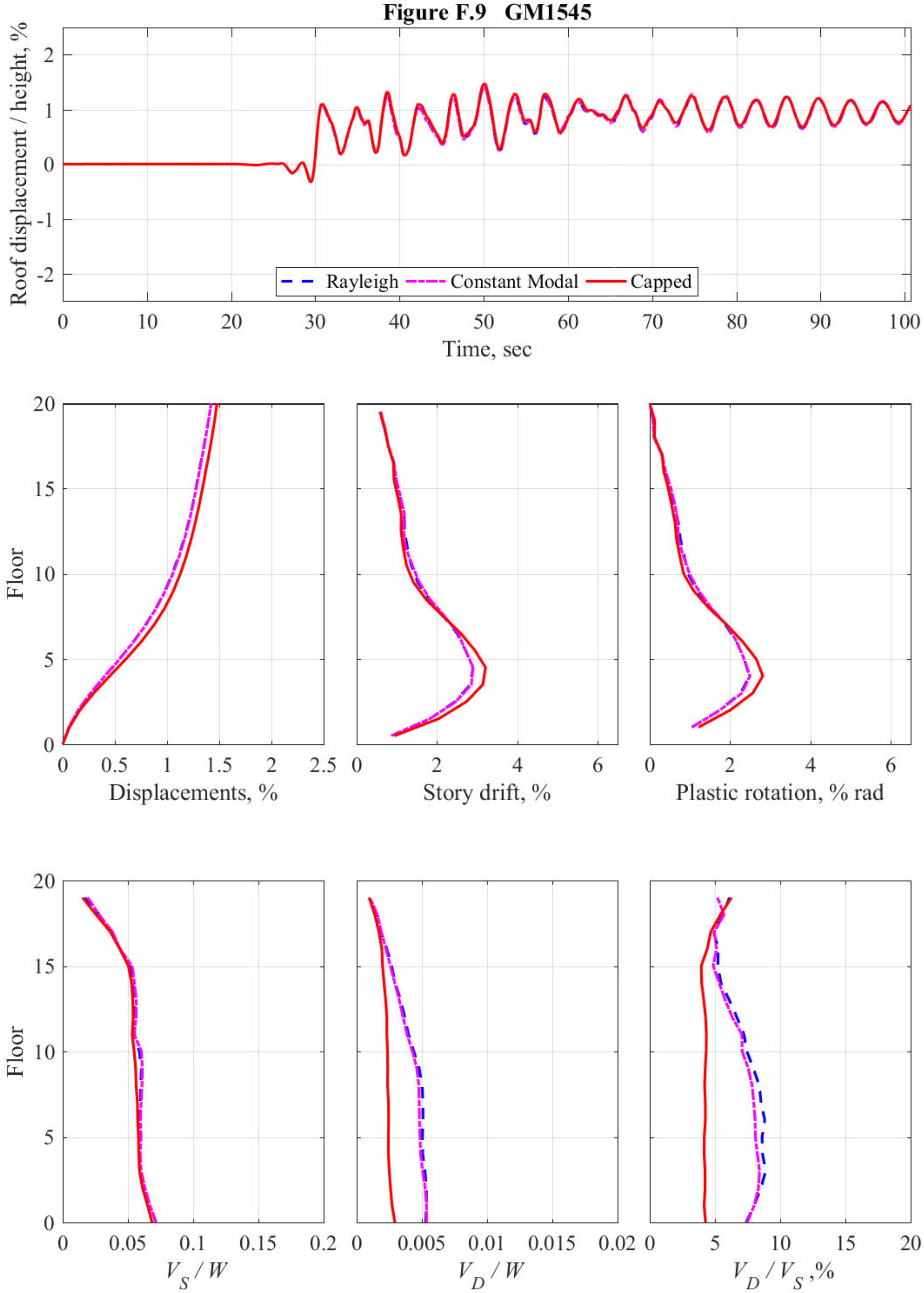

Figure F.10 GM3747

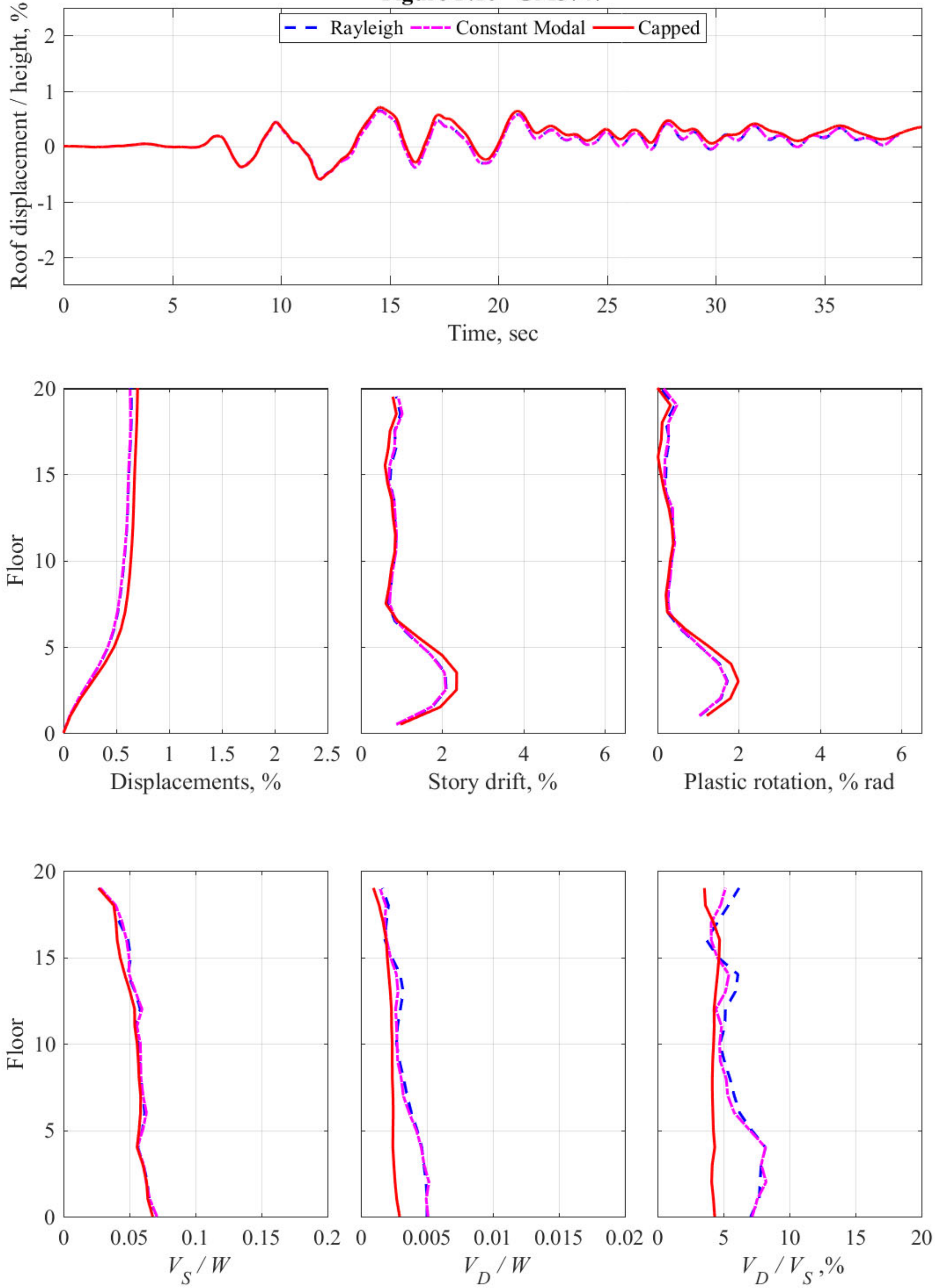

Figure F.11 GM5825

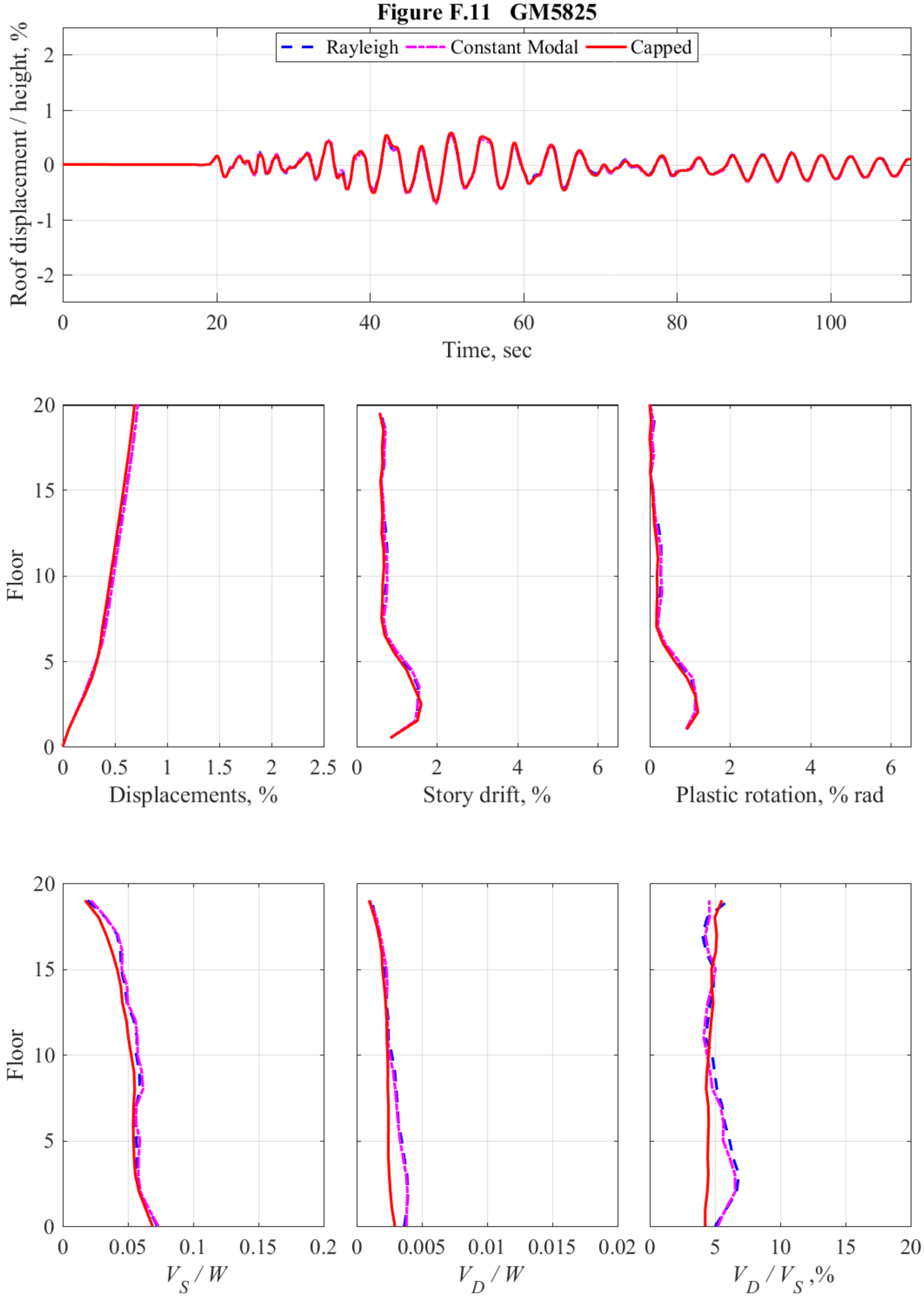

Table F.2 Response of a simple model of the 20-story frame to 11 GMs corresponding to 2% PE in 50 years; 5% damping.

GM#	Story drift, %			Plastic rotations, % radian			V_D/V_S at base, %		
	Rayleigh	Constant modal	Capped	Rayleigh	Constant modal	Capped	Rayleigh	Constant modal	Capped
1183	1.91	1.83	2.14	1.53	1.45	1.75	17.1	17.1	11.9
1188	3.88	4.22	4.44	3.50	3.85	4.02	16.0	16.3	12.0
1213	1.54	1.51	1.38	1.15	1.13	0.99	15.5	16.4	11.9
1237	2.34	2.42	2.27	1.90	2.00	1.81	18.0	19.4	11.2
1261	1.76	1.78	1.72	1.35	1.38	1.31	14.2	15.8	10.6
1436	1.45	1.37	1.34	1.02	0.94	0.91	16.6	16.8	11.9
1471	1.39	1.42	1.36	0.99	1.03	0.96	11.9	12.7	10.1
1490	2.40	2.42	2.61	2.00	2.01	2.23	15.6	17.5	10.7
1545	2.33	2.42	2.69	1.94	2.03	2.30	18.5	19.1	10.8
3747	2.12	2.10	2.39	1.73	1.72	2.02	16.1	17.3	10.5
5825	1.35	1.32	1.24	0.94	0.91	0.84	14.3	15.3	11.2

Response of a simple model of the 20-story frame to 11 GMs corresponding to 2% PE in 50 years; 5% damping

Figures F.12–F.22

Results for 11 GMs listed in Table F.2 are presented in Figures F.12–F.22. Each figure is organized as follows:

Top row	Roof displacement history
Middle row	Peak values of floor displacement, story drifts, and plastic rotations
Bottom row	Peak story shears, V_S, peak story damping forces, V_D, and ratio V_D / V_S

Figure F.12 GM1183

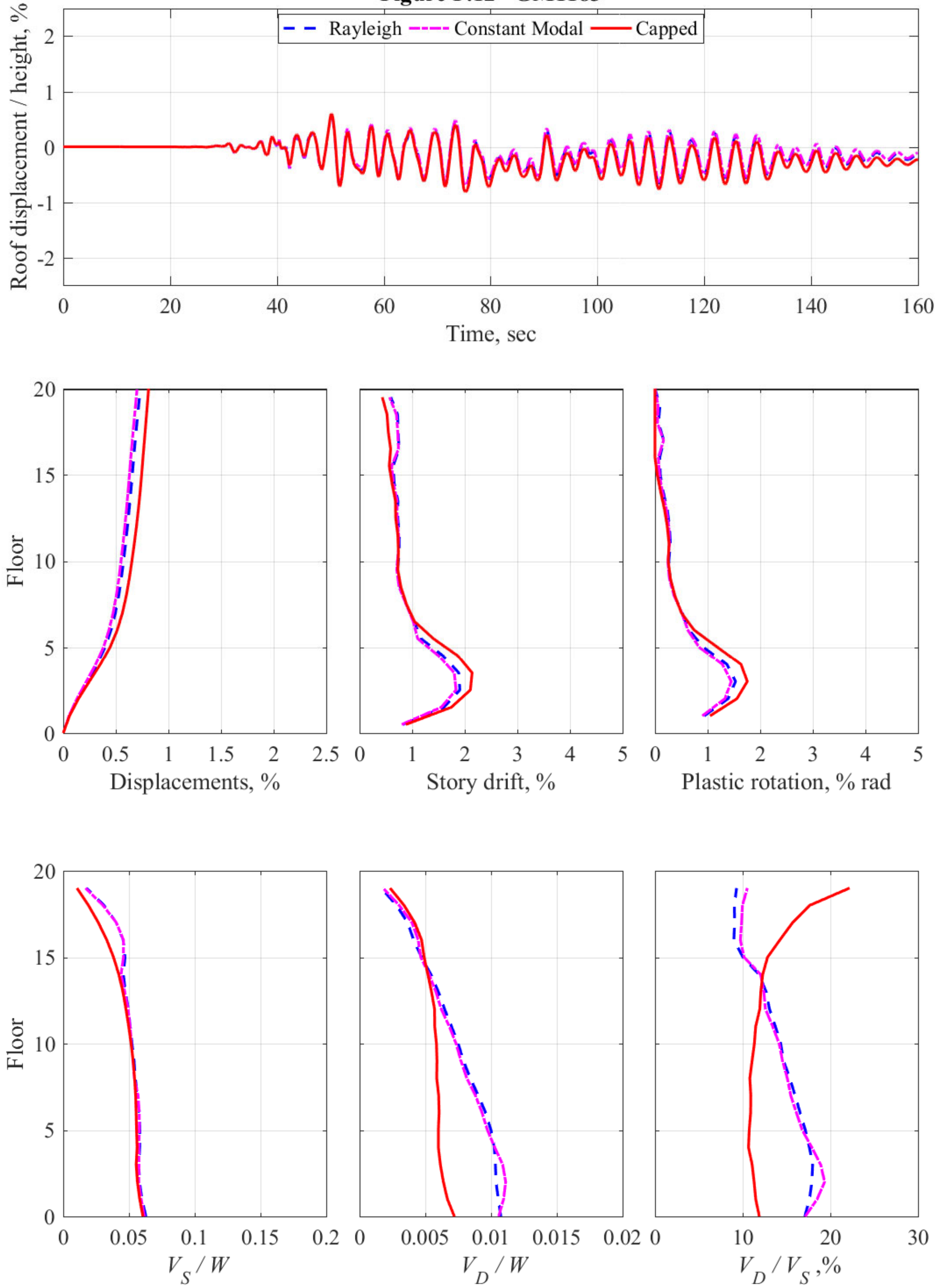

Figure F.13 GM1188

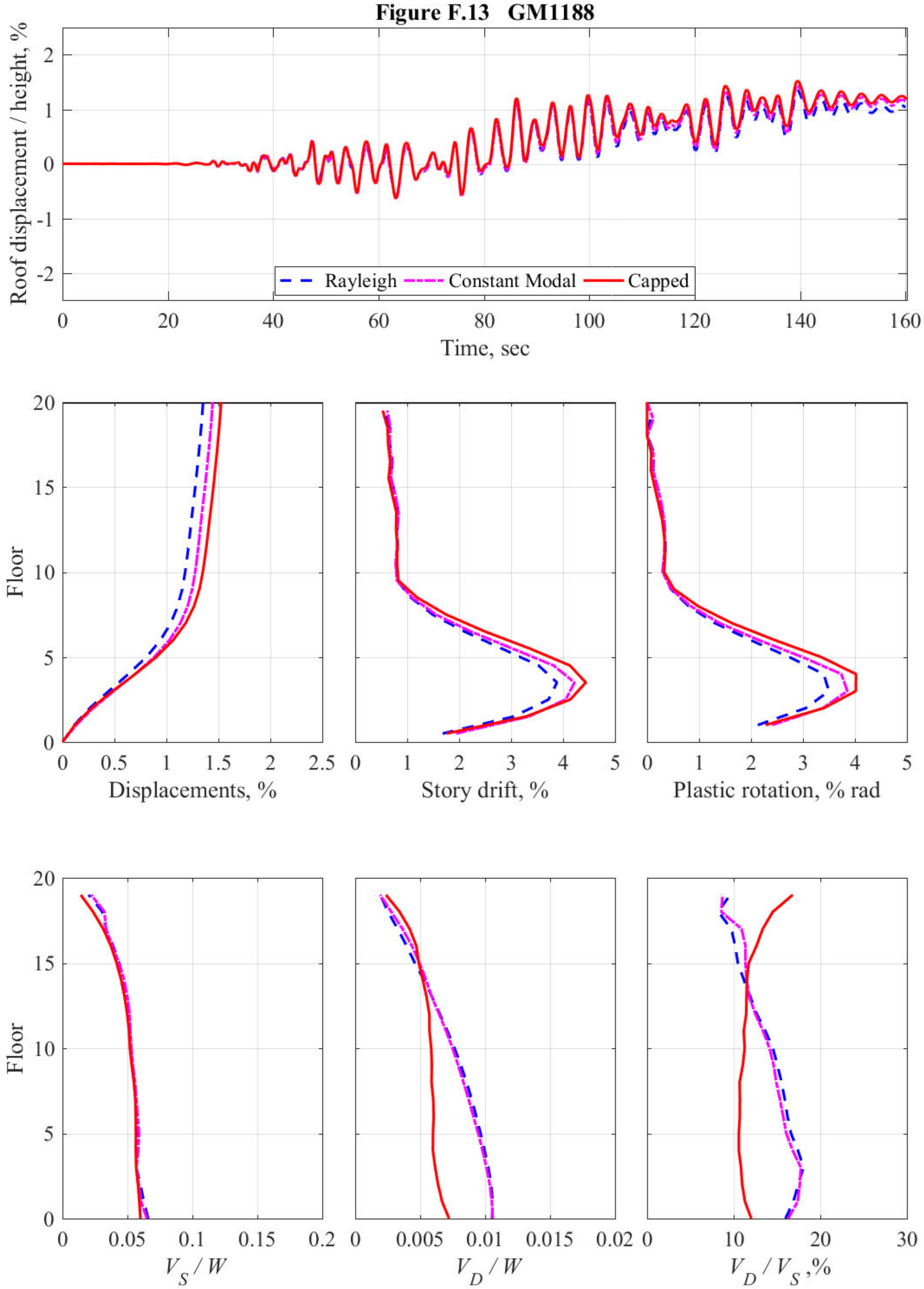

Figure F.14 GM1213

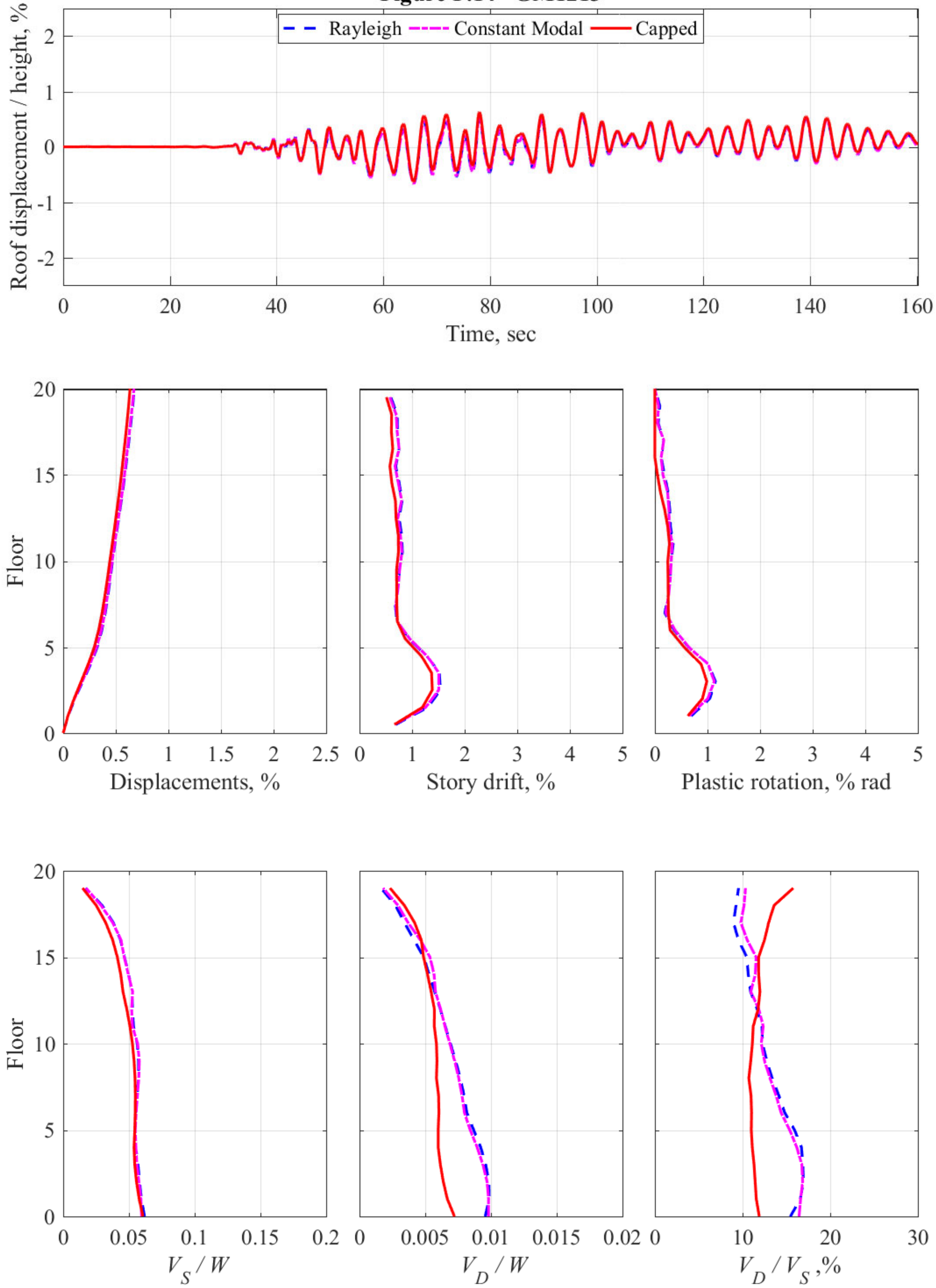

Figure F.15 GM1237

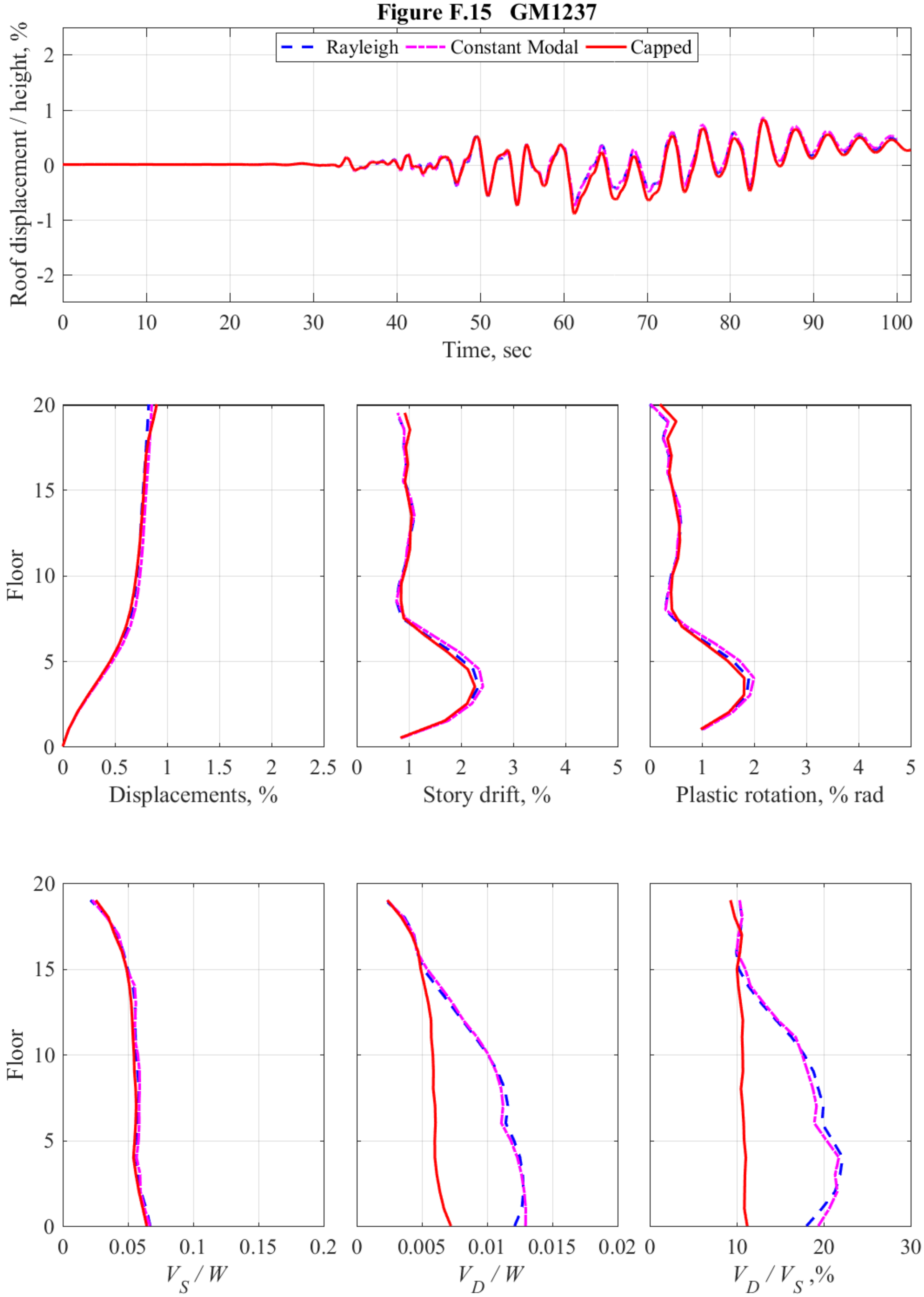

Figure F.16 GM1261

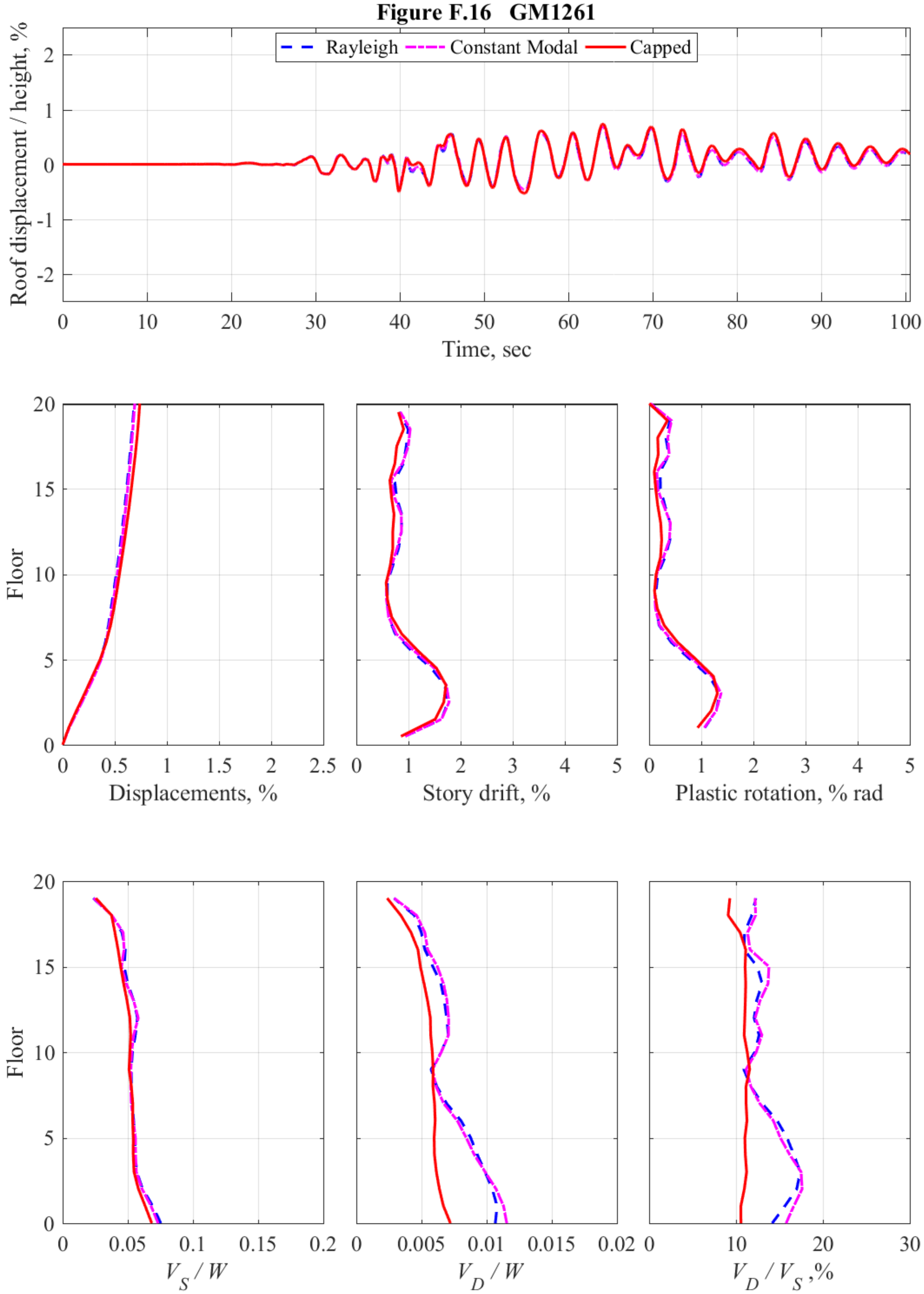

Figure F.17 GM1436

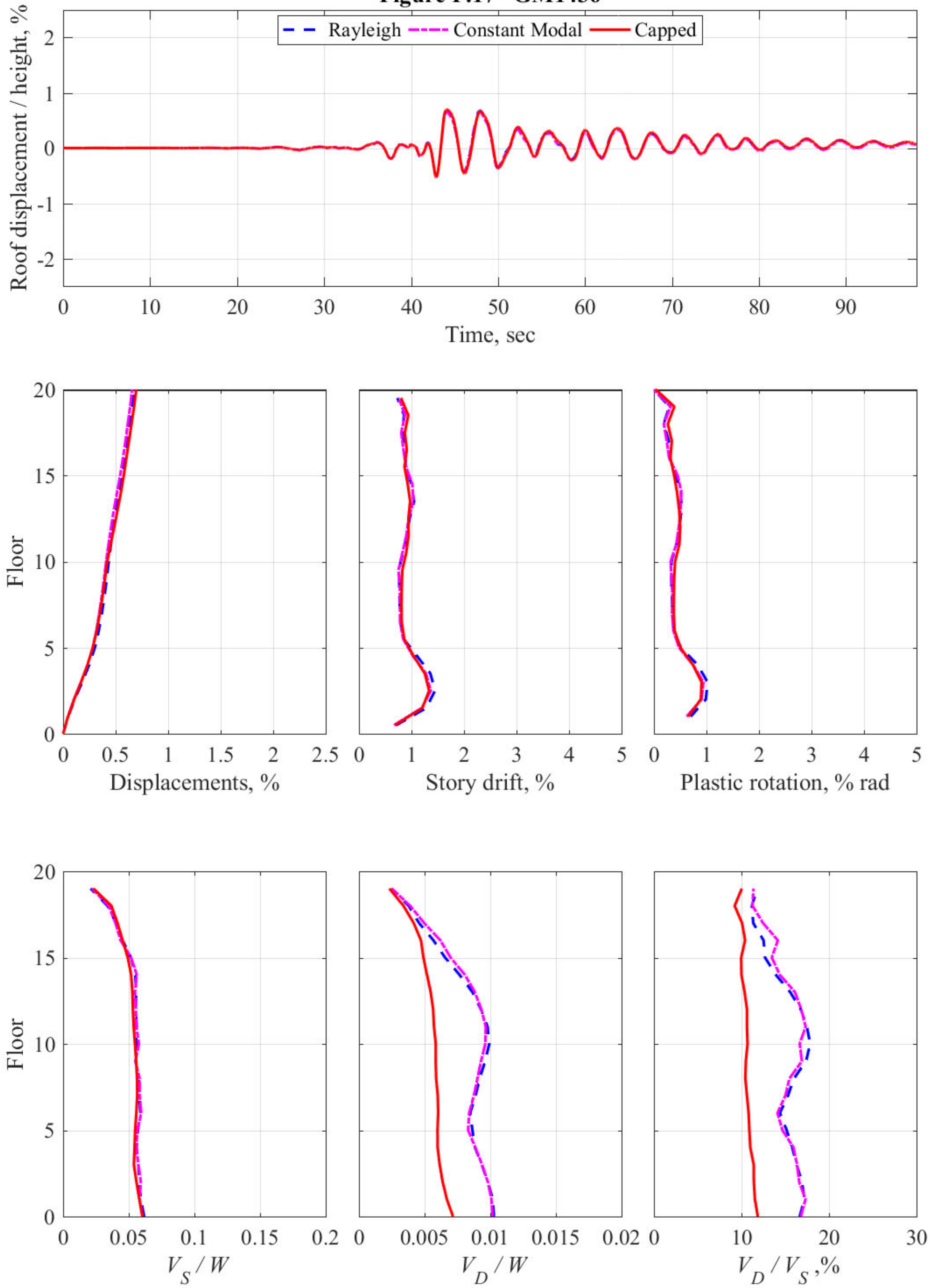

Figure F.18   GM1471

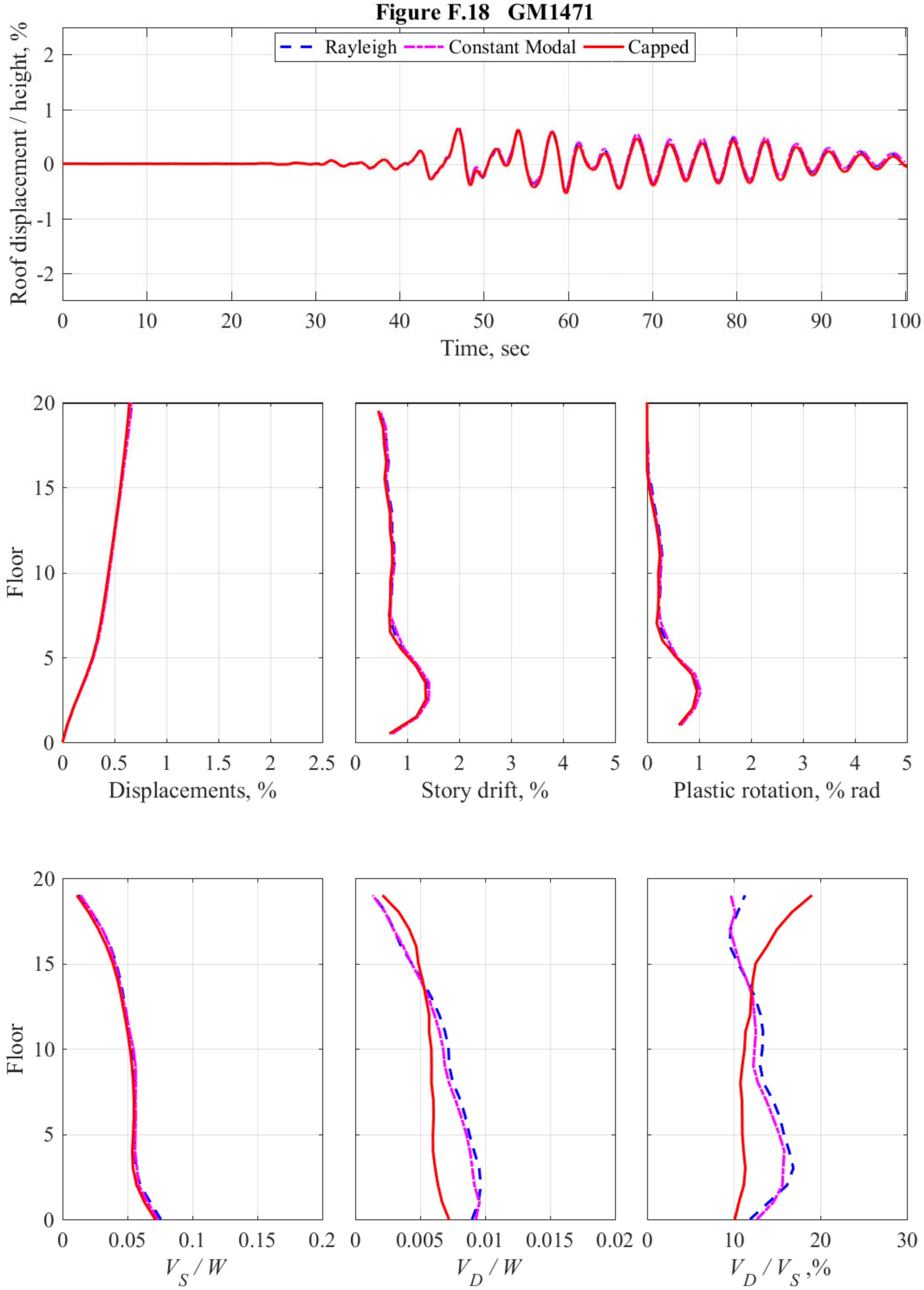

Note: the V_D/V_S ratio is approximately 10%, which is equal to 2ζ according to the definition of capped damping, in the lower ten stories. This ratio is significantly larger in stories 15–20 because these stories did not yield (as evidenced by zero plastic hinge rotation), and the story shears were lower than story strengths.

Figure F.19 GM1490

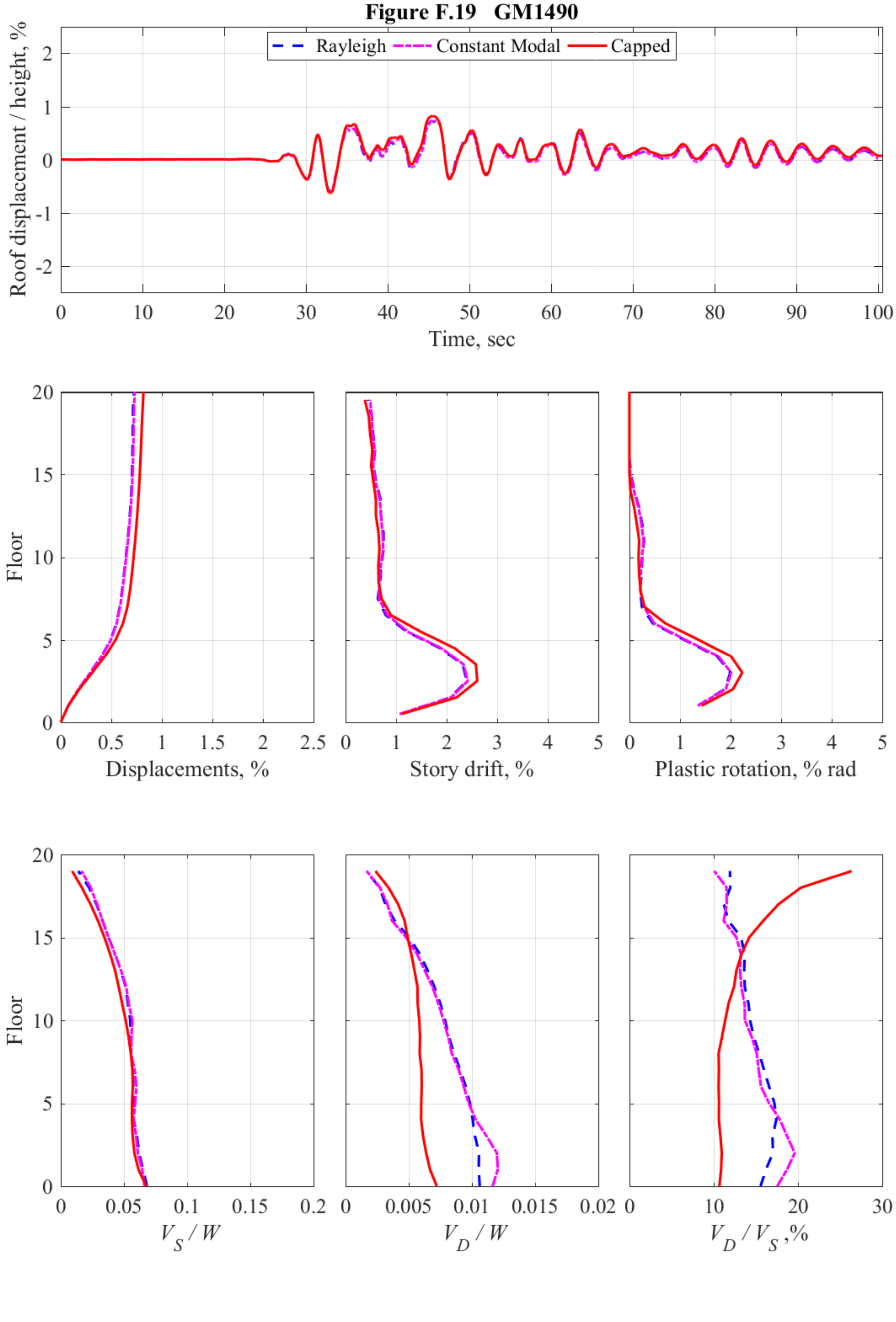

Figure F.20 GM1545

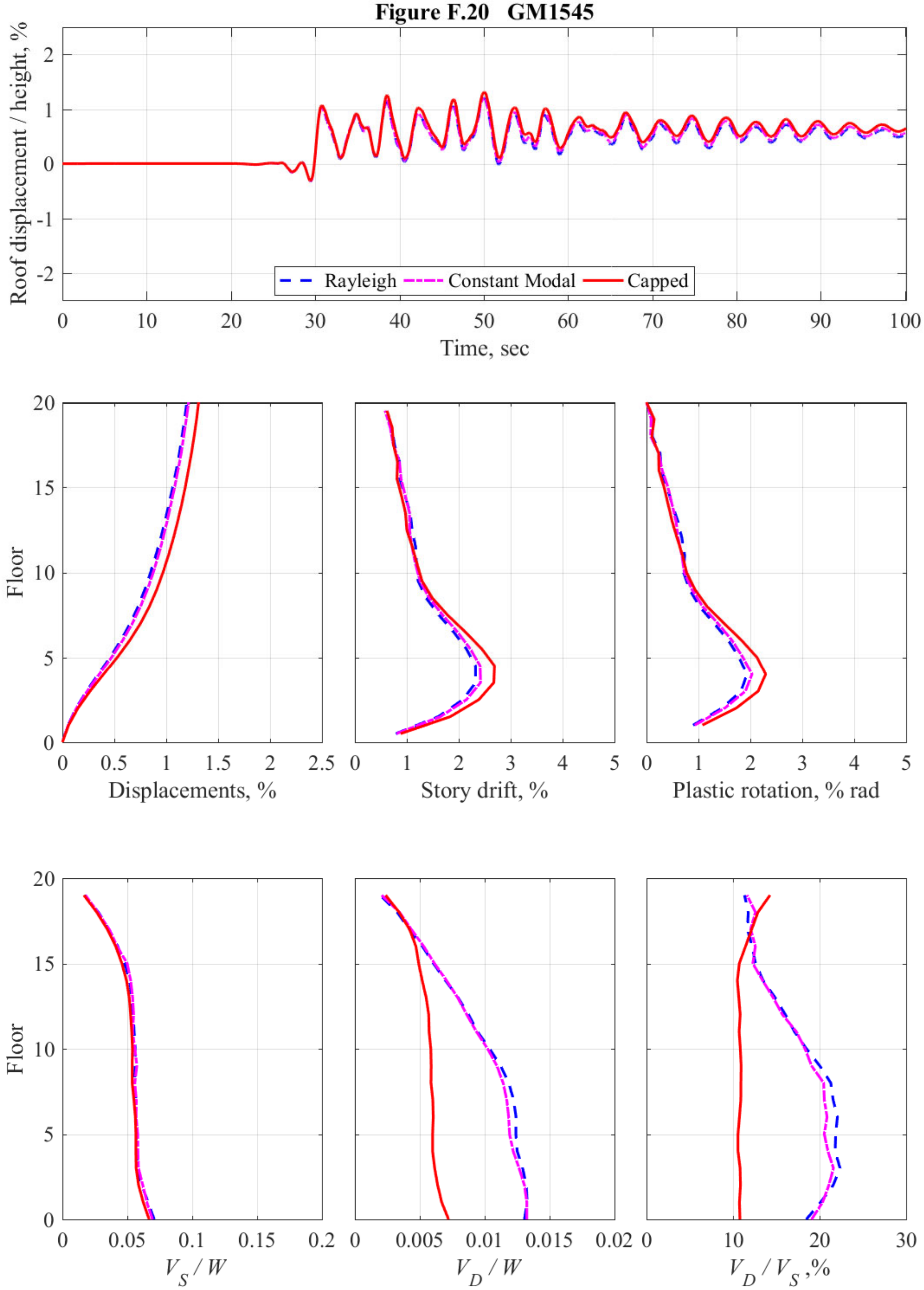

Figure F.21 GM3747

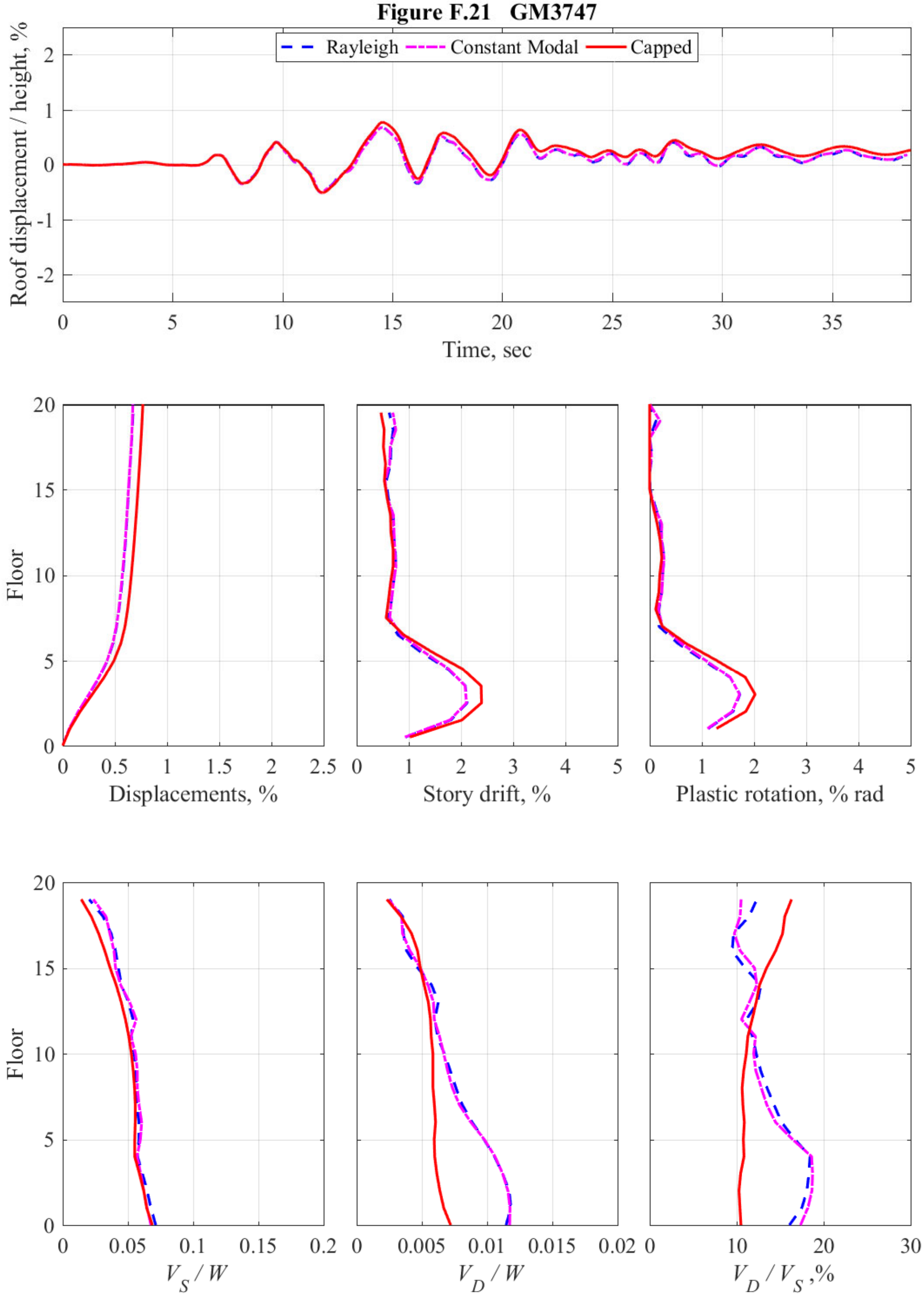

Figure F.22 GM5825

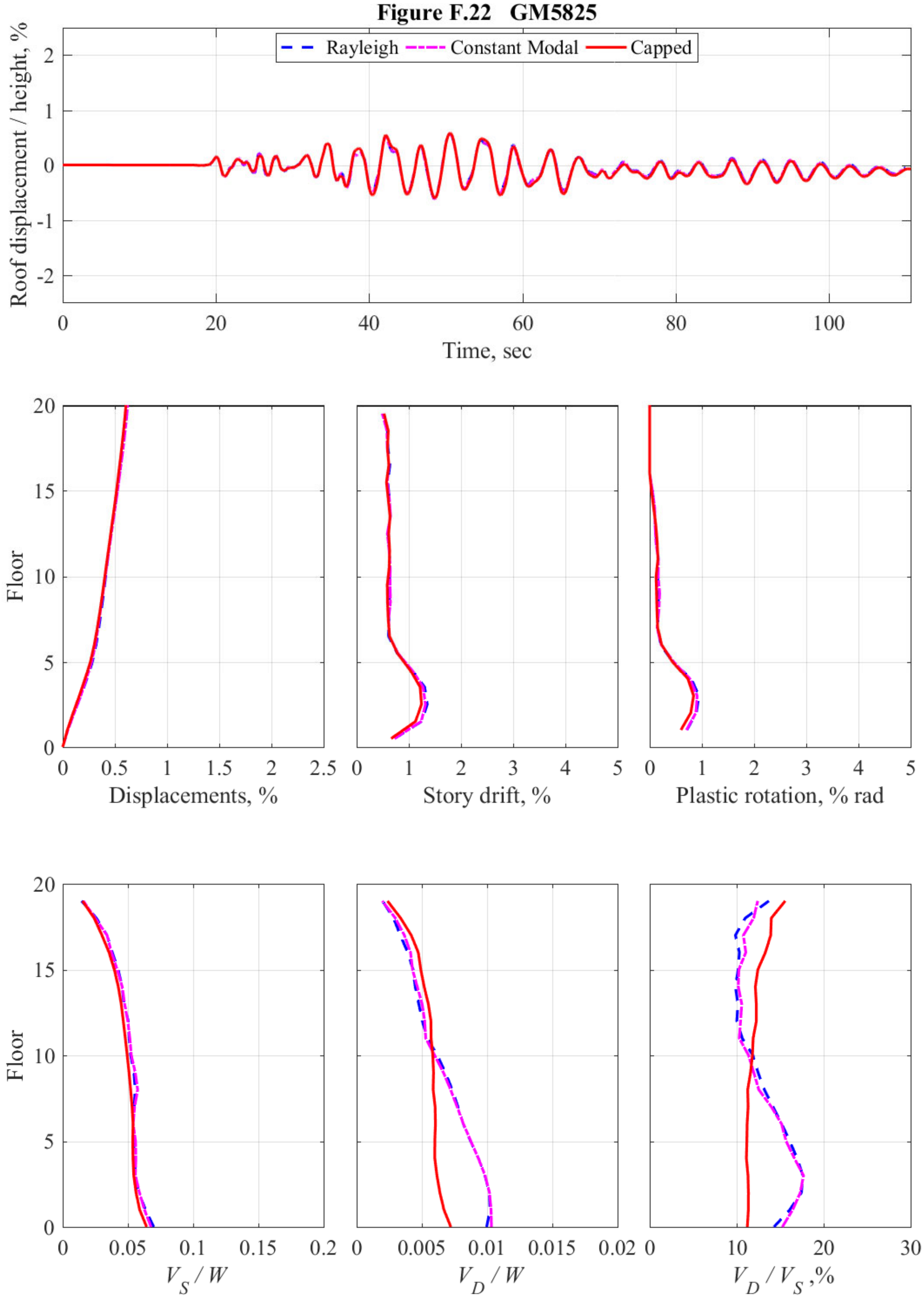

Table F.3 Response of an enhanced model of the 20-story building to 11 GMs corresponding to 2% PE in 50 years.

GM#	Story drift, %			Plastic rotations, % radian			V_D/V_S at base, %		
	Rayleigh	Constant modal	Capped	Rayleigh	Constant modal	Capped	Rayleigh	Constant modal	Capped
185	2.05	2.13	2.26	1.81	1.91	2.10	9.5	9.7	5.9
838	1.39	1.41	1.37	1.02	1.05	0.99	7.4	7.3	6.1
1193	2.10	2.10	2.18	1.92	1.92	2.04	8.3	8.6	5.8
1213	1.68	1.68	1.73	1.36	1.37	1.36	8.4	8.4	5.8
1223	1.61	1.60	1.61	1.32	1.31	1.32	10.3	10.2	6.2
1430	1.47	1.50	1.57	1.10	1.13	1.25	8.9	9.0	6.2
1436	1.28	1.28	1.28	0.90	0.90	0.88	7.4	7.2	6.1
1541	1.64	1.64	1.75	1.30	1.30	1.44	8.4	8.6	6.0
1545	1.77	1.79	1.74	1.25	1.26	1.30	10.5	10.7	5.9
1551	1.61	1.66	1.65	1.30	1.35	1.37	6.9	6.9	6.0
6953	2.48	2.55	2.56	2.49	2.61	2.64	9.2	9.2	5.5

Response of an enhanced model of the 20-story building to 11 GMs corresponding to 2% PE in 50 years.

Figures F.23–F.33

Results for 11 GMs listed in Table F.3 are presented in Figures F.23–F.33. Each figure is organized as follows:

Top row	Roof displacement history
Middle row	Peak values of floor displacement, story drifts, and plastic rotations
Bottom row	Peak story shears, V_S, peak story damping forces, V_D, and ratio V_D / V_S

Figure F.23 GM185

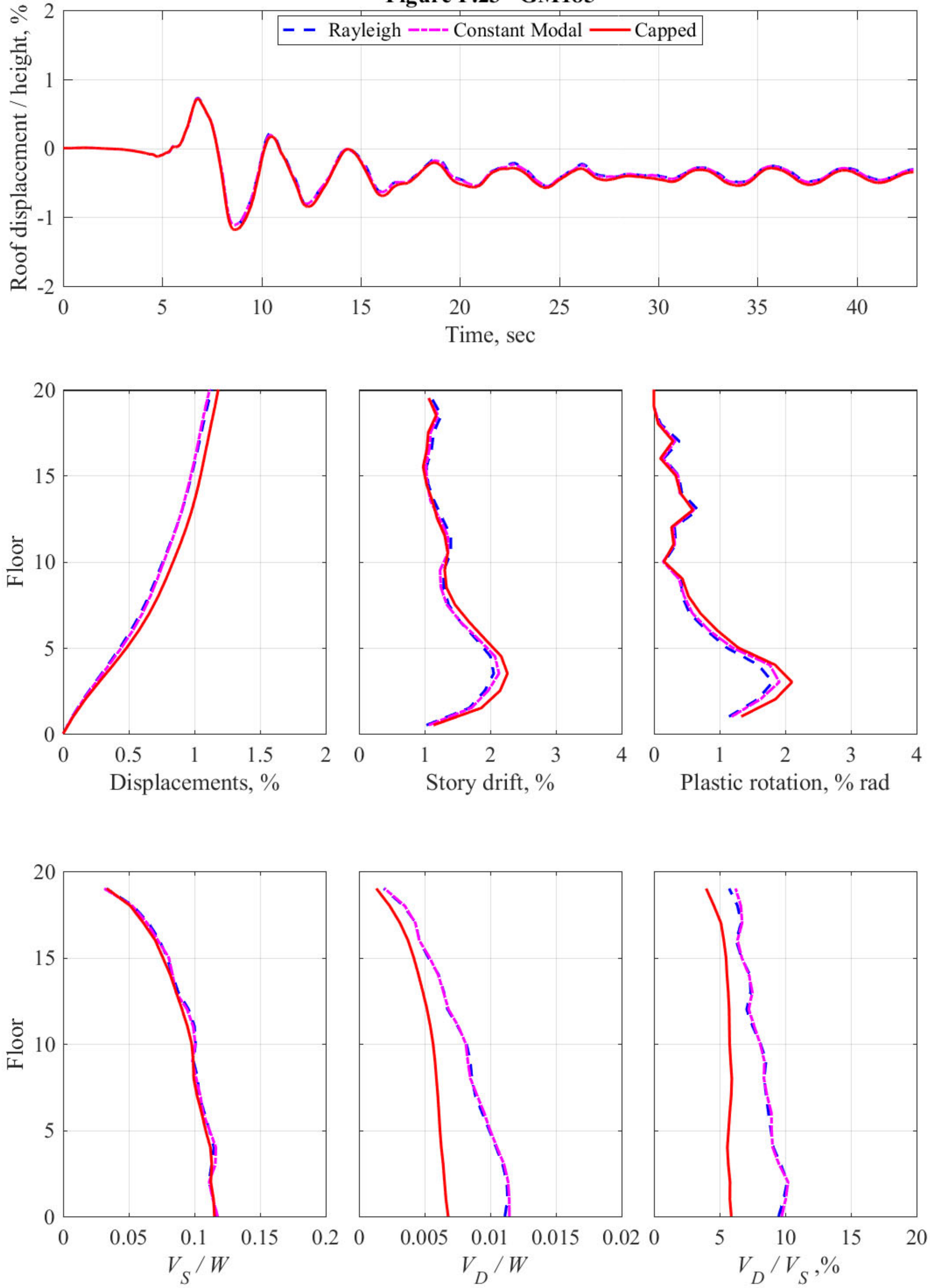

Figure F.24   GM838

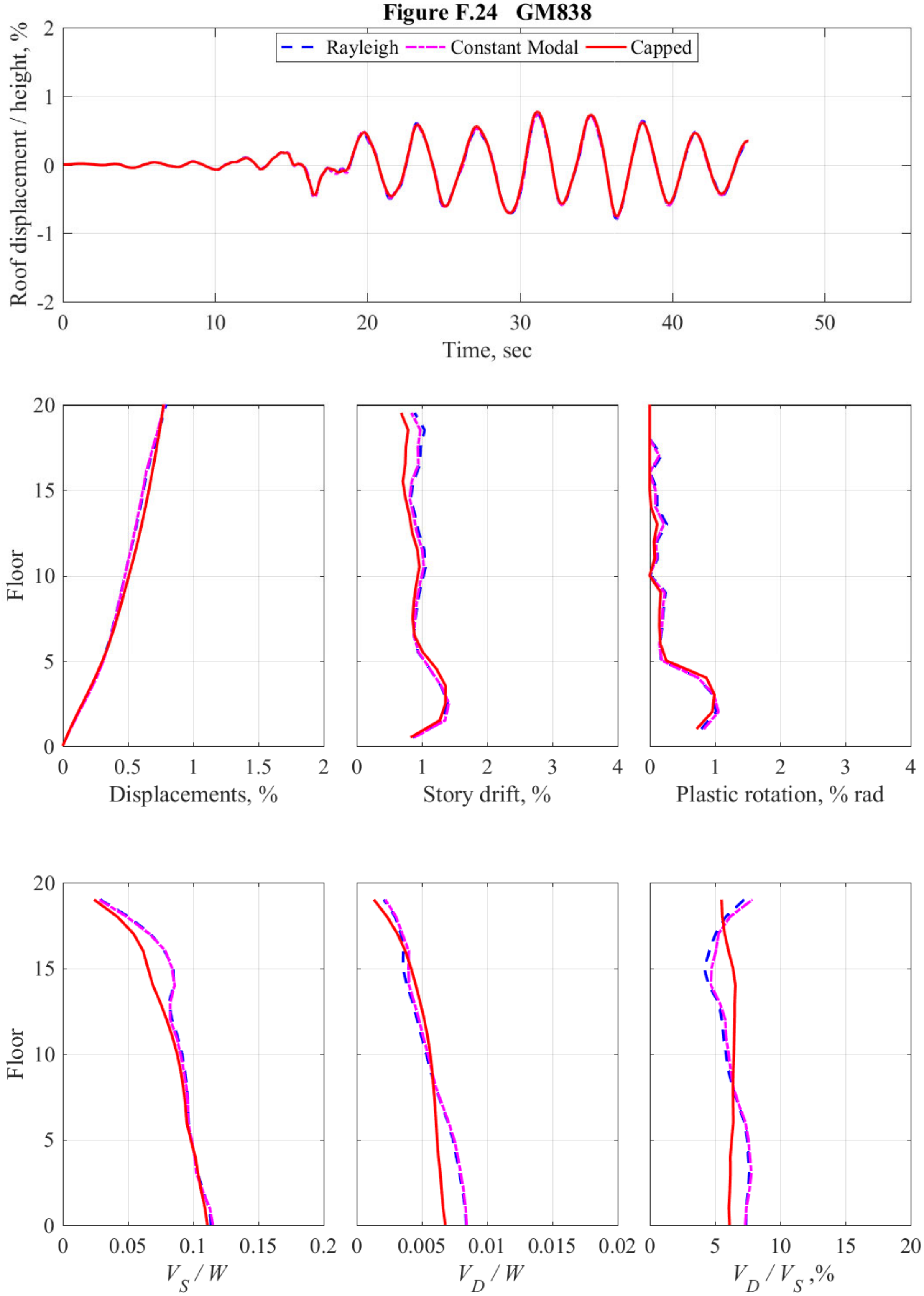

Figure F.25 GM1193

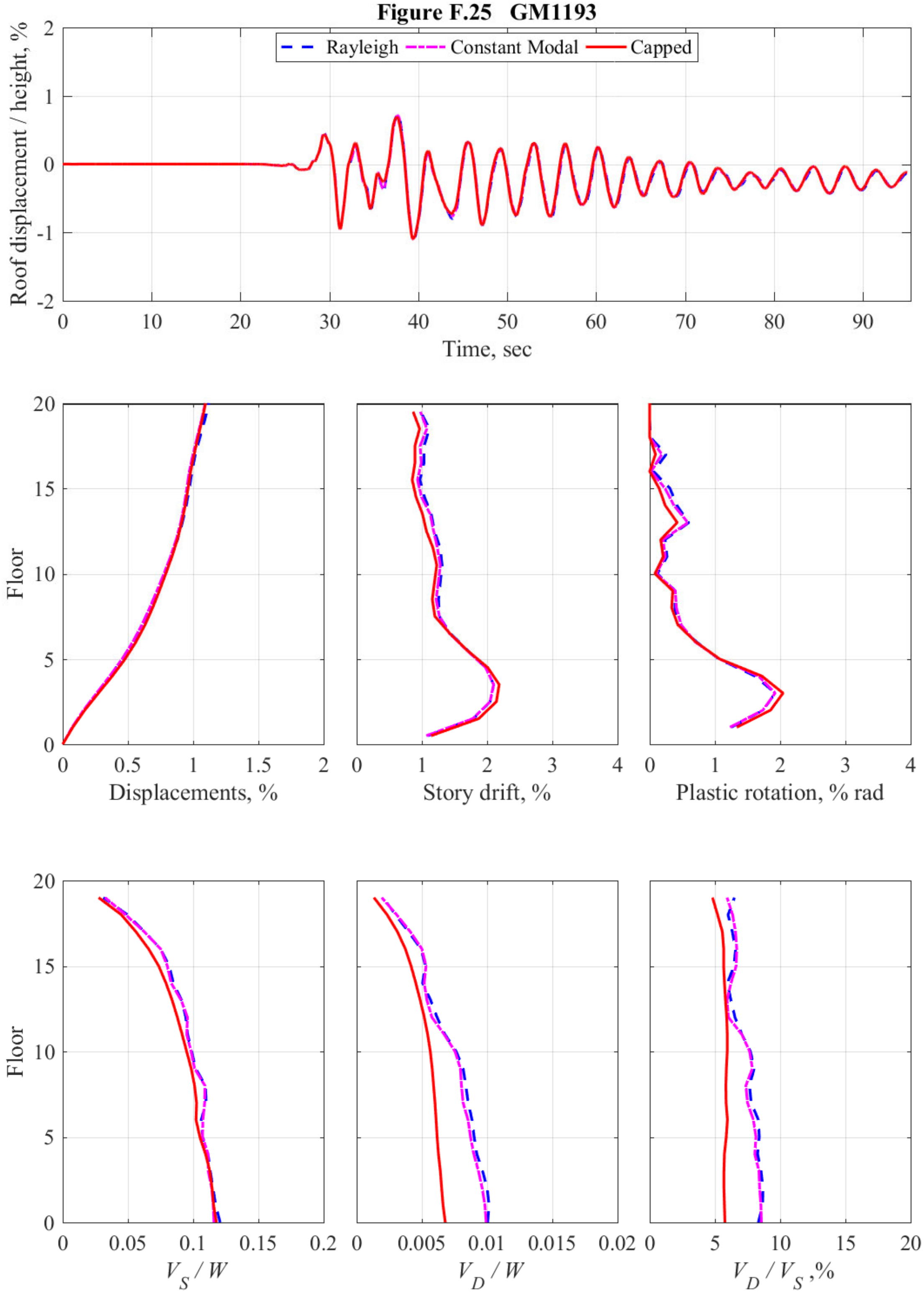

Figure F.26   GM1213

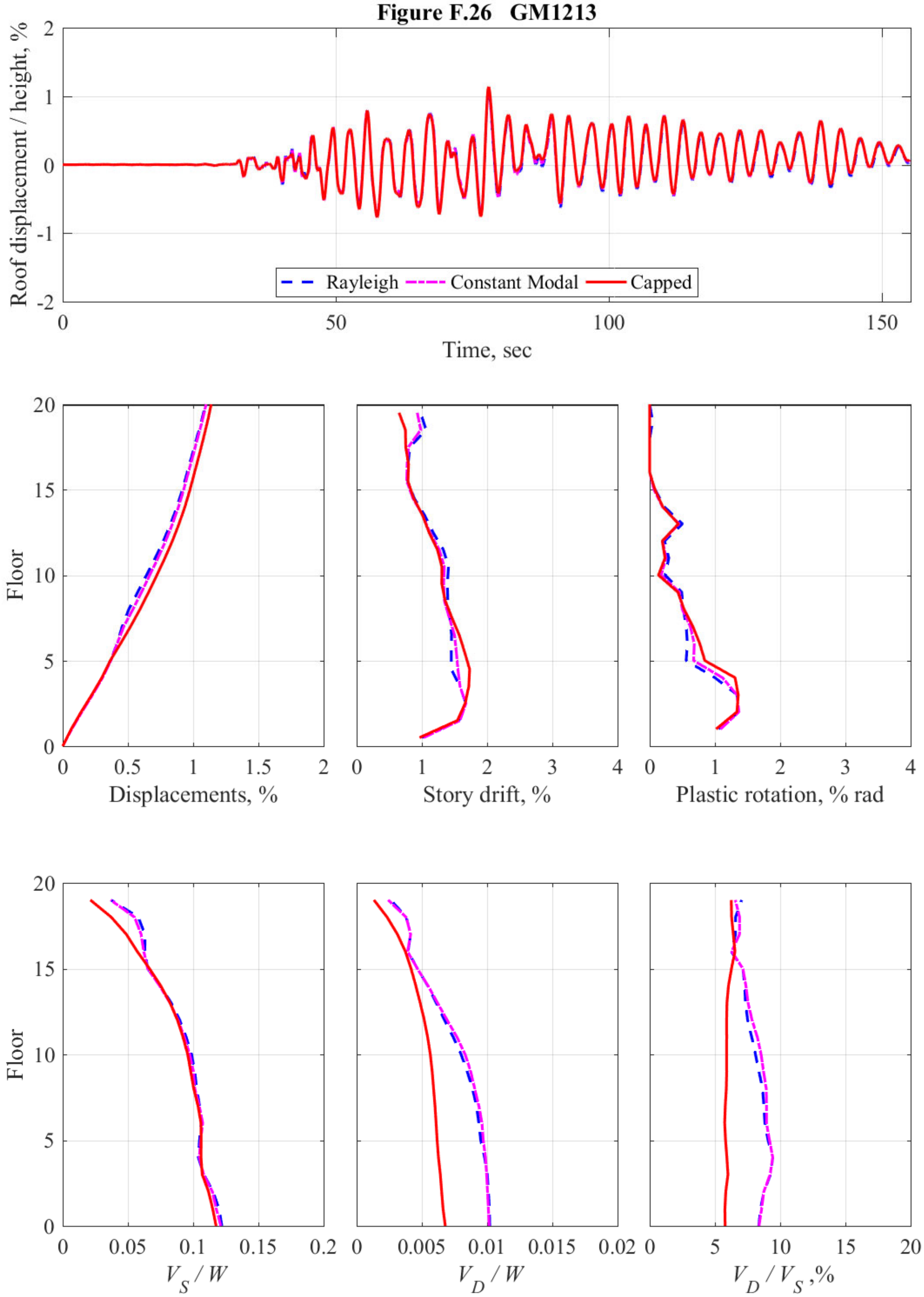

Figure F.27   GM1223

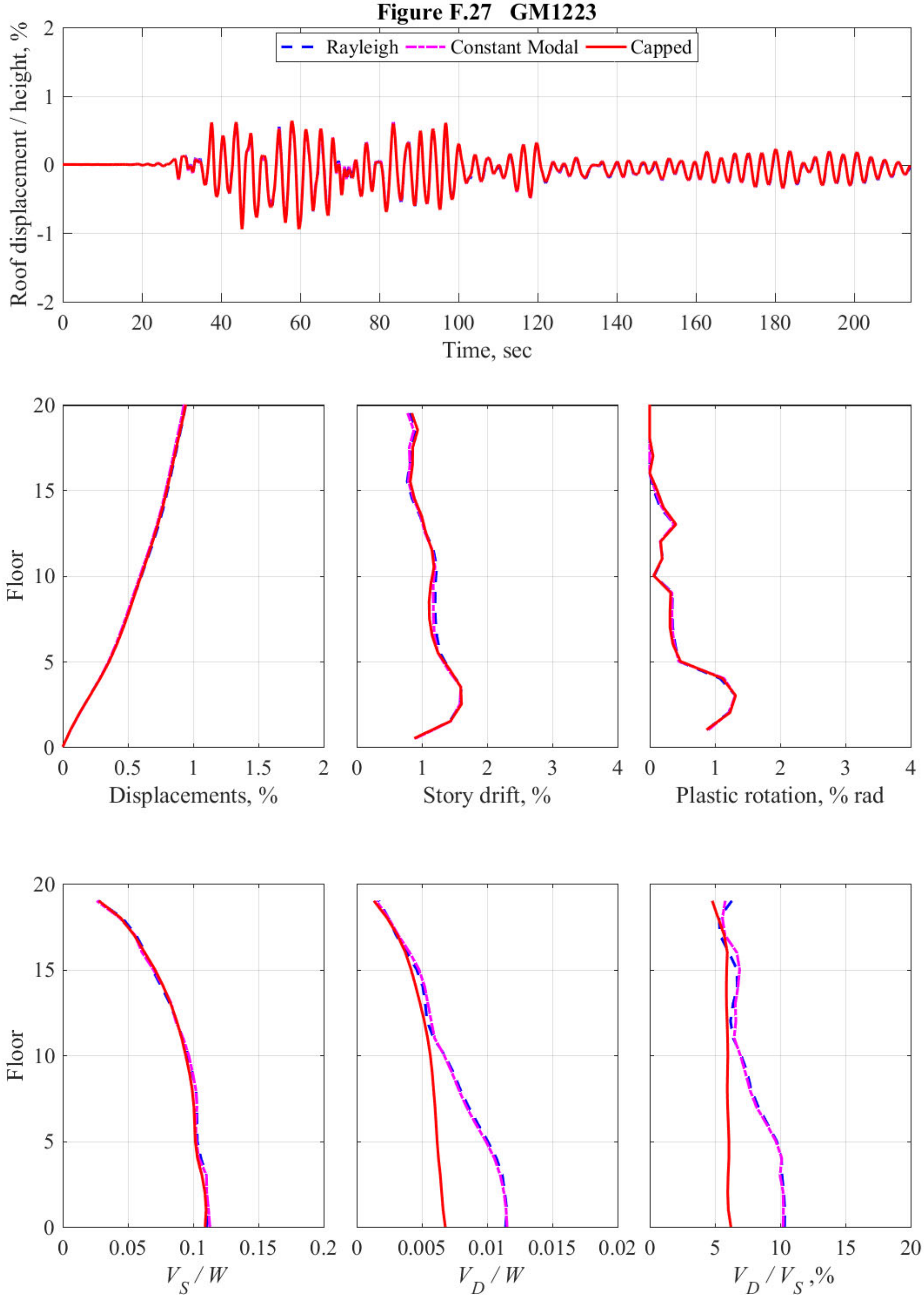

Figure F.28 GM1430

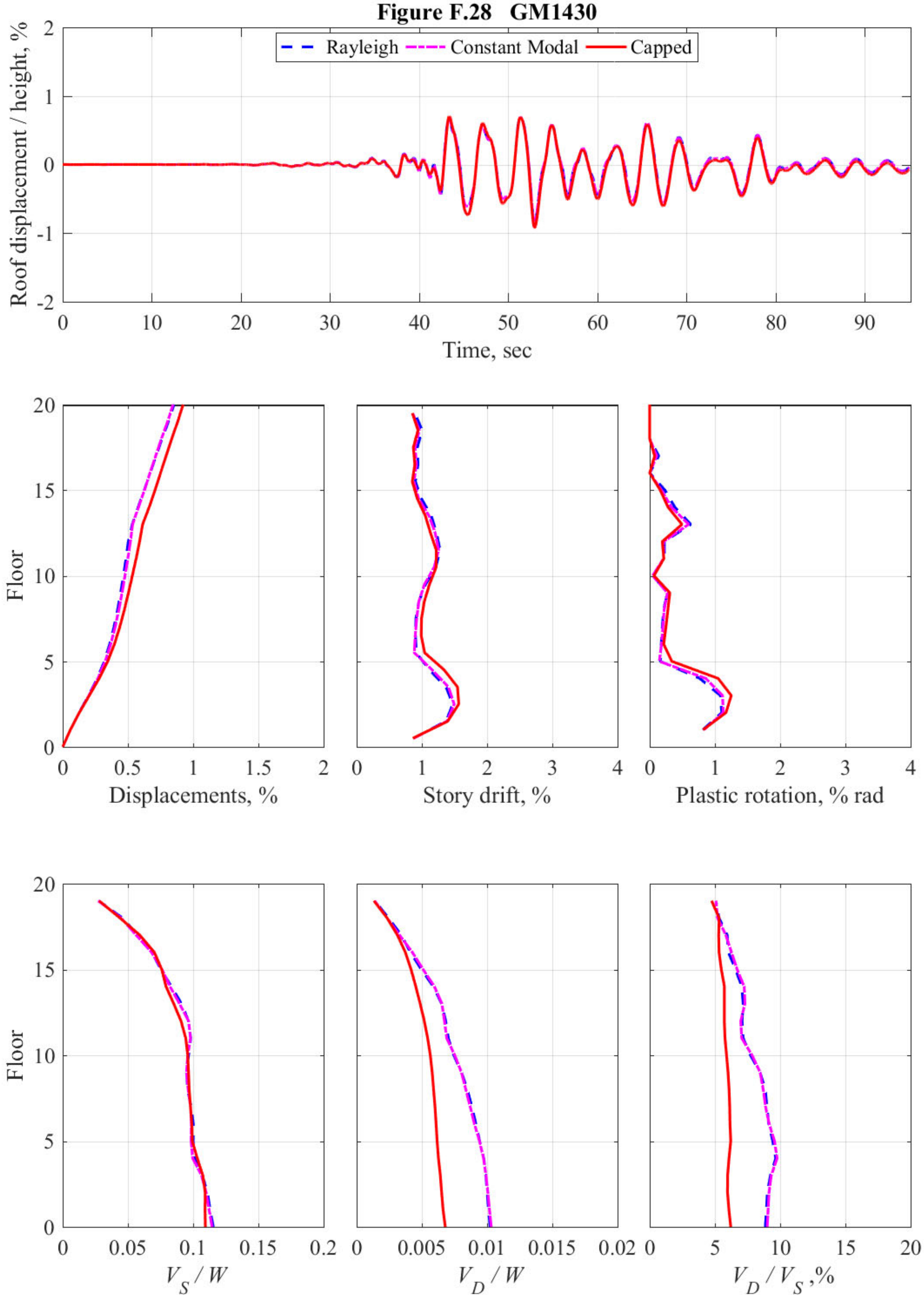

Figure F.29 GM1436

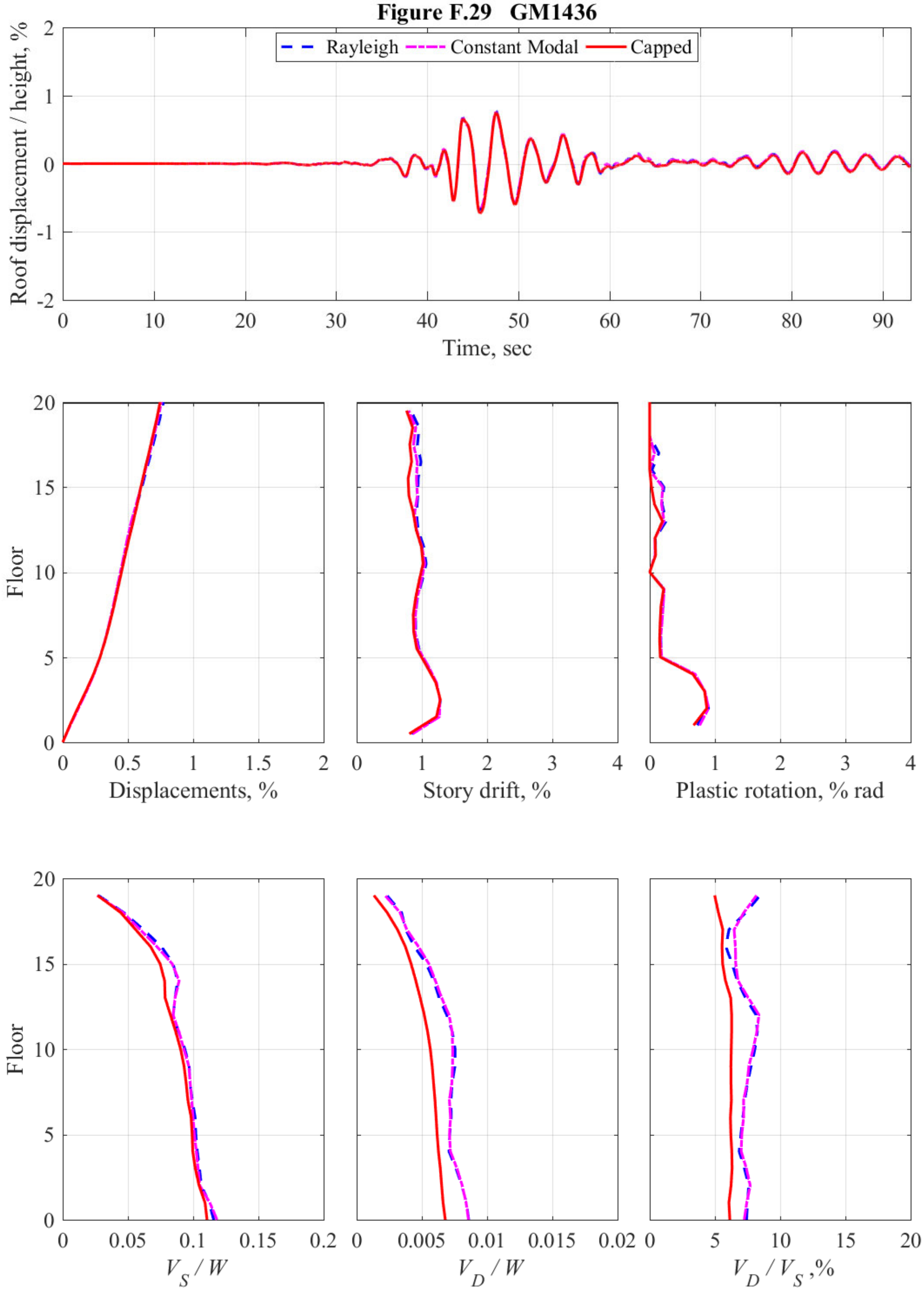

Figure F.30 GM1541

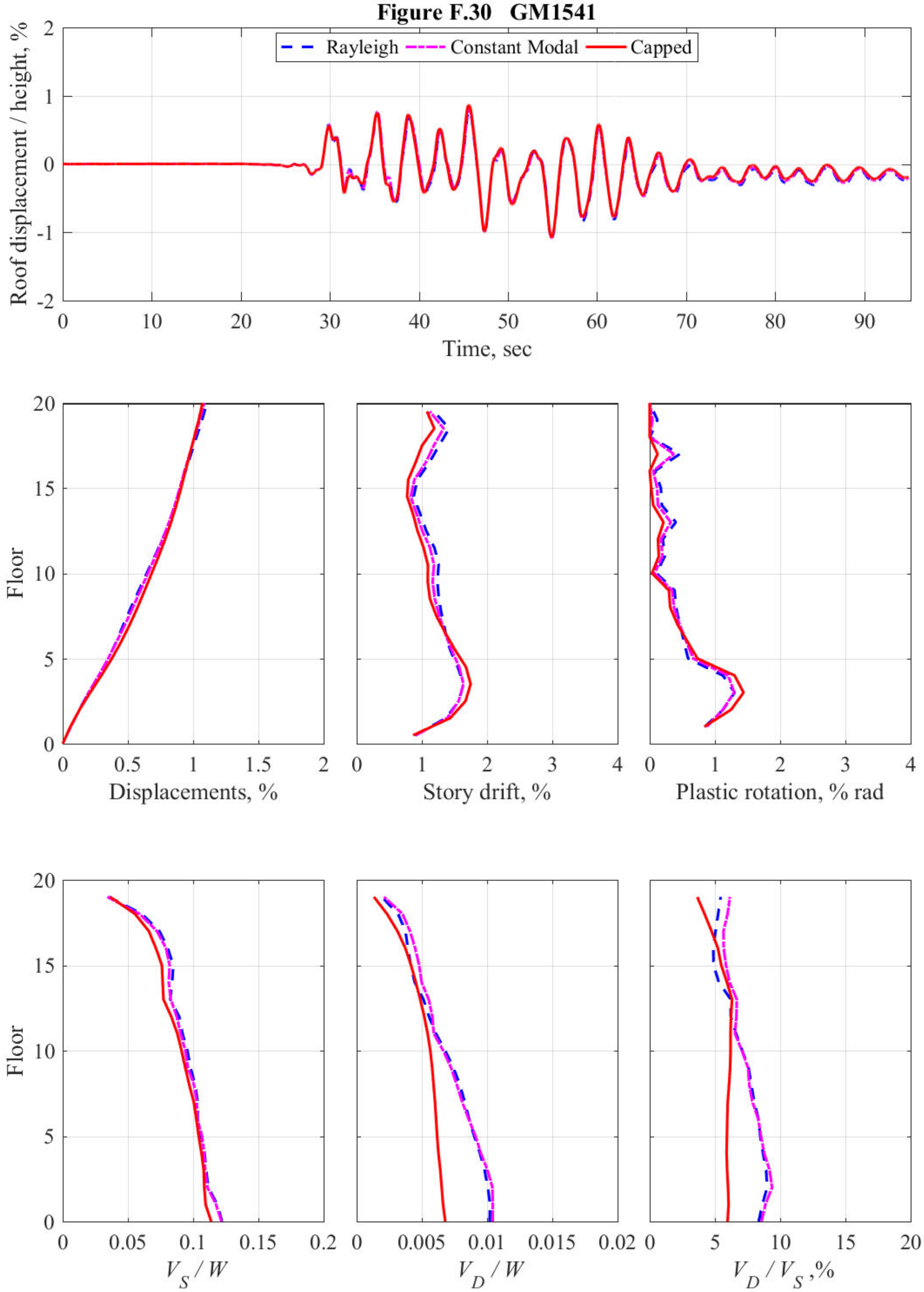

Figure F.31 GM1545

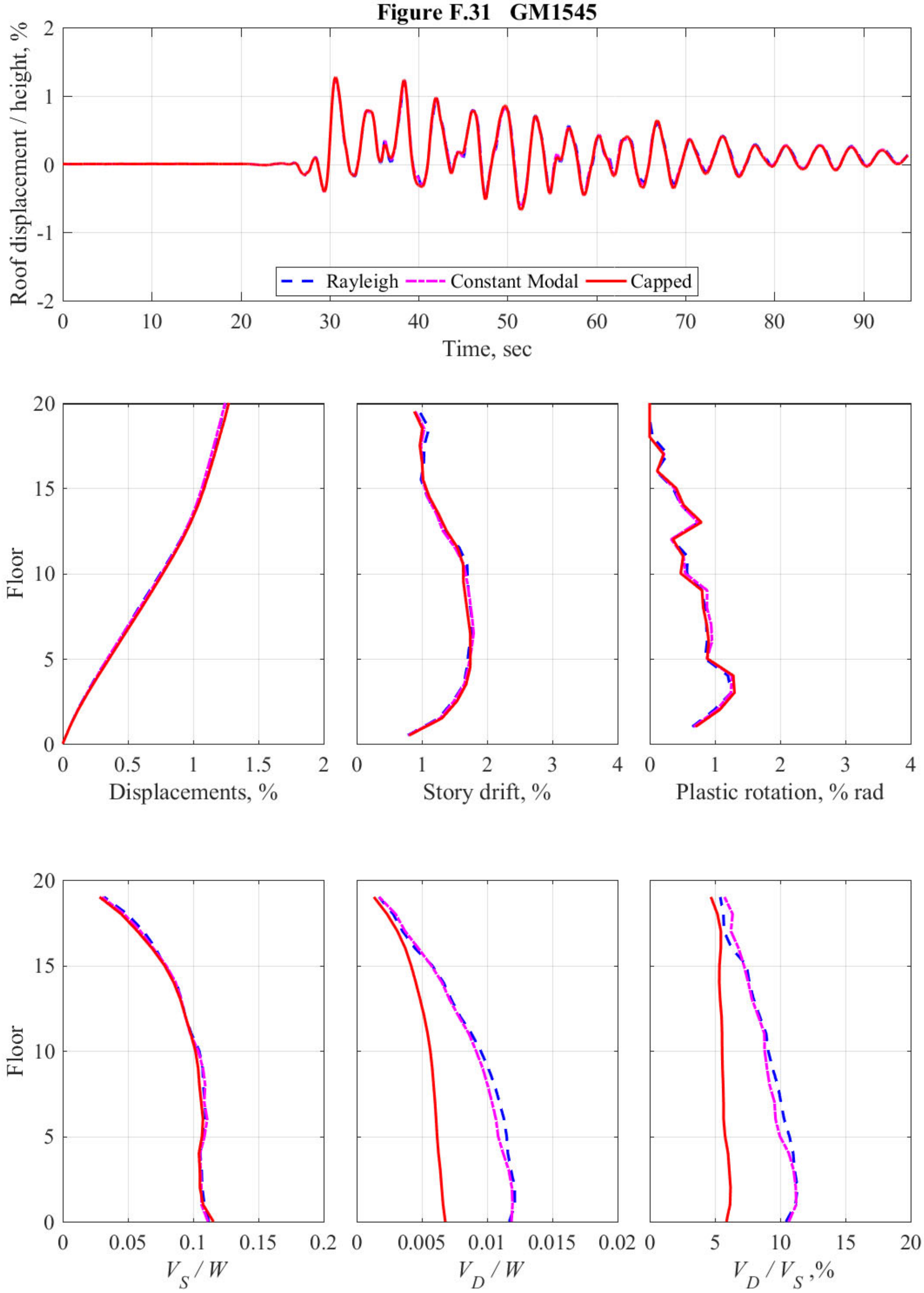

Figure F.32 GM1551

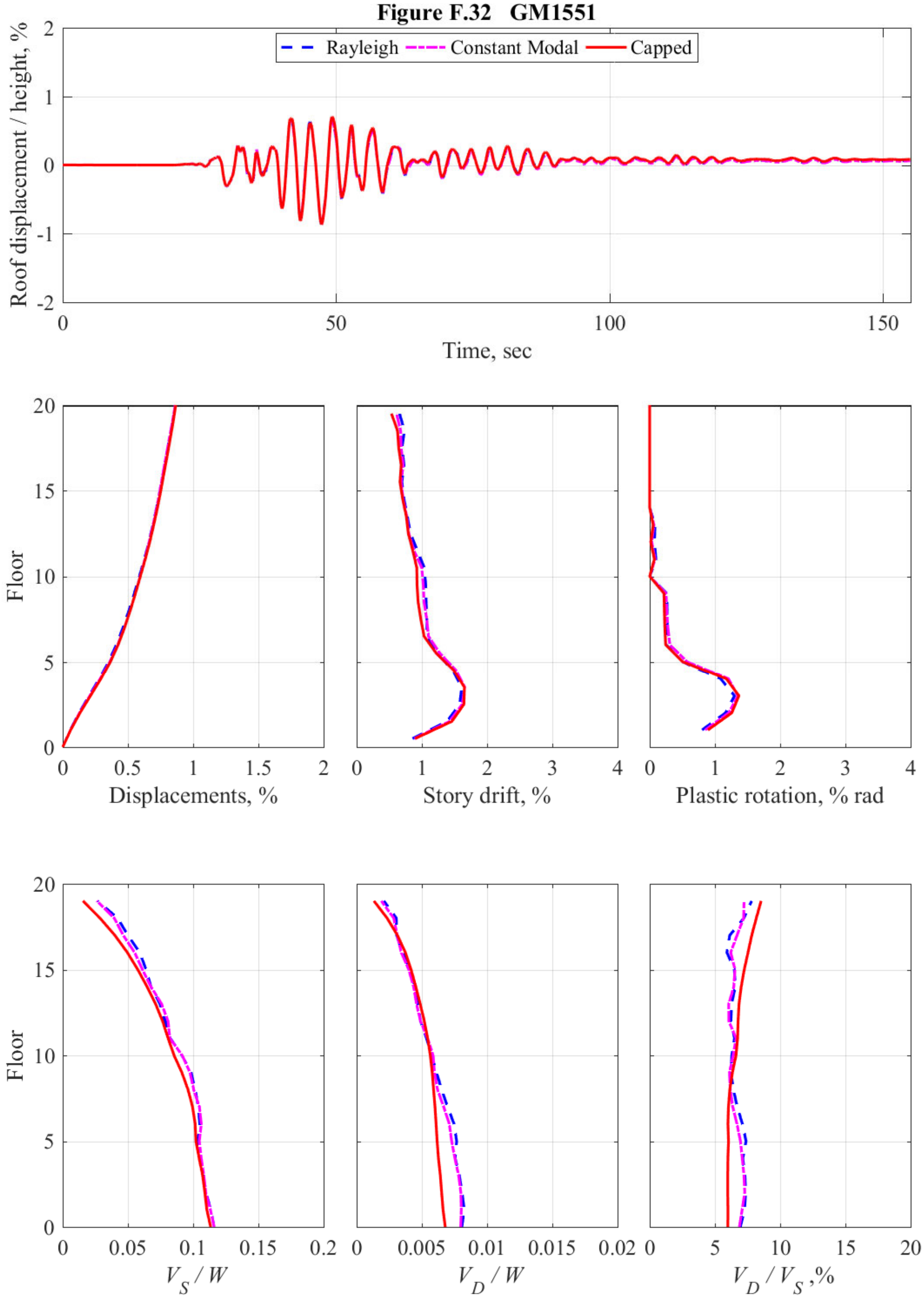

Figure F.33 GM6953

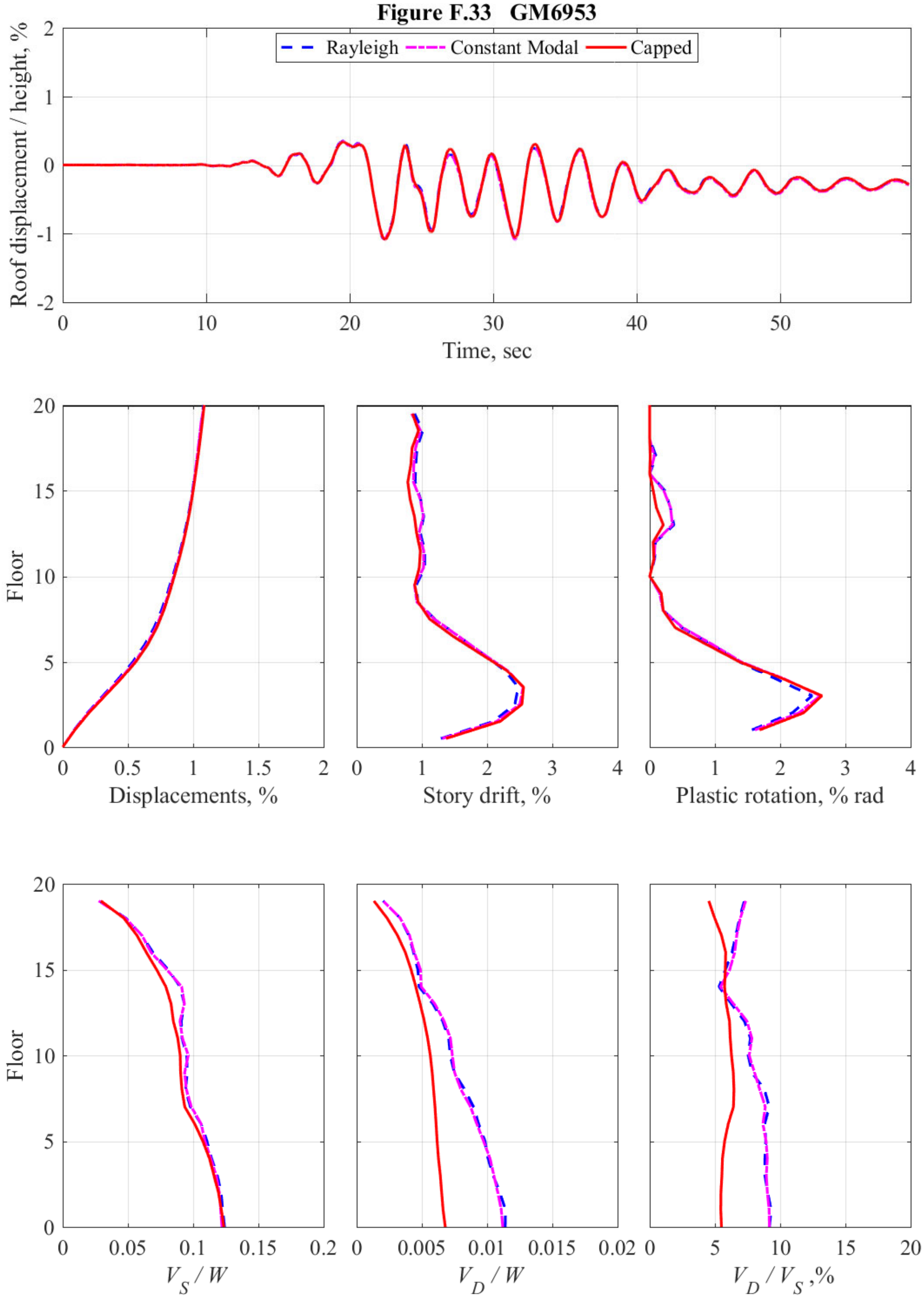

Table F.4 Response of an enhanced model of the 20-story building to 11 GMs corresponding to 1% PE in 50 years.

GM#	Story drift, %			Plastic rotations, % radian			V_D/V_S at base, %		
	Rayleigh	Constant modal	Capped	Rayleigh	Constant modal	Capped	Rayleigh	Constant modal	Capped
185	2.32	2.41	2.66	2.22	2.32	2.77	10.2	10.6	5.8
736	1.46	1.46	1.49	1.11	1.11	1.16	11.0	11.2	5.9
838	1.76	1.80	1.86	1.47	1.53	1.62	8.2	8.1	5.8
1193	2.27	2.25	2.17	2.12	2.08	2.01	9.1	9.3	5.6
1277	1.70	1.71	1.82	1.41	1.43	1.56	9.2	9.8	5.9
1430	1.85	1.86	1.94	1.62	1.63	1.73	8.6	8.9	5.4
1436	1.45	1.46	1.57	1.10	1.12	1.23	7.4	7.2	6.0
1541	1.81	1.96	2.12	1.50	1.62	1.87	8.9	9.5	5.5
1545	2.70	2.75	2.76	2.05	2.11	2.20	11.7	12.1	5.5
2655	1.73	1.77	1.83	1.44	1.52	1.59	10.5	11.0	5.7
6953	4.03	4.35	4.35	4.96	5.42	5.39	9.2	9.3	5.2

Response of an enhanced model of the 20-story building to 11 GMs corresponding to 1% PE in 50 years.

Figures F.34–F.44

Results for 11 GMs listed in Table F.4 are presented in Figures F.34–F.44. Each figure is organized as follows:

Top row	Roof displacement history
Middle row	Peak values of floor displacement, story drifts, and plastic rotations
Bottom row	Peak story shears, V_S, peak story damping forces, V_D, and ratio V_D / V_S

Figure F.34 GM185

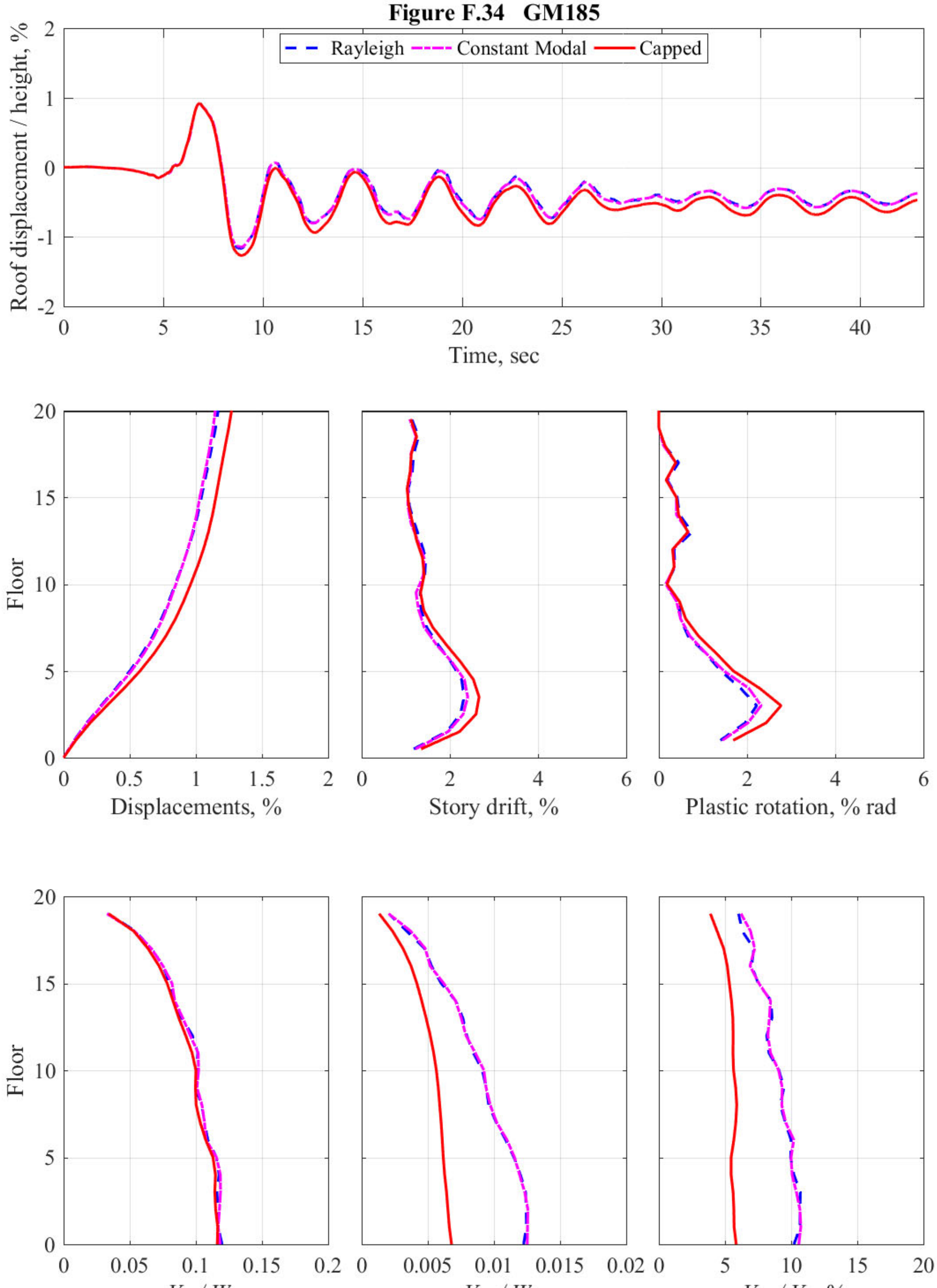

Figure F.35 GM736

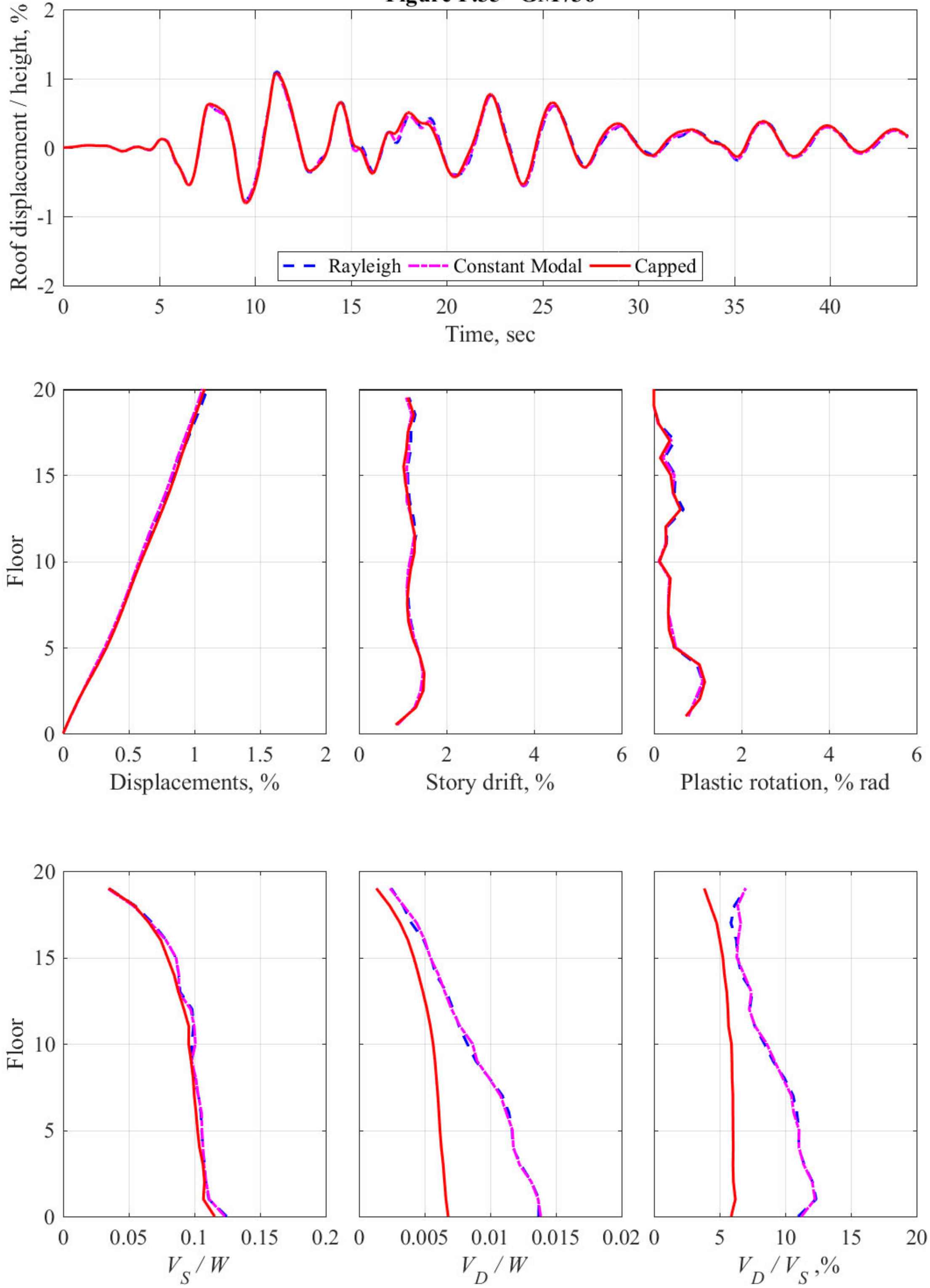

Figure F.36 GM838

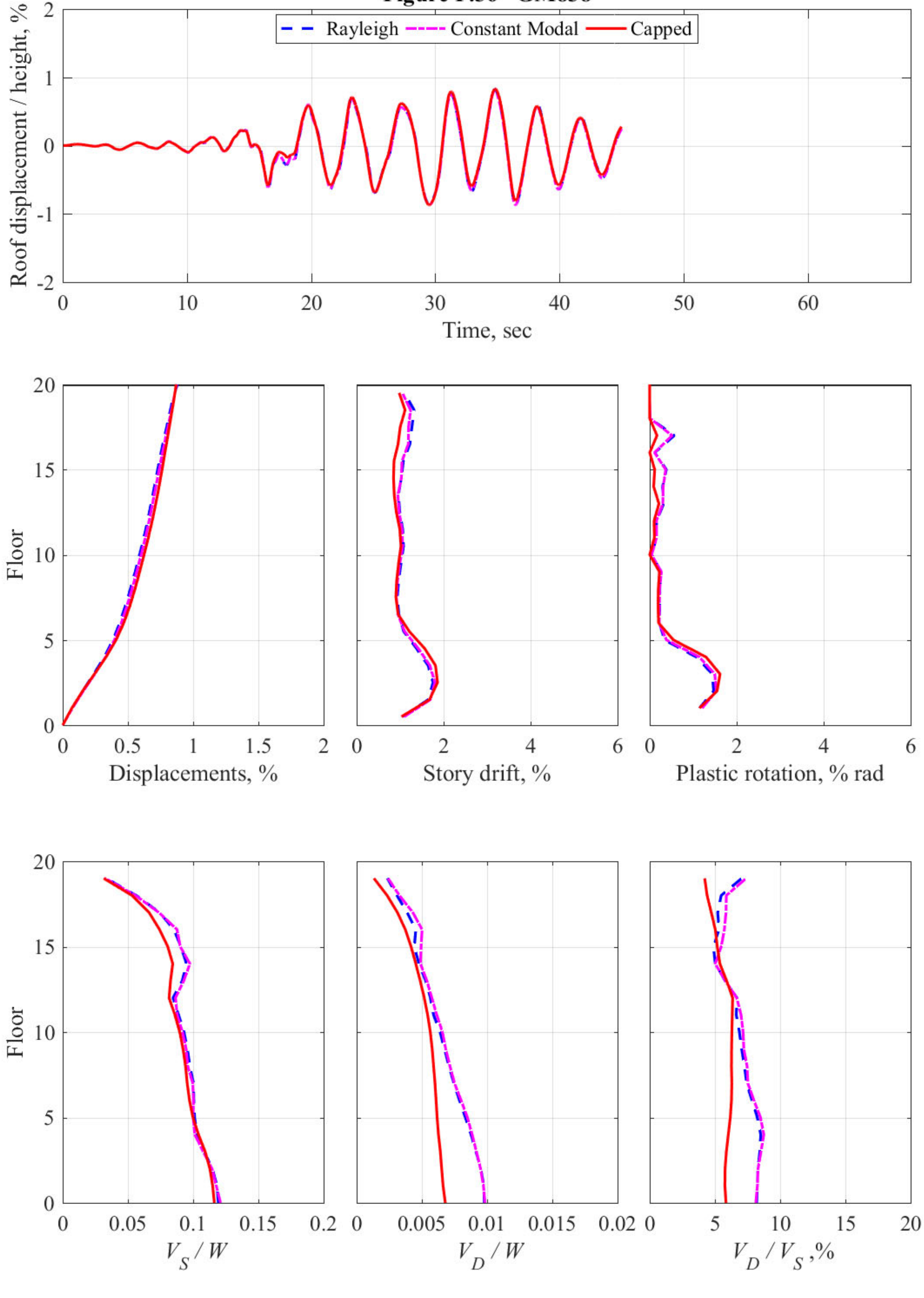

Figure F.37 GM1193

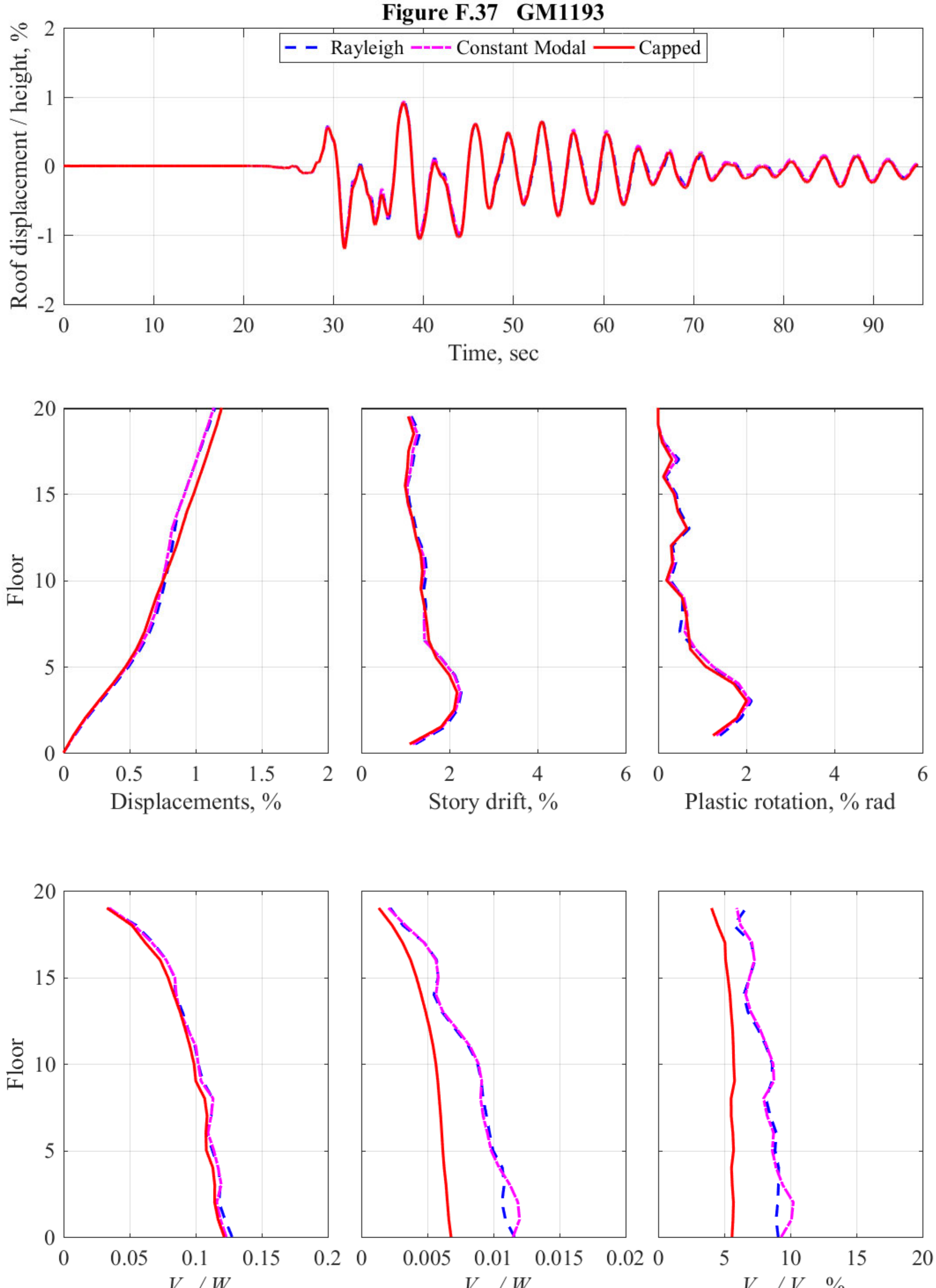

Figure F.38 GM1277

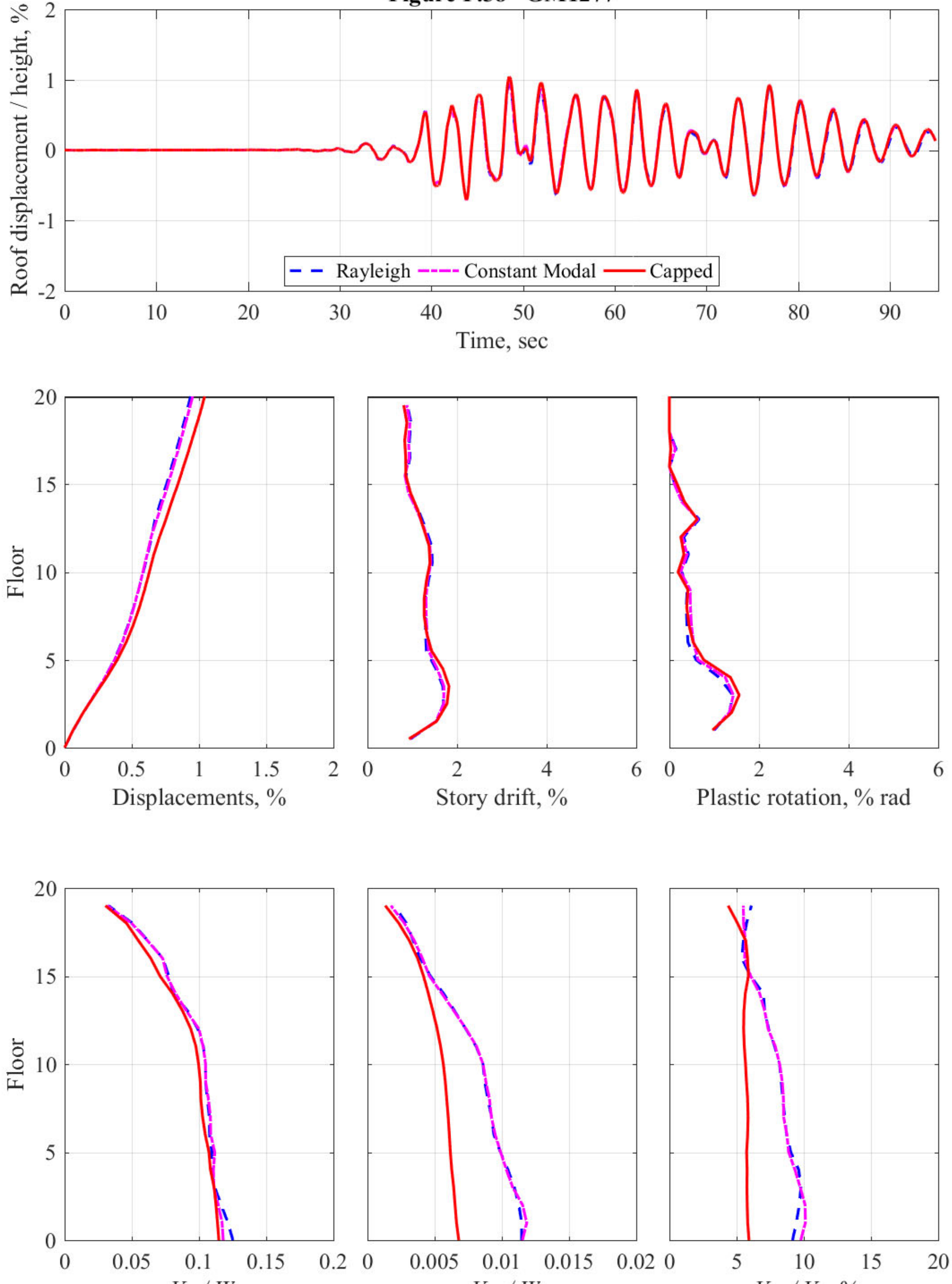

Figure F.39 GM1430

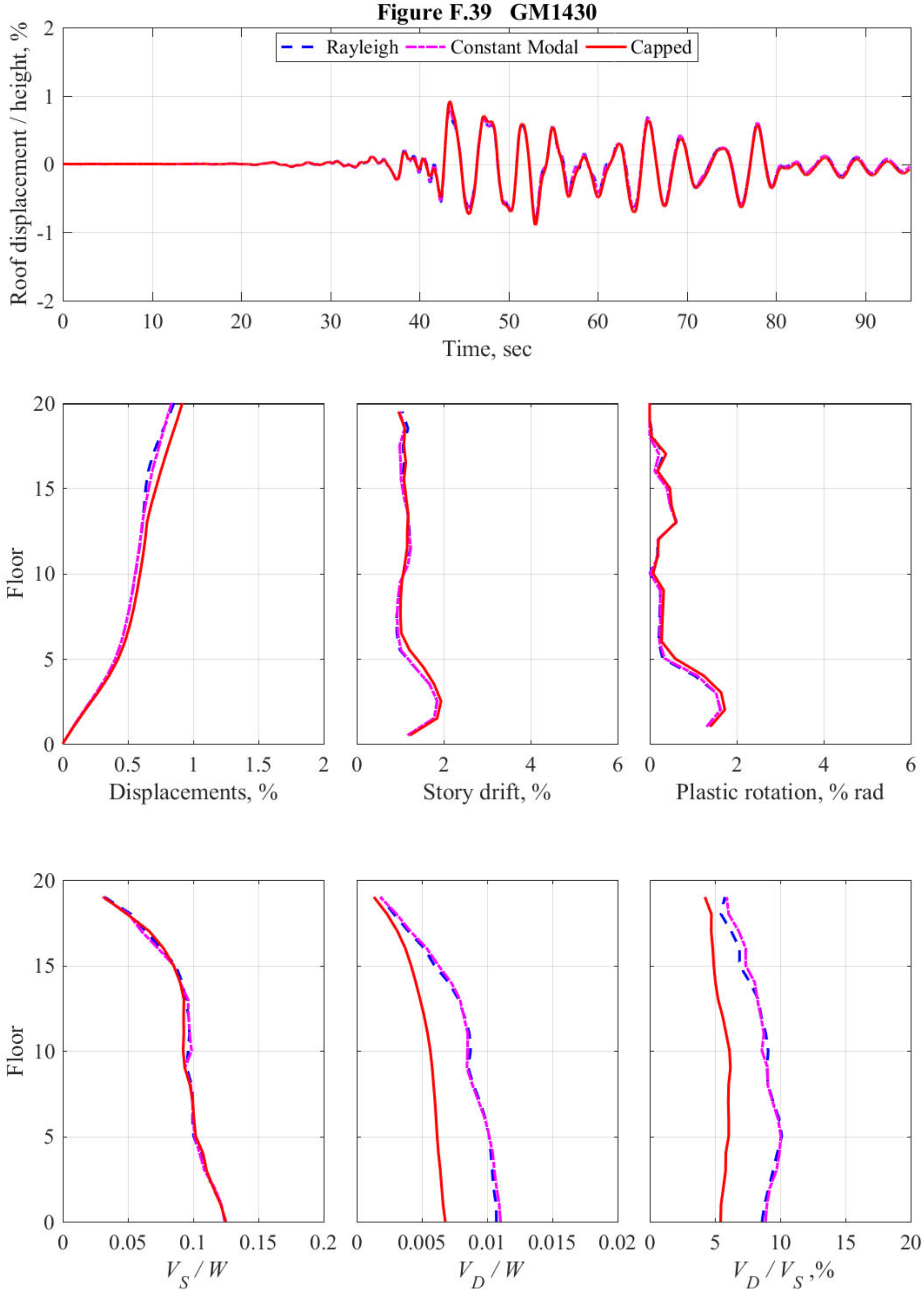

Figure F.40 GM1436

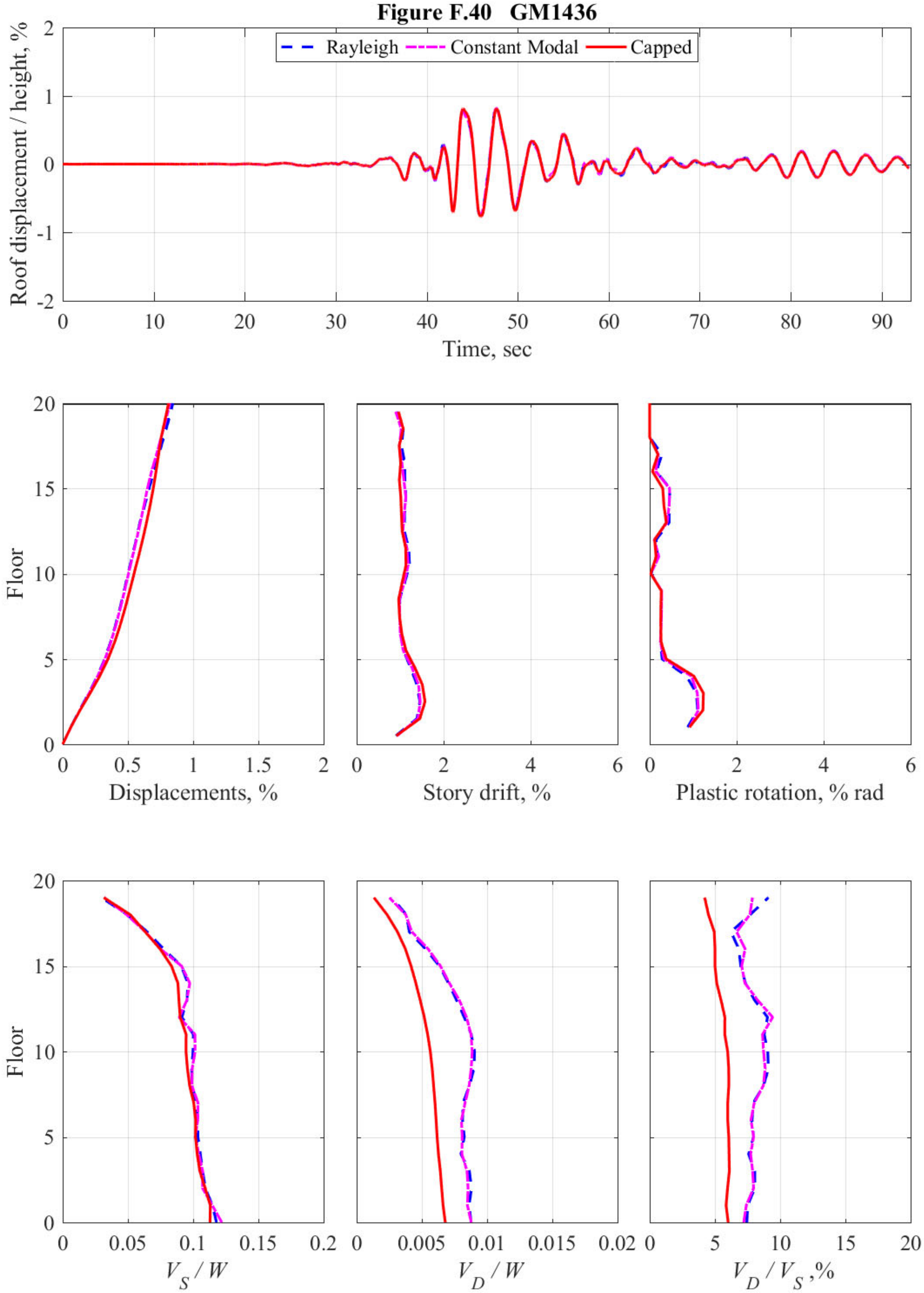

Figure F.41 GM1541

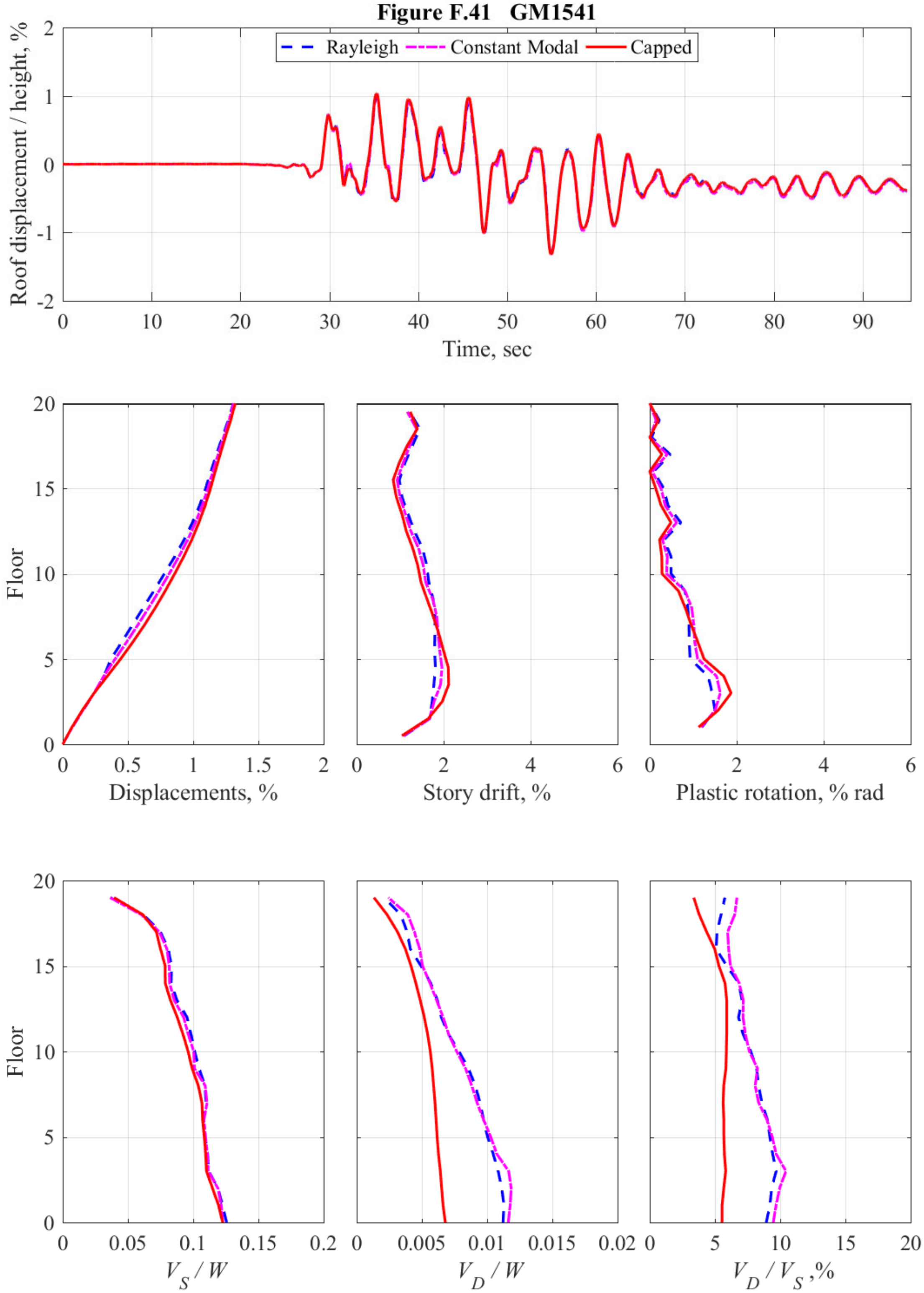

Figure F.42 GM1545

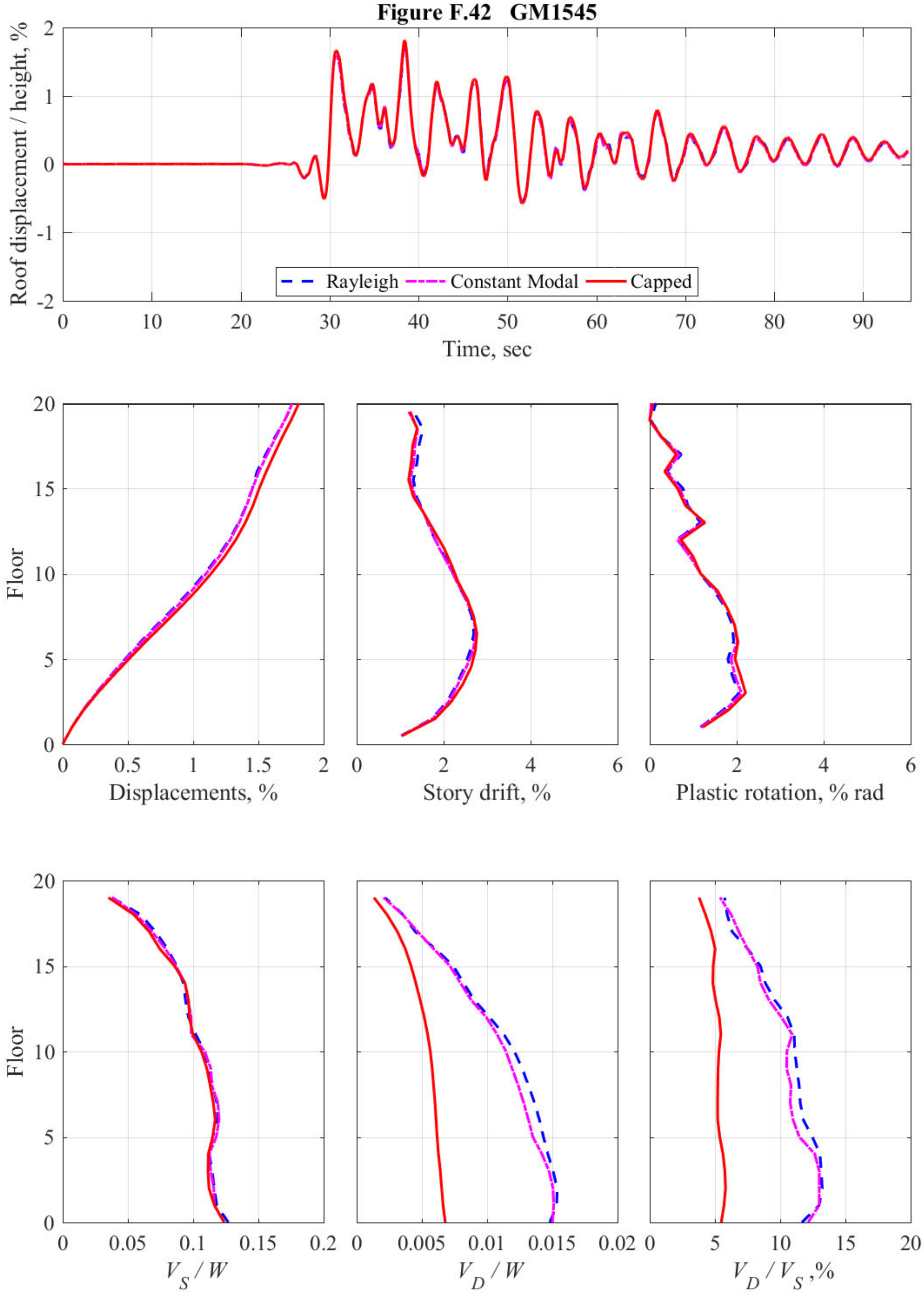

Figure F.43 GM2655

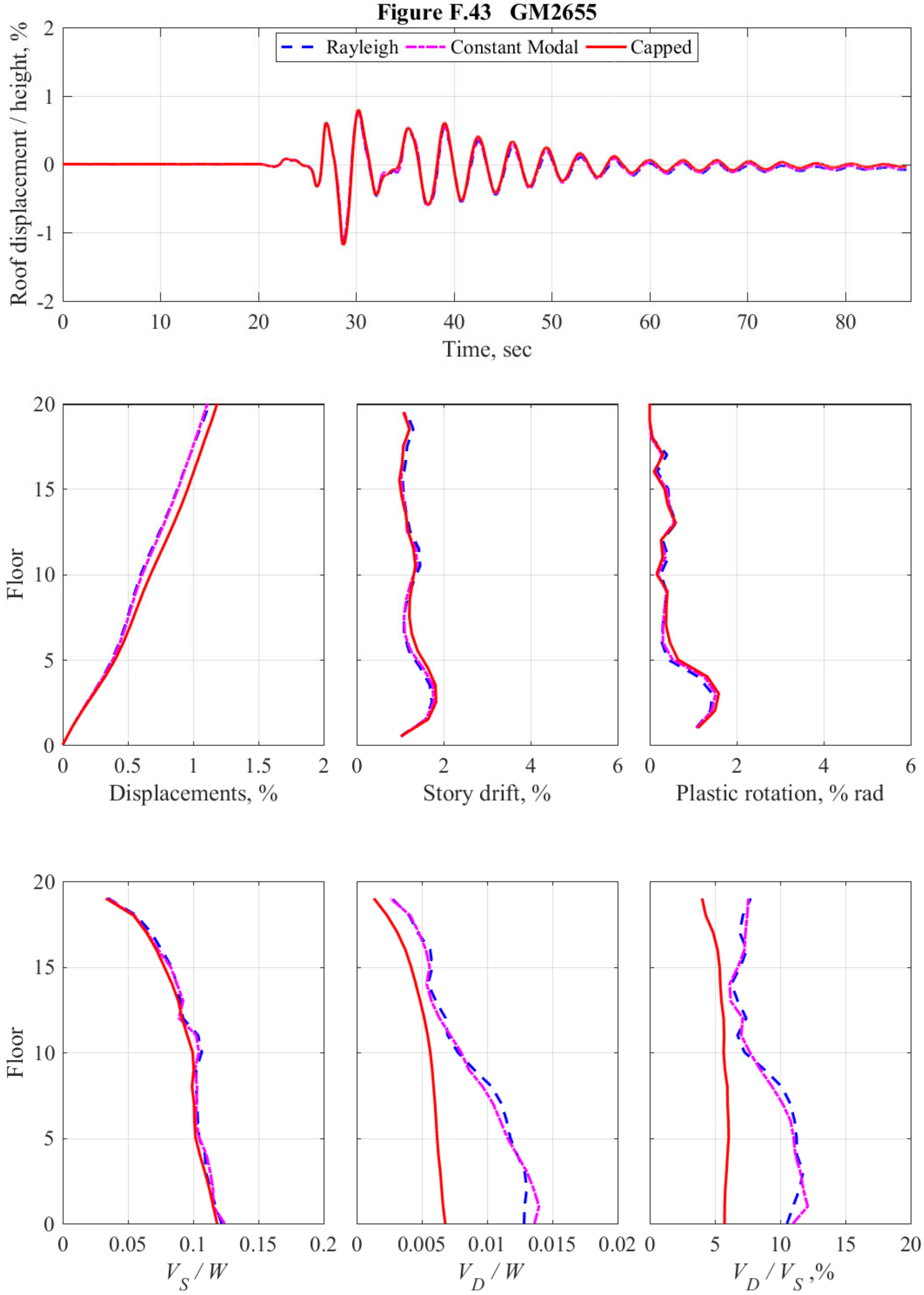

Figure F.44 GM6953

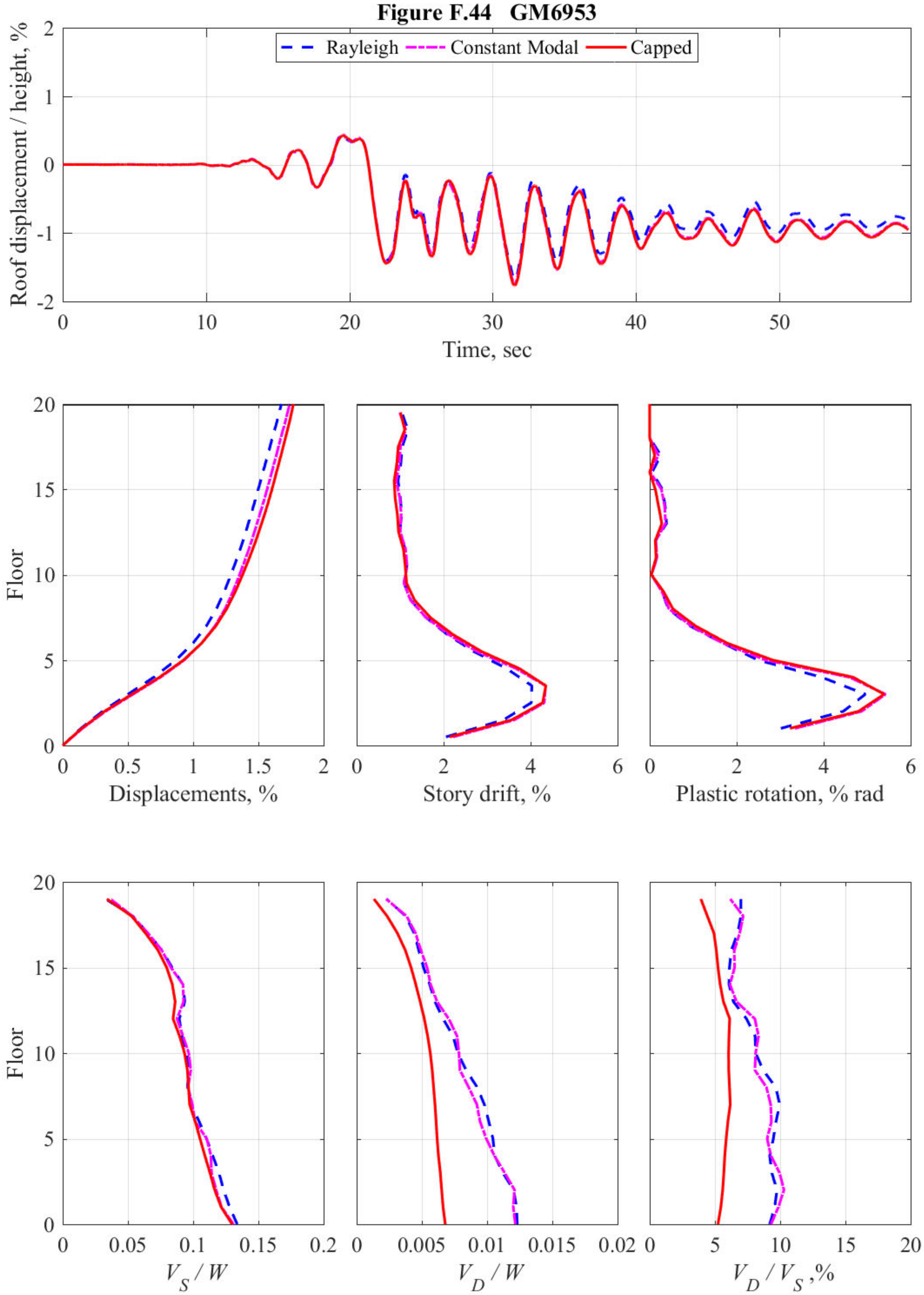

PEER REPORTS

PEER reports are available as a free PDF download from https://peer.berkeley.edu/peer-reports. In addition, printed hard copies of PEER reports can be ordered directly from our printer by following the instructions at https://peer.berkeley.edu/peer-reports. For other related questions about the PEER Report Series, contact the Pacific Earthquake Engineering Research Center, 325 Davis Hall, Mail Code 1792, Berkeley, CA 94720. Tel.: (510) 642-3437; and Email: peer_center@berkeley.edu.

PEER 2019/09 Seismic Behavior of Special Concentric Braced Frames under Short- and Long-Duration Ground Motions. Ali Hammad and Mohamed A. Moustafa. December 2019.

PEER 2019/08 Influence of Vertical Ground Motion on Bridges Isolated with Spherical Sliding Bearings. Rushil Mojidra and Keri L. Ryan. December 2019.

PEER 2019/07 *PEER Hub ImageNet* (ϕ-Net): *A Large-Scale Multi-Attribute Benchmark Dataset of Structural Images*. Yuqing Gao, and Khalid. M. Mosalam. November 2019.

PEER 2019/06 *Fluid-Structure Interaction and Python-Scripting Capabilities in OpenSees*. Minjie Zhu and Michael H. Scott. August 2019.

PEER 2019/05 *Expected Earthquake Performance of Buildings Designed to the California Building Code (California Alfred E. Alquist Seismic Safety Publication 19-01).* Grace S. Kang, Sifat Muin, Jorge Archbold, Bitanoosh Woods, and Khalid Mosalam. July 2019.

PEER 2019/04 *Aftershock Seismic Vulnerability and Time-Dependent Risk Assessment of Bridges*. Sujith Mangalathu, Mehrdad Shokrabadi, and Henry V. Burton. May 2019.

PEER 2019/03 *Ground-Motion Directivity Modeling for Seismic Hazard Applications.* Jennifer L. Donahue, Jonathan P. Stewart, Nicolas Gregor, and Yousef Bozorgnia. Review Panel: Jonathan D. Bray, Stephen A. Mahin, I. M. Idriss, Robert W. Graves, and Tom Shantz. May 2019.

PEER 2019/02 *Direct-Finite-Element Method for Nonlinear Earthquake Analysis of Concrete Dams Including Dam–Water–Foundation Rock Interaction.* Arnkjell Løkke and Anil K. Chopra. March 2019.

PEER 2019/01 *Flow-Failure Case History of the Las Palmas, Chile, Tailings Dam.* R. E. S. Moss, T. R. Gebhart, D. J. Frost, and C. Ledezma. January 2019.

PEER 2018/08 *Central and Eastern North America Ground-Motion Characterization: NGA-East Final Report*. Christine Goulet, Yousef Bozorgnia, Norman Abrahamson, Nicolas Kuehn, Linda Al Atik, Robert Youngs, Robert Graves, and Gail Atkinson. December 2018.

PEER 2018/07 *An Empirical Model for Fourier Amplitude Spectra using the NGA-West2 Database*. Jeff Bayless, and Norman A. Abrahamson. December 2018.

PEER 2018/06 *Estimation of Shear Demands on Rock-Socketed Drilled Shafts subjected to Lateral Loading*. Pedro Arduino, Long Chen, and Christopher R. McGann. December 2018.

PEER 2018/05 *Selection of Random Vibration Procedures for the NGA-East Project*. Albert Kottke, Norman A. Abrahamson, David M. Boore, Yousef Bozorgnia, Christine Goulet, Justin Hollenback, Tadahiro Kishida, Armen Der Kiureghian, Olga-Joan Ktenidou, Nicolas Kuehn, Ellen M. Rathje, Walter J. Silva, Eric Thompson, and Xiaoyue Wang. December 2018.

PEER 2018/04 *Capturing Directivity Effects in the Mean and Aleatory Variability of the NGA-West 2 Ground Motion Prediction Equations.* Jennie A. Watson-Lamprey. November 2018.

PEER 2018/03 *Probabilistic Seismic Hazard Analysis Code Verification*. Christie Hale, Norman Abrahamson, and Yousef Bozorgnia. July 2018.

PEER 2018/02 *Update of the BCHydro Subduction Ground-Motion Model using the NGA-Subduction Dataset.* Norman Abrahamson, Nicolas Kuehn, Zeynep Gulerce, Nicholas Gregor, Yousef Bozorgnia, Grace Parker, Jonathan Stewart, Brian Chiou, I. M. Idriss, Kenneth Campbell, and Robert Youngs. June 2018.

PEER 2018/01 *PEER Annual Report 2017–2018*. Khalid Mosalam, Amarnath Kasalanati, and Selim Günay. June 2018.

PEER 2017/12 *Experimental Investigation of the Behavior of Vintage and Retrofit Concentrically Braced Steel Frames under Cyclic Loading*. Barbara G. Simpson, Stephen A. Mahin, and Jiun-Wei Lai, December 2017.

PEER 2017/11 *Preliminary Studies on the Dynamic Response of a Seismically Isolated Prototype Gen-IV Sodium-Cooled Fast Reactor* (*PGSFR*). Benshun Shao, Andreas H. Schellenberg, Matthew J. Schoettler, and Stephen A. Mahin. December 2017.

PEER 2017/10 *Development of Time Histories for IEEE693 Testing and Analysis (including Seismically Isolated Equipment).* Shakhzod M. Takhirov, Eric Fujisaki, Leon Kempner, Michael Riley, and Brian Low. December 2017.

PEER 2017/09 *“”R” Package for Computation of Earthquake Ground-Motion Response Spectra.* Pengfei Wang, Jonathan P. Stewart, Yousef Bozorgnia, David M. Boore, and Tadahiro Kishida. December 2017.

PEER 2017/08 *Influence of Kinematic SSI on Foundation Input Motions for Bridges on Deep Foundations*. Benjamin J. Turner, Scott J. Brandenberg, and Jonathan P. Stewart. November 2017.

PEER 2017/07 *A Nonlinear Kinetic Model for Multi-Stage Friction Pendulum Systems*. Paul L. Drazin and Sanjay Govindjee. September 2017.

PEER 2017/06 *Guidelines for Performance-Based Seismic Design of Tall Buildings, Version 2.02*. TBI Working Group led by co-chairs Ron Hamburger and Jack Moehle: Jack Baker, Jonathan Bray, C.B. Crouse, Greg Deierlein, John Hooper, Marshall Lew, Joe Maffei, Stephen Mahin, James Malley, Farzad Naeim, Jonathan Stewart, and John Wallace. May 2017.

PEER 2017/05 *Recommendations for Ergodic Nonlinear Site Amplification in Central and Eastern North America*. Youssef M.A. Hashash, Joseph A. Harmon, Okan Ilhan, Grace A. Parker, and Jonathan P. Stewart. March 2017.

PEER 2017/04 *Expert Panel Recommendations for Ergodic Site Amplification in Central and Eastern North America*. Jonathan P. Stewart, Grace A. Parker, Joseph P. Harmon, Gail M. Atkinson, David M. Boore, Robert B. Darragh, Walter J. Silva, and Youssef M.A. Hashash. March 2017.

PEER 2017/03 *NGA-East Ground-Motion Models for the U.S. Geological Survey National Seismic Hazard Maps*. Christine A. Goulet, Yousef Bozorgnia, Nicolas Kuehn, Linda Al Atik, Robert R. Youngs, Robert W. Graves, and Gail M. Atkinson. March 2017.

PEER 2017/02 *U.S.–New Zealand–Japan Workshop: Liquefaction-Induced Ground Movements Effects, University of California, Berkeley, California, 2–4 November 2016.* Jonathan D. Bray, Ross W. Boulanger, Misko Cubrinovski, Kohji Tokimatsu, Steven L. Kramer, Thomas O’Rourke, Ellen Rathje, Russell A. Green, Peter K. Robinson, and Christine Z. Beyzaei. March 2017.

PEER 2017/01 *2016 PEER Annual Report*. Khalid M. Mosalam, Amarnath Kasalanati, and Grace Kang. March 2017.

PEER 2016/10 *Performance-Based Robust Nonlinear Seismic Analysis with Application to Reinforced Concrete Bridge Systems*. Xiao Ling and Khalid M. Mosalam. December 2016.

PEER 2017/09 *Detailing Requirements for Column Plastic Hinges subjected to Combined Flexural, Axial, and Torsional Seismic Loading.* Gabriel Hurtado and Jack P. Moehle. December 2016.

PEER 2016/08 *Resilience of Critical Structures, Infrastructure, and Communities*. Gian Paolo Cimellaro, Ali Zamani-Noori, Omar Kamouh, Vesna Terzic, and Stephen A. Mahin. December 2016.

PEER 2016/07 *Hybrid Simulation Theory for a Classical Nonlinear Dynamical System*. Paul L. Drazin and Sanjay Govindjee. September 2016.

PEER 2016/06 *California Earthquake Early Warning System Benefit Study*. Laurie A. Johnson, Sharyl Rabinovici, Grace S. Kang, and Stephen A. Mahin. July 2006.

PEER 2016/05 *Ground-Motion Prediction Equations for Arias Intensity Consistent with the NGA-West2 Ground-Motion Models.* Charlotte Abrahamson, Hao-Jun Michael Shi, and Brian Yang. July 2016.

PEER 2016/04 *The M_W 6.0 South Napa Earthquake of August 24, 2014: A Wake-Up Call for Renewed Investment in Seismic Resilience Across California.* Prepared for the California Seismic Safety Commission, Laurie A. Johnson and Stephen A. Mahin. May 2016.

PEER 2016/03 *Simulation Confidence in Tsunami-Driven Overland Flow.* Patrick Lynett. May 2016.

PEER 2016/02 *Semi-Automated Procedure for Windowing time Series and Computing Fourier Amplitude Spectra for the NGA-West2 Database.* Tadahiro Kishida, Olga-Joan Ktenidou, Robert B. Darragh, and Walter J. Silva. May 2016.

PEER 2016/01 *A Methodology for the Estimation of Kappa (κ) from Large Datasets: Example Application to Rock Sites in the NGA-East Database and Implications on Design Motions.* Olga-Joan Ktenidou, Norman A. Abrahamson, Robert B. Darragh, and Walter J. Silva. April 2016.

PEER 2015/13 *Self-Centering Precast Concrete Dual-Steel-Shell Columns for Accelerated Bridge Construction: Seismic Performance, Analysis, and Design*. Gabriele Guerrini, José I. Restrepo, Athanassios Vervelidis, and Milena Massari. December 2015.

PEER 2015/12 *Shear-Flexure Interaction Modeling for Reinforced Concrete Structural Walls and Columns under Reversed Cyclic Loading*. Kristijan Kolozvari, Kutay Orakcal, and John Wallace. December 2015.

PEER 2015/11 *Selection and Scaling of Ground Motions for Nonlinear Response History Analysis of Buildings in Performance-Based Earthquake Engineering*. N. Simon Kwong and Anil K. Chopra. December 2015.

PEER 2015/10 *Structural Behavior of Column-Bent Cap Beam-Box Girder Systems in Reinforced Concrete Bridges Subjected to Gravity and Seismic Loads. Part II: Hybrid Simulation and Post-Test Analysis*. Mohamed A. Moustafa and Khalid M. Mosalam. November 2015.

PEER 2015/09 *Structural Behavior of Column-Bent Cap Beam-Box Girder Systems in Reinforced Concrete Bridges Subjected to Gravity and Seismic Loads. Part I: Pre-Test Analysis and Quasi-Static Experiments*. Mohamed A. Moustafa and Khalid M. Mosalam. September 2015.

PEER 2015/08 *NGA-East: Adjustments to Median Ground-Motion Models for Center and Eastern North America*. August 2015.

PEER 2015/07 *NGA-East: Ground-Motion Standard-Deviation Models for Central and Eastern North America*. Linda Al Atik. June 2015.

PEER 2015/06 *Adjusting Ground-Motion Intensity Measures to a Reference Site for which V_{S30} = 3000 m/sec*. David M. Boore. May 2015.

PEER 2015/05 *Hybrid Simulation of Seismic Isolation Systems Applied to an APR-1400 Nuclear Power Plant.* Andreas H. Schellenberg, Alireza Sarebanha, Matthew J. Schoettler, Gilberto Mosqueda, Gianmario Benzoni, and Stephen A. Mahin. April 2015.

PEER 2015/04 *NGA-East: Median Ground-Motion Models for the Central and Eastern North America Region*. April 2015.

PEER 2015/03 *Single Series Solution for the Rectangular Fiber-Reinforced Elastomeric Isolator Compression Modulus*. James M. Kelly and Niel C. Van Engelen. March 2015.

PEER 2015/02 *A Full-Scale, Single-Column Bridge Bent Tested by Shake-Table Excitation.* Matthew J. Schoettler, José I. Restrepo, Gabriele Guerrini, David E. Duck, and Francesco Carrea. March 2015.

PEER 2015/01 *Concrete Column Blind Prediction Contest 2010: Outcomes and Observations.* Vesna Terzic, Matthew J. Schoettler, José I. Restrepo, and Stephen A Mahin. March 2015.

PEER 2014/20 *Stochastic Modeling and Simulation of Near-Fault Ground Motions for Performance-Based Earthquake Engineering*. Mayssa Dabaghi and Armen Der Kiureghian. December 2014.

PEER 2014/19 *Seismic Response of a Hybrid Fiber-Reinforced Concrete Bridge Column Detailed for Accelerated Bridge Construction*. Wilson Nguyen, William Trono, Marios Panagiotou, and Claudia P. Ostertag. December 2014.

PEER 2014/18 *Three-Dimensional Beam-Truss Model for Reinforced Concrete Walls and Slabs Subjected to Cyclic Static or Dynamic Loading*. Yuan Lu, Marios Panagiotou, and Ioannis Koutromanos. December 2014.

PEER 2014/17 *PEER NGA-East Database.* Christine A. Goulet, Tadahiro Kishida, Timothy D. Ancheta, Chris H. Cramer, Robert B. Darragh, Walter J. Silva, Youssef M.A. Hashash, Joseph Harmon, Jonathan P. Stewart, Katie E. Wooddell, and Robert R. Youngs. October 2014.

PEER 2014/16 *Guidelines for Performing Hazard-Consistent One-Dimensional Ground Response Analysis for Ground Motion Prediction*. Jonathan P. Stewart, Kioumars Afshari, and Youssef M.A. Hashash. October 2014.

PEER 2014/15 *NGA-East Regionalization Report: Comparison of Four Crustal Regions within Central and Eastern North America using Waveform Modeling and 5%-Damped Pseudo-Spectral Acceleration Response*. Jennifer Dreiling, Marius P. Isken, Walter D. Mooney, Martin C. Chapman, and Richard W. Godbee. October 2014.

PEER 2014/14 *Scaling Relations between Seismic Moment and Rupture Area of Earthquakes in Stable Continental Regions*. Paul Somerville. August 2014.

PEER 2014/13 *PEER Preliminary Notes and Observations on the August 24, 2014, South Napa Earthquake*. Grace S. Kang and Stephen A. Mahin, Editors. September 2014.

PEER 2014/12 *Reference-Rock Site Conditions for Central and Eastern North America: Part II – Attenuation (Kappa) Definition*. Kenneth W. Campbell, Youssef M.A. Hashash, Byungmin Kim, Albert R. Kottke, Ellen M. Rathje, Walter J. Silva, and Jonathan P. Stewart. August 2014.

PEER 2014/11 *Reference-Rock Site Conditions for Central and Eastern North America: Part I - Velocity Definition*. Youssef M.A. Hashash, Albert R. Kottke, Jonathan P. Stewart, Kenneth W. Campbell, Byungmin Kim, Ellen M. Rathje, Walter J. Silva, Sissy Nikolaou, and Cheryl Moss. August 2014.

PEER 2014/10 *Evaluation of Collapse and Non-Collapse of Parallel Bridges Affected by Liquefaction and Lateral Spreading*. Benjamin Turner, Scott J. Brandenberg, and Jonathan P. Stewart. August 2014.

PEER 2014/09 *PEER Arizona Strong-Motion Database and GMPEs Evaluation*. Tadahiro Kishida, Robert E. Kayen, Olga-Joan Ktenidou, Walter J. Silva, Robert B. Darragh, and Jennie Watson-Lamprey. June 2014.

PEER 2014/08 *Unbonded Pretensioned Bridge Columns with Rocking Detail*. Jeffrey A. Schaefer, Bryan Kennedy, Marc O. Eberhard, and John F. Stanton. June 2014.

PEER 2014/07 *Northridge 20 Symposium Summary Report: Impacts, Outcomes, and Next Steps*. May 2014.

PEER 2014/06 *Report of the Tenth Planning Meeting of NEES/E-Defense Collaborative Research on Earthquake Engineering*. December 2013.

PEER 2014/05 *Seismic Velocity Site Characterization of Thirty-One Chilean Seismometer Stations by Spectral Analysis of Surface Wave Dispersion*. Robert Kayen, Brad D. Carkin, Skye Corbet, Camilo Pinilla, Allan Ng, Edward Gorbis, and Christine Truong. April 2014.

PEER 2014/04 Effect of Vertical Acceleration on Shear Strength of Reinforced Concrete Columns. Hyerin Lee and Khalid M. Mosalam. April 2014.

PEER 2014/03 *Retest of Thirty-Year-Old Neoprene Isolation Bearings.* James M. Kelly and Niel C. Van Engelen. March 2014.

PEER 2014/02 *Theoretical Development of Hybrid Simulation Applied to Plate Structures.* Ahmed A. Bakhaty, Khalid M. Mosalam, and Sanjay Govindjee. January 2014.

PEER 2014/01 *Performance-Based Seismic Assessment of Skewed Bridges.* Peyman Kaviani, Farzin Zareian, and Ertugrul Taciroglu. January 2014.

PEER 2013/26 *Urban Earthquake Engineerin*g. Proceedings of the U.S.-Iran Seismic Workshop. December 2013.

PEER 2013/25 *Earthquake Engineering for Resilient Communities: 2013 PEER Internship Program Research Report Collection.* Heidi Tremayne (Editor), Stephen A. Mahin (Editor), Jorge Archbold Monterossa, Matt Brosman, Shelly Dean, Katherine deLaveaga, Curtis Fong, Donovan Holder, Rakeeb Khan, Elizabeth Jachens, David Lam, Daniela Martinez Lopez, Mara Minner, Geffen Oren, Julia Pavicic, Melissa Quinonez, Lorena Rodriguez, Sean Salazar, Kelli Slaven, Vivian Steyert, Jenny Taing, and Salvador Tena. December 2013.

PEER 2013/24 *NGA-West2 Ground Motion Prediction Equations for Vertical Ground Motions*. September 2013.

PEER 2013/23 *Coordinated Planning and Preparedness for Fire Following Major Earthquakes*. Charles Scawthorn. November 2013.

PEER 2013/22 *GEM-PEER Task 3 Project: Selection of a Global Set of Ground Motion Prediction Equations.* Jonathan P. Stewart, John Douglas, Mohammad B. Javanbarg, Carola Di Alessandro, Yousef Bozorgnia, Norman A. Abrahamson, David M. Boore, Kenneth W. Campbell, Elise Delavaud, Mustafa Erdik, and Peter J. Stafford. December 2013.

PEER 2013/21 *Seismic Design and Performance of Bridges with Columns on Rocking Foundations*. Grigorios Antonellis and Marios Panagiotou. September 2013.

PEER 2013/20 *Experimental and Analytical Studies on the Seismic Behavior of Conventional and Hybrid Braced Frames*. Jiun-Wei Lai and Stephen A. Mahin. September 2013.

PEER 2013/19 *Toward Resilient Communities: A Performance-Based Engineering Framework for Design and Evaluation of the Built Environment.* Michael William Mieler, Bozidar Stojadinovic, Robert J. Budnitz, Stephen A. Mahin, and Mary C. Comerio. September 2013.

PEER 2013/18 *Identification of Site Parameters that Improve Predictions of Site Amplification*. Ellen M. Rathje and Sara Navidi. July 2013.

PEER 2013/17 *Response Spectrum Analysis of Concrete Gravity Dams Including Dam-Water-Foundation Interaction*. Arnkjell Løkke and Anil K. Chopra. July 2013.

PEER 2013/16 *Effect of Hoop Reinforcement Spacing on the Cyclic Response of Large Reinforced Concrete Special Moment Frame Beams.* Marios Panagiotou, Tea Visnjic, Grigorios Antonellis, Panagiotis Galanis, and Jack P. Moehle. June 2013.

PEER 2013/15 *A Probabilistic Framework to Include the Effects of Near-Fault Directivity in Seismic Hazard Assessment*. Shrey Kumar Shahi, Jack W. Baker. October 2013.

PEER 2013/14 *Hanging-Wall Scaling using Finite-Fault Simulations.* Jennifer L. Donahue and Norman A. Abrahamson. September 2013.

PEER 2013/13 *Semi-Empirical Nonlinear Site Amplification and its Application in NEHRP Site Factors*. Jonathan P. Stewart and Emel Seyhan. November 2013.

PEER 2013/12 *Nonlinear Horizontal Site Response for the NGA-West2 Project.* Ronnie Kamai, Norman A. Abramson, Walter J. Silva. May 2013.

PEER 2013/11 *Epistemic Uncertainty for NGA-West2 Models.* Linda Al Atik and Robert R. Youngs. May 2013.

PEER 2013/10 *NGA-West 2 Models for Ground-Motion Directionality.* Shrey K. Shahi and Jack W. Baker. May 2013.

PEER 2013/09 *Final Report of the NGA-West2 Directivity Working Group.* Paul Spudich, Jeffrey R. Bayless, Jack W. Baker, Brian S.J. Chiou, Badie Rowshandel, Shrey Shahi, and Paul Somerville. May 2013.

PEER 2013/08 *NGA-West2 Model for Estimating Average Horizontal Values of Pseudo-Absolute Spectral Accelerations Generated by Crustal Earthquakes*. I. M. Idriss. May 2013.

PEER 2013/07 *Update of the Chiou and Youngs NGA Ground Motion Model for Average Horizontal Component of Peak Ground Motion and Response Spectra*. Brian Chiou and Robert Youngs. May 2013.

PEER 2013/06 *NGA-West2 Campbell-Bozorgnia Ground Motion Model for the Horizontal Components of PGA, PGV, and 5%-Damped Elastic Pseudo-Acceleration Response Spectra for Periods Ranging from 0.01 to 10 sec.* Kenneth W. Campbell and Yousef Bozorgnia. May 2013.

PEER 2013/05 *NGA-West 2 Equations for Predicting Response Spectral Accelerations for Shallow Crustal Earthquakes*. David M. Boore, Jonathan P. Stewart, Emel Seyhan, and Gail M. Atkinson. May 2013.

PEER 2013/04 *Update of the AS08 Ground-Motion Prediction Equations Based on the NGA-West2 Data Set*. Norman Abrahamson, Walter Silva, and Ronnie Kamai. May 2013.

PEER 2013/03 *PEER NGA-West2 Database.* Timothy D. Ancheta, Robert B. Darragh, Jonathan P. Stewart, Emel Seyhan, Walter J. Silva, Brian S.J. Chiou, Katie E. Wooddell, Robert W. Graves, Albert R. Kottke, David M. Boore, Tadahiro Kishida, and Jennifer L. Donahue. May 2013.

PEER 2013/02 *Hybrid Simulation of the Seismic Response of Squat Reinforced Concrete Shear Walls*. Catherine A. Whyte and Bozidar Stojadinovic. May 2013.

PEER 2013/01 *Housing Recovery in Chile: A Qualitative Mid-program Review*. Mary C. Comerio. February 2013.

PEER 2012/08 *Guidelines for Estimation of Shear Wave Velocity.* Bernard R. Wair, Jason T. DeJong, and Thomas Shantz. December 2012.

PEER 2012/07 *Earthquake Engineering for Resilient Communities: 2012 PEER Internship Program Research Report Collection.* Heidi Tremayne (Editor), Stephen A. Mahin (Editor), Collin Anderson, Dustin Cook, Michael Erceg, Carlos Esparza, Jose Jimenez, Dorian Krausz, Andrew Lo, Stephanie Lopez, Nicole McCurdy, Paul Shipman, Alexander Strum, Eduardo Vega. December 2012.

PEER 2012/06 *Fragilities for Precarious Rocks at Yucca Mountain.* Matthew D. Purvance, Rasool Anooshehpoor, and James N. Brune. December 2012.

PEER 2012/05 *Development of Simplified Analysis Procedure for Piles in Laterally Spreading Layered Soils.* Christopher R. McGann, Pedro Arduino, and Peter Mackenzie–Helnwein. December 2012.

PEER 2012/04 *Unbonded Pre-Tensioned Columns for Bridges in Seismic Regions.* Phillip M. Davis, Todd M. Janes, Marc O. Eberhard, and John F. Stanton. December 2012.

PEER 2012/03 *Experimental and Analytical Studies on Reinforced Concrete Buildings with Seismically Vulnerable Beam-Column Joints*. Sangjoon Park and Khalid M. Mosalam. October 2012.

PEER 2012/02 *Seismic Performance of Reinforced Concrete Bridges Allowed to Uplift during Multi-Directional Excitation*. Andres Oscar Espinoza and Stephen A. Mahin. July 2012.

PEER 2012/01 *Spectral Damping Scaling Factors for Shallow Crustal Earthquakes in Active Tectonic Regions.* Sanaz Rezaeian, Yousef Bozorgnia, I. M. Idriss, Kenneth Campbell, Norman Abrahamson, and Walter Silva. July 2012.

PEER 2011/10 *Earthquake Engineering for Resilient Communities: 2011 PEER Internship Program Research Report Collection*. Heidi Faison and Stephen A. Mahin, Editors. December 2011.

PEER 2011/09 *Calibration of Semi-Stochastic Procedure for Simulating High-Frequency Ground Motions*. Jonathan P. Stewart, Emel Seyhan, and Robert W. Graves. December 2011.

PEER 2011/08 *Water Supply in regard to Fire Following Earthquake*. Charles Scawthorn. November 2011.

PEER 2011/07 *Seismic Risk Management in Urban Areas*. Proceedings of a U.S.-Iran-Turkey Seismic Workshop. September 2011.

PEER 2011/06 *The Use of Base Isolation Systems to Achieve Complex Seismic Performance Objectives*. Troy A. Morgan and Stephen A. Mahin. July 2011.

PEER 2011/05 *Case Studies of the Seismic Performance of Tall Buildings Designed by Alternative Means.* Task 12 Report for the Tall Buildings Initiative. Jack Moehle, Yousef Bozorgnia, Nirmal Jayaram, Pierson Jones, Mohsen Rahnama, Nilesh Shome, Zeynep Tuna, John Wallace, Tony Yang, and Farzin Zareian. July 2011.

PEER 2011/04 *Recommended Design Practice for Pile Foundations in Laterally Spreading Ground.* Scott A. Ashford, Ross W. Boulanger, and Scott J. Brandenberg. June 2011.

PEER 2011/03 *New Ground Motion Selection Procedures and Selected Motions for the PEER Transportation Research Program*. Jack W. Baker, Ting Lin, Shrey K. Shahi, and Nirmal Jayaram. March 2011.

PEER 2011/02 *A Bayesian Network Methodology for Infrastructure Seismic Risk Assessment and Decision Support*. Michelle T. Bensi, Armen Der Kiureghian, and Daniel Straub. March 2011.

PEER 2011/01 *Demand Fragility Surfaces for Bridges in Liquefied and Laterally Spreading Ground.* Scott J. Brandenberg, Jian Zhang, Pirooz Kashighandi, Yili Huo, and Minxing Zhao. March 2011.

PEER 2010/05 *Guidelines for Performance-Based Seismic Design of Tall Buildings.* Developed by the Tall Buildings Initiative. November 2010.

PEER 2010/04 *Application Guide for the Design of Flexible and Rigid Bus Connections between Substation Equipment Subjected to Earthquakes.* Jean-Bernard Dastous and Armen Der Kiureghian. September 2010.

PEER 2010/03 *Shear Wave Velocity as a Statistical Function of Standard Penetration Test Resistance and Vertical Effective Stress at Caltrans Bridge Sites.* Scott J. Brandenberg, Naresh Bellana, and Thomas Shantz. June 2010.

PEER 2010/02 *Stochastic Modeling and Simulation of Ground Motions for Performance-Based Earthquake Engineering.* Sanaz Rezaeian and Armen Der Kiureghian. June 2010.

PEER 2010/01 *Structural Response and Cost Characterization of Bridge Construction Using Seismic Performance Enhancement Strategies.* Ady Aviram, Božidar Stojadinović, Gustavo J. Parra-Montesinos, and Kevin R. Mackie. March 2010.

PEER 2009/03 *The Integration of Experimental and Simulation Data in the Study of Reinforced Concrete Bridge Systems Including Soil-Foundation-Structure Interaction.* Matthew Dryden and Gregory L. Fenves. November 2009.

PEER 2009/02 *Improving Earthquake Mitigation through Innovations and Applications in Seismic Science, Engineering, Communication, and Response*. Proceedings of a U.S.-Iran Seismic Workshop. October 2009.

PEER 2009/01 *Evaluation of Ground Motion Selection and Modification Methods: Predicting Median Interstory Drift Response of Buildings*. Curt B. Haselton, Editor. June 2009.

PEER 2008/10 *Technical Manual for Strata.* Albert R. Kottke and Ellen M. Rathje. February 2009.

PEER 2008/09 *NGA Model for Average Horizontal Component of Peak Ground Motion and Response Spectra.* Brian S.-J. Chiou and Robert R. Youngs. November 2008.

PEER 2008/08 *Toward Earthquake-Resistant Design of Concentrically Braced Steel Structures*. Patxi Uriz and Stephen A. Mahin. November 2008.

PEER 2008/07 *Using OpenSees for Performance-Based Evaluation of Bridges on Liquefiable Soils*. Stephen L. Kramer, Pedro Arduino, and HyungSuk Shin. November 2008.

PEER 2008/06 *Shaking Table Tests and Numerical Investigation of Self-Centering Reinforced Concrete Bridge Columns*. Hyung IL Jeong, Junichi Sakai, and Stephen A. Mahin. September 2008.

PEER 2008/05 *Performance-Based Earthquake Engineering Design Evaluation Procedure for Bridge Foundations Undergoing Liquefaction-Induced Lateral Ground Displacement*. Christian A. Ledezma and Jonathan D. Bray. August 2008.

PEER 2008/04 *Benchmarking of Nonlinear Geotechnical Ground Response Analysis Procedures.* Jonathan P. Stewart, Annie On-Lei Kwok, Youssef M. A. Hashash, Neven Matasovic, Robert Pyke, Zhiliang Wang, and Zhaohui Yang. August 2008.

PEER 2008/03 *Guidelines for Nonlinear Analysis of Bridge Structures in California.* Ady Aviram, Kevin R. Mackie, and Božidar Stojadinović. August 2008.

PEER 2008/02 *Treatment of Uncertainties in Seismic-Risk Analysis of Transportation Systems*. Evangelos Stergiou and Anne S. Kiremidjian. July 2008.

PEER 2008/01 *Seismic Performance Objectives for Tall Buildings.* William T. Holmes, Charles Kircher, William Petak, and Nabih Youssef. August 2008.

PEER 2007/12 *An Assessment to Benchmark the Seismic Performance of a Code-Conforming Reinforced Concrete Moment-Frame Building.* Curt Haselton, Christine A. Goulet, Judith Mitrani-Reiser, James L. Beck, Gregory G. Deierlein, Keith A. Porter, Jonathan P. Stewart, and Ertugrul Taciroglu. August 2008.

PEER 2007/11 *Bar Buckling in Reinforced Concrete Bridge Columns.* Wayne A. Brown, Dawn E. Lehman, and John F. Stanton. February 2008.

PEER 2007/10 *Computational Modeling of Progressive Collapse in Reinforced Concrete Frame Structures*. Mohamed M. Talaat and Khalid M. Mosalam. May 2008.

PEER 2007/09 *Integrated Probabilistic Performance-Based Evaluation of Benchmark Reinforced Concrete Bridges*. Kevin R. Mackie, John-Michael Wong, and Božidar Stojadinović. January 2008.

PEER 2007/08 *Assessing Seismic Collapse Safety of Modern Reinforced Concrete Moment-Frame Buildings*. Curt B. Haselton and Gregory G. Deierlein. February 2008.

PEER 2007/07 *Performance Modeling Strategies for Modern Reinforced Concrete Bridge Columns*. Michael P. Berry and Marc O. Eberhard. April 2008.

PEER 2007/06 *Development of Improved Procedures for Seismic Design of Buried and Partially Buried Structures*. Linda Al Atik and Nicholas Sitar. June 2007.

PEER 2007/05 *Uncertainty and Correlation in Seismic Risk Assessment of Transportation Systems*. Renee G. Lee and Anne S. Kiremidjian. July 2007.

PEER 2007/04 *Numerical Models for Analysis and Performance-Based Design of Shallow Foundations Subjected to Seismic Loading.* Sivapalan Gajan, Tara C. Hutchinson, Bruce L. Kutter, Prishati Raychowdhury, José A. Ugalde, and Jonathan P. Stewart. May 2008.

PEER 2007/03 *Beam-Column Element Model Calibrated for Predicting Flexural Response Leading to Global Collapse of RC Frame Buildings*. Curt B. Haselton, Abbie B. Liel, Sarah Taylor Lange, and Gregory G. Deierlein. May 2008.

PEER 2007/02 *Campbell-Bozorgnia NGA Ground Motion Relations for the Geometric Mean Horizontal Component of Peak and Spectral Ground Motion Parameters*. Kenneth W. Campbell and Yousef Bozorgnia. May 2007.

PEER 2007/01 *Boore-Atkinson NGA Ground Motion Relations for the Geometric Mean Horizontal Component of Peak and Spectral Ground Motion Parameters*. David M. Boore and Gail M. Atkinson. May 2007.

PEER 2006/12 Societal Implications of Performance-Based Earthquake Engineering. Peter J. May. May 2007.

PEER 2006/11 *Probabilistic Seismic Demand Analysis Using Advanced Ground Motion Intensity Measures, Attenuation Relationships, and Near-Fault Effects*. Polsak Tothong and C. Allin Cornell. March 2007.

PEER 2006/10 *Application of the PEER PBEE Methodology to the I-880 Viaduct*. Sashi Kunnath. February 2007.

PEER 2006/09 *Quantifying Economic Losses from Travel Forgone Following a Large Metropolitan Earthquake*. James Moore, Sungbin Cho, Yue Yue Fan, and Stuart Werner. November 2006.

PEER 2006/08 *Vector-Valued Ground Motion Intensity Measures for Probabilistic Seismic Demand Analysis*. Jack W. Baker and C. Allin Cornell. October 2006.

PEER 2006/07 *Analytical Modeling of Reinforced Concrete Walls for Predicting Flexural and Coupled–Shear-Flexural Responses*. Kutay Orakcal, Leonardo M. Massone, and John W. Wallace. October 2006.

PEER 2006/06 *Nonlinear Analysis of a Soil-Drilled Pier System under Static and Dynamic Axial Loading*. Gang Wang and Nicholas Sitar. November 2006.

PEER 2006/05 *Advanced Seismic Assessment Guidelines.* Paolo Bazzurro, C. Allin Cornell, Charles Menun, Maziar Motahari, and Nicolas Luco. September 2006.

PEER 2006/04 *Probabilistic Seismic Evaluation of Reinforced Concrete Structural Components and Systems*. Tae Hyung Lee and Khalid M. Mosalam. August 2006.

PEER 2006/03 *Performance of Lifelines Subjected to Lateral Spreading.* Scott A. Ashford and Teerawut Juirnarongrit. July 2006.

PEER 2006/02 *Pacific Earthquake Engineering Research Center Highway Demonstration Project.* Anne Kiremidjian, James Moore, Yue Yue Fan, Nesrin Basoz, Ozgur Yazali, and Meredith Williams. April 2006.

PEER 2006/01 *Bracing Berkeley. A Guide to Seismic Safety on the UC Berkeley Campus.* Mary C. Comerio, Stephen Tobriner, and Ariane Fehrenkamp. January 2006.

PEER 2005/17 *Earthquake Simulation Tests on Reducing Residual Displacements of Reinforced Concrete Bridges.* Junichi Sakai, Stephen A Mahin, and Andres Espinoza. December 2005.

PEER 2005/16 *Seismic Response and Reliability of Electrical Substation Equipment and Systems.* Junho Song, Armen Der Kiureghian, and Jerome L. Sackman. April 2006.

PEER 2005/15 *CPT-Based Probabilistic Assessment of Seismic Soil Liquefaction Initiation.* R. E. S. Moss, R. B. Seed, R. E. Kayen, J. P. Stewart, and A. Der Kiureghian. April 2006.

PEER 2005/14 *Workshop on Modeling of Nonlinear Cyclic Load-Deformation Behavior of Shallow Foundations.* Bruce L. Kutter, Geoffrey Martin, Tara Hutchinson, Chad Harden, Sivapalan Gajan, and Justin Phalen. March 2006.

PEER 2005/13 *Stochastic Characterization and Decision Bases under Time-Dependent Aftershock Risk in Performance-Based Earthquake Engineering*. Gee Liek Yeo and C. Allin Cornell. July 2005.

PEER 2005/12 *PEER Testbed Study on a Laboratory Building: Exercising Seismic Performance Assessment.* Mary C. Comerio, Editor. November 2005.

PEER 2005/11 *Van Nuys Hotel Building Testbed Report: Exercising Seismic Performance Assessment.* Helmut Krawinkler, Editor. October 2005.

PEER 2005/10 *First NEES/E-Defense Workshop on Collapse Simulation of Reinforced Concrete Building Structures.* September 2005.

PEER 2005/09 *Test Applications of Advanced Seismic Assessment Guidelines.* Joe Maffei, Karl Telleen, Danya Mohr, William Holmes, and Yuki Nakayama. August 2006.

PEER 2005/08 *Damage Accumulation in Lightly Confined Reinforced Concrete Bridge Columns.* R. Tyler Ranf, Jared M. Nelson, Zach Price, Marc O. Eberhard, and John F. Stanton. April 2006.

PEER 2005/07 *Experimental and Analytical Studies on the Seismic Response of Freestanding and Anchored Laboratory Equipment.* Dimitrios Konstantinidis and Nicos Makris. January 2005.

PEER 2005/06 *Global Collapse of Frame Structures under Seismic Excitations*. Luis F. Ibarra and Helmut Krawinkler. September 2005.

PEER 2005//05 *Performance Characterization of Bench- and Shelf-Mounted Equipment.* Samit Ray Chaudhuri and Tara C. Hutchinson. May 2006.

PEER 2005/04 *Numerical Modeling of the Nonlinear Cyclic Response of Shallow Foundations.* Chad Harden, Tara Hutchinson, Geoffrey R. Martin, and Bruce L. Kutter. August 2005.

PEER 2005/03 *A Taxonomy of Building Components for Performance-Based Earthquake Engineering.* Keith A. Porter. September 2005.

PEER 2005/02 *Fragility Basis for California Highway Overpass Bridge Seismic Decision Making*. Kevin R. Mackie and Božidar Stojadinović. June 2005.

PEER 2005/01 *Empirical Characterization of Site Conditions on Strong Ground Motion.* Jonathan P. Stewart, Yoojoong Choi, and Robert W. Graves. June 2005.

PEER 2004/09 *Electrical Substation Equipment Interaction: Experimental Rigid Conductor Studies.* Christopher Stearns and André Filiatrault. February 2005.

PEER 2004/08 *Seismic Qualification and Fragility Testing of Line Break 550-kV Disconnect Switches.* Shakhzod M. Takhirov, Gregory L. Fenves, and Eric Fujisaki. January 2005.

PEER 2004/07 *Ground Motions for Earthquake Simulator Qualification of Electrical Substation Equipment.* Shakhzod M. Takhirov, Gregory L. Fenves, Eric Fujisaki, and Don Clyde. January 2005.

PEER 2004/06 *Performance-Based Regulation and Regulatory Regimes.* Peter J. May and Chris Koski. September 2004.

PEER 2004/05 *Performance-Based Seismic Design Concepts and Implementation: Proceedings of an International Workshop.* Peter Fajfar and Helmut Krawinkler, Editors. September 2004.

PEER 2004/04 *Seismic Performance of an Instrumented Tilt-up Wall Building.* James C. Anderson and Vitelmo V. Bertero. July 2004.

PEER 2004/03 *Evaluation and Application of Concrete Tilt-up Assessment Methodologies.* Timothy Graf and James O. Malley. October 2004.

PEER 2004/02 *Analytical Investigations of New Methods for Reducing Residual Displacements of Reinforced Concrete Bridge Columns.* Junichi Sakai and Stephen A. Mahin. August 2004.

PEER 2004/01 *Seismic Performance of Masonry Buildings and Design Implications.* Kerri Anne Taeko Tokoro, James C. Anderson, and Vitelmo V. Bertero. February 2004.

PEER 2003/18 *Performance Models for Flexural Damage in Reinforced Concrete Columns.* Michael Berry and Marc Eberhard. August 2003.

PEER 2003/17 *Predicting Earthquake Damage in Older Reinforced Concrete Beam-Column Joints.* Catherine Pagni and Laura Lowes. October 2004.

PEER 2003/16 *Seismic Demands for Performance-Based Design of Bridges.* Kevin Mackie and Božidar Stojadinović. August 2003.

PEER 2003/15 *Seismic Demands for Nondeteriorating Frame Structures and Their Dependence on Ground Motions.* Ricardo Antonio Medina and Helmut Krawinkler. May 2004.

PEER 2003/14 *Finite Element Reliability and Sensitivity Methods for Performance-Based Earthquake Engineering*. Terje Haukaas and Armen Der Kiureghian. April 2004.

PEER 2003/13 *Effects of Connection Hysteretic Degradation on the Seismic Behavior of Steel Moment-Resisting Frames.* Janise E. Rodgers and Stephen A. Mahin. March 2004.

PEER 2003/12 *Implementation Manual for the Seismic Protection of Laboratory Contents: Format and Case Studies*. William T. Holmes and Mary C. Comerio. October 2003.

PEER 2003/11 *Fifth U.S.-Japan Workshop on Performance-Based Earthquake Engineering Methodology for Reinforced Concrete Building Structures*. February 2004.

PEER 2003/10 *A Beam-Column Joint Model for Simulating the Earthquake Response of Reinforced Concrete Frames.* Laura N. Lowes, Nilanjan Mitra, and Arash Altoontash. February 2004.

PEER 2003/09 *Sequencing Repairs after an Earthquake: An Economic Approach.* Marco Casari and Simon J. Wilkie. April 2004.

PEER 2003/08 *A Technical Framework for Probability-Based Demand and Capacity Factor Design (DCFD) Seismic Formats*. Fatemeh Jalayer and C. Allin Cornell. November 2003.

PEER 2003/07 *Uncertainty Specification and Propagation for Loss Estimation Using FOSM Methods.* Jack W. Baker and C. Allin Cornell. September 2003.

PEER 2003/06 *Performance of Circular Reinforced Concrete Bridge Columns under Bidirectional Earthquake Loading*. Mahmoud M. Hachem, Stephen A. Mahin, and Jack P. Moehle. February 2003.

PEER 2003/05 *Response Assessment for Building-Specific Loss Estimation.* Eduardo Miranda and Shahram Taghavi. September 2003.

PEER 2003/04 *Experimental Assessment of Columns with Short Lap Splices Subjected to Cyclic Loads*. Murat Melek, John W. Wallace, and Joel Conte. April 2003.

PEER 2003/03 *Probabilistic Response Assessment for Building-Specific Loss Estimation*. Eduardo Miranda and Hesameddin Aslani. September 2003.

PEER 2003/02 *Software Framework for Collaborative Development of Nonlinear Dynamic Analysis Program*. Jun Peng and Kincho H. Law. September 2003.

PEER 2003/01 *Shake Table Tests and Analytical Studies on the Gravity Load Collapse of Reinforced Concrete Frames.* Kenneth John Elwood and Jack P. Moehle. November 2003.

PEER 2002/24 *Performance of Beam to Column Bridge Joints Subjected to a Large Velocity Pulse.* Natalie Gibson, André Filiatrault, and Scott A. Ashford. April 2002.

PEER 2002/23 *Effects of Large Velocity Pulses on Reinforced Concrete Bridge Columns.* Greg L. Orozco and Scott A. Ashford. April 2002.

PEER 2002/22 *Characterization of Large Velocity Pulses for Laboratory Testing.* Kenneth E. Cox and Scott A. Ashford. April 2002.

PEER 2002/21 *Fourth U.S.-Japan Workshop on Performance-Based Earthquake Engineering Methodology for Reinforced Concrete Building Structures*. December 2002.

PEER 2002/20 *Barriers to Adoption and Implementation of PBEE Innovations.* Peter J. May. August 2002.

PEER 2002/19 *Economic-Engineered Integrated Models for Earthquakes: Socioeconomic Impacts.* Peter Gordon, James E. Moore II, and Harry W. Richardson. July 2002.

PEER 2002/18 *Assessment of Reinforced Concrete Building Exterior Joints with Substandard Details.* Chris P. Pantelides, Jon Hansen, Justin Nadauld, and Lawrence D. Reaveley. May 2002.

PEER 2002/17 *Structural Characterization and Seismic Response Analysis of a Highway Overcrossing Equipped with Elastomeric Bearings and Fluid Dampers: A Case Study*. Nicos Makris and Jian Zhang. November 2002.

PEER 2002/16 *Estimation of Uncertainty in Geotechnical Properties for Performance-Based Earthquake Engineering*. Allen L. Jones, Steven L. Kramer, and Pedro Arduino. December 2002.

PEER 2002/15 *Seismic Behavior of Bridge Columns Subjected to Various Loading Patterns*. Asadollah Esmaeily-Gh. and Yan Xiao. December 2002.

PEER 2002/14 *Inelastic Seismic Response of Extended Pile Shaft Supported Bridge Structures.* T.C. Hutchinson, R.W. Boulanger, Y.H. Chai, and I.M. Idriss. December 2002.

PEER 2002/13 *Probabilistic Models and Fragility Estimates for Bridge Components and Systems.* Paolo Gardoni, Armen Der Kiureghian, and Khalid M. Mosalam. June 2002.

PEER 2002/12 *Effects of Fault Dip and Slip Rake on Near-Source Ground Motions: Why Chi-Chi Was a Relatively Mild M7.6 Earthquake*. Brad T. Aagaard, John F. Hall, and Thomas H. Heaton. December 2002.

PEER 2002/11 *Analytical and Experimental Study of Fiber-Reinforced Strip Isolators*. James M. Kelly and Shakhzod M. Takhirov. September 2002.

PEER 2002/10 *Centrifuge Modeling of Settlement and Lateral Spreading with Comparisons to Numerical Analyses***.** Sivapalan Gajan and Bruce L. Kutter. January 2003.

PEER 2002/09 *Documentation and Analysis of Field Case Histories of Seismic Compression during the 1994 Northridge, California, Earthquake*. Jonathan P. Stewart, Patrick M. Smith, Daniel H. Whang, and Jonathan D. Bray. October 2002.

PEER 2002/08 *Component Testing, Stability Analysis and Characterization of Buckling-Restrained Unbonded Braces^{TM}*. Cameron Black, Nicos Makris, and Ian Aiken. September 2002.

PEER 2002/07 *Seismic Performance of Pile-Wharf Connections.* Charles W. Roeder, Robert Graff, Jennifer Soderstrom, and Jun Han Yoo. December 2001.

PEER 2002/06 *The Use of Benefit-Cost Analysis for Evaluation of Performance-Based Earthquake Engineering Decisions*. Richard O. Zerbe and Anthony Falit-Baiamonte. September 2001.

PEER 2002/05 *Guidelines, Specifications, and Seismic Performance Characterization of Nonstructural Building Components and Equipment*. André Filiatrault, Constantin Christopoulos, and Christopher Stearns. September 2001.

PEER 2002/04 *Consortium of Organizations for Strong-Motion Observation Systems and the Pacific Earthquake Engineering Research Center Lifelines Program: Invited Workshop on Archiving and Web Dissemination of Geotechnical Data, 4–5 October 2001*. September 2002.

PEER 2002/03 *Investigation of Sensitivity of Building Loss Estimates to Major Uncertain Variables for the Van Nuys Testbed*. Keith A. Porter, James L. Beck, and Rustem V. Shaikhutdinov. August 2002.

PEER 2002/02 *The Third U.S.-Japan Workshop on Performance-Based Earthquake Engineering Methodology for Reinforced Concrete Building Structures*. July 2002.

PEER 2002/01 *Nonstructural Loss Estimation: The UC Berkeley Case Study.* Mary C. Comerio and John C. Stallmeyer. December 2001.

PEER 2001/16 *Statistics of SDF-System Estimate of Roof Displacement for Pushover Analysis of Buildings.* Anil K. Chopra, Rakesh K. Goel, and Chatpan Chintanapakdee. December 2001.

PEER 2001/15 *Damage to Bridges during the 2001 Nisqually Earthquake.* R. Tyler Ranf, Marc O. Eberhard, and Michael P. Berry. November 2001.

PEER 2001/14 *Rocking Response of Equipment Anchored to a Base Foundation.* Nicos Makris and Cameron J. Black. September 2001.

PEER 2001/13 *Modeling Soil Liquefaction Hazards for Performance-Based Earthquake Engineering*. Steven L. Kramer and Ahmed-W. Elgamal. February 2001.

PEER 2001/12 *Development of Geotechnical Capabilities in OpenSees*. Boris Jeremić. September 2001.

PEER 2001/11 *Analytical and Experimental Study of Fiber-Reinforced Elastomeric Isolators*. James M. Kelly and Shakhzod M. Takhirov. September 2001.

PEER 2001/10 *Amplification Factors for Spectral Acceleration in Active Regions.* Jonathan P. Stewart, Andrew H. Liu, Yoojoong Choi, and Mehmet B. Baturay. December 2001.

PEER 2001/09 *Ground Motion Evaluation Procedures for Performance-Based Design.* Jonathan P. Stewart, Shyh-Jeng Chiou, Jonathan D. Bray, Robert W. Graves, Paul G. Somerville, and Norman A. Abrahamson. September 2001.

PEER 2001/08 *Experimental and Computational Evaluation of Reinforced Concrete Bridge Beam-Column Connections for Seismic Performance.* Clay J. Naito, Jack P. Moehle, and Khalid M. Mosalam. November 2001.

PEER 2001/07 *The Rocking Spectrum and the Shortcomings of Design Guidelines.* Nicos Makris and Dimitrios Konstantinidis. August 2001.

PEER 2001/06 *Development of an Electrical Substation Equipment Performance Database for Evaluation of Equipment Fragilities*. Thalia Agnanos. April 1999.

PEER 2001/05 *Stiffness Analysis of Fiber-Reinforced Elastomeric Isolators.* Hsiang-Chuan Tsai and James M. Kelly. May 2001.

PEER 2001/04 *Organizational and Societal Considerations for Performance-Based Earthquake Engineering*. Peter J. May. April 2001.

PEER 2001/03 *A Modal Pushover Analysis Procedure to Estimate Seismic Demands for Buildings: Theory and Preliminary Evaluation*. Anil K. Chopra and Rakesh K. Goel. January 2001.

PEER 2001/02 *Seismic Response Analysis of Highway Overcrossings Including Soil-Structure Interaction*. Jian Zhang and Nicos Makris. March 2001.

PEER 2001/01 *Experimental Study of Large Seismic Steel Beam-to-Column Connections.* Egor P. Popov and Shakhzod M. Takhirov. November 2000.

PEER 2000/10 *The Second U.S.-Japan Workshop on Performance-Based Earthquake Engineering Methodology for Reinforced Concrete Building Structures*. March 2000.

PEER 2000/09 *Structural Engineering Reconnaissance of the August 17, 1999 Earthquake: Kocaeli (Izmit), Turkey.* Halil Sezen, Kenneth J. Elwood, Andrew S. Whittaker, Khalid Mosalam, John J. Wallace, and John F. Stanton. December 2000.

PEER 2000/08 *Behavior of Reinforced Concrete Bridge Columns Having Varying Aspect Ratios and Varying Lengths of Confinement*. Anthony J. Calderone, Dawn E. Lehman, and Jack P. Moehle. January 2001.

PEER 2000/07 *Cover-Plate and Flange-Plate Reinforced Steel Moment-Resisting Connections.* Taejin Kim, Andrew S. Whittaker, Amir S. Gilani, Vitelmo V. Bertero, and Shakhzod M. Takhirov. September 2000.

PEER 2000/06 *Seismic Evaluation and Analysis of 230-kV Disconnect Switches.* Amir S. J. Gilani, Andrew S. Whittaker, Gregory L. Fenves, Chun-Hao Chen, Henry Ho, and Eric Fujisaki. July 2000.

PEER 2000/05 *Performance-Based Evaluation of Exterior Reinforced Concrete Building Joints for Seismic Excitation*. Chandra Clyde, Chris P. Pantelides, and Lawrence D. Reaveley. July 2000.

PEER 2000/04 *An Evaluation of Seismic Energy Demand: An Attenuation Approach*. Chung-Che Chou and Chia-Ming Uang. July 1999.

PEER 2000/03 *Framing Earthquake Retrofitting Decisions: The Case of Hillside Homes in Los Angeles.* Detlof von Winterfeldt, Nels Roselund, and Alicia Kitsuse. March 2000.

PEER 2000/02 *U.S.-Japan Workshop on the Effects of Near-Field Earthquake Shaking*. Andrew Whittaker, Editor. July 2000.

PEER 2000/01 *Further Studies on Seismic Interaction in Interconnected Electrical Substation Equipment.* Armen Der Kiureghian, Kee-Jeung Hong, and Jerome L. Sackman. November 1999.

PEER 1999/14 *Seismic Evaluation and Retrofit of 230-kV Porcelain Transformer Bushings*. Amir S. Gilani, Andrew S. Whittaker, Gregory L. Fenves, and Eric Fujisaki. December 1999.

PEER 1999/13 *Building Vulnerability Studies: Modeling and Evaluation of Tilt-up and Steel Reinforced Concrete Buildings*. John W. Wallace, Jonathan P. Stewart, and Andrew S. Whittaker, Editors. December 1999.

PEER 1999/12 *Rehabilitation of Nonductile RC Frame Building Using Encasement Plates and Energy-Dissipating Devices*. Mehrdad Sasani, Vitelmo V. Bertero, James C. Anderson. December 1999.

PEER 1999/11 *Performance Evaluation Database for Concrete Bridge Components and Systems under Simulated Seismic Loads*. Yael D. Hose and Frieder Seible. November 1999.

PEER 1999/10 *U.S.-Japan Workshop on Performance-Based Earthquake Engineering Methodology for Reinforced Concrete Building Structures*. December 1999.

PEER 1999/09 *Performance Improvement of Long Period Building Structures Subjected to Severe Pulse-Type Ground Motions*. James C. Anderson, Vitelmo V. Bertero, and Raul Bertero. October 1999.

PEER 1999/08 *Envelopes for Seismic Response Vectors.* Charles Menun and Armen Der Kiureghian. July 1999.

PEER 1999/07 *Documentation of Strengths and Weaknesses of Current Computer Analysis Methods for Seismic Performance of Reinforced Concrete Members*. William F. Cofer. November 1999.

PEER 1999/06 *Rocking Response and Overturning of Anchored Equipment under Seismic Excitations*. Nicos Makris and Jian Zhang. November 1999.

PEER 1999/05 *Seismic Evaluation of 550 kV Porcelain Transformer Bushings.* Amir S. Gilani, Andrew S. Whittaker, Gregory L. Fenves, and Eric Fujisaki. October 1999.

PEER 1999/04 *Adoption and Enforcement of Earthquake Risk-Reduction Measures.* Peter J. May, Raymond J. Burby, T. Jens Feeley, and Robert Wood. August 1999.

PEER 1999/03 *Task 3 Characterization of Site Response General Site Categories*. Adrian Rodriguez-Marek, Jonathan D. Bray and Norman Abrahamson. February 1999.

PEER 1999/02 *Capacity-Demand-Diagram Methods for Estimating Seismic Deformation of Inelastic Structures: SDF Systems*. Anil K. Chopra and Rakesh Goel. April 1999.

PEER 1999/01 *Interaction in Interconnected Electrical Substation Equipment Subjected to Earthquake Ground Motions*. Armen Der Kiureghian, Jerome L. Sackman, and Kee-Jeung Hong. February 1999.

PEER 1998/08 *Behavior and Failure Analysis of a Multiple-Frame Highway Bridge in the 1994 Northridge Earthquake*. Gregory L. Fenves and Michael Ellery. December 1998.

PEER 1998/07 *Empirical Evaluation of Inertial Soil-Structure Interaction Effects.* Jonathan P. Stewart, Raymond B. Seed, and Gregory L. Fenves. November 1998.

PEER 1998/06 *Effect of Damping Mechanisms on the Response of Seismic Isolated Structures*. Nicos Makris and Shih-Po Chang. November 1998.

PEER 1998/05 *Rocking Response and Overturning of Equipment under Horizontal Pulse-Type Motions*. Nicos Makris and Yiannis Roussos. October 1998.

PEER 1998/04 *Pacific Earthquake Engineering Research Invitational Workshop Proceedings, May 14–15, 1998: Defining the Links between Planning, Policy Analysis, Economics and Earthquake Engineering*. Mary Comerio and Peter Gordon. September 1998.

PEER 1998/03 *Repair/Upgrade Procedures for Welded Beam to Column Connections*. James C. Anderson and Xiaojing Duan. May 1998.

PEER 1998/02 *Seismic Evaluation of 196 kV Porcelain Transformer Bushings.* Amir S. Gilani, Juan W. Chavez, Gregory L. Fenves, and Andrew S. Whittaker. May 1998.

PEER 1998/01 *Seismic Performance of Well-Confined Concrete Bridge Columns.* Dawn E. Lehman and Jack P. Moehle. December 2000.

PEER REPORTS: ONE HUNDRED SERIES

PEER 2012/103 *Performance-Based Seismic Demand Assessment of Concentrically Braced Steel Frame Buildings.* Chui-Hsin Chen and Stephen A. Mahin. December 2012.

PEER 2012/102 *Procedure to Restart an Interrupted Hybrid Simulation: Addendum to PEER Report 2010/103.* Vesna Terzic and Bozidar Stojadinovic. October 2012.

PEER 2012/101 *Mechanics of Fiber Reinforced Bearings.* James M. Kelly and Andrea Calabrese. February 2012.

PEER 2011/107 *Nonlinear Site Response and Seismic Compression at Vertical Array Strongly Shaken by 2007 Niigata-ken Chuetsu-oki Earthquake.* Eric Yee, Jonathan P. Stewart, and Kohji Tokimatsu. December 2011.

PEER 2011/106 *Self Compacting Hybrid Fiber Reinforced Concrete Composites for Bridge Columns.* Pardeep Kumar, Gabriel Jen, William Trono, Marios Panagiotou, and Claudia Ostertag. September 2011.

PEER 2011/105 *Stochastic Dynamic Analysis of Bridges Subjected to Spacially Varying Ground Motions.* Katerina Konakli and Armen Der Kiureghian. August 2011.

PEER 2011/104 *Design and Instrumentation of the 2010 E-Defense Four-Story Reinforced Concrete and Post-Tensioned Concrete Buildings.* Takuya Nagae, Kenichi Tahara, Taizo Matsumori, Hitoshi Shiohara, Toshimi Kabeyasawa, Susumu Kono, Minehiro Nishiyama (Japanese Research Team) and John Wallace, Wassim Ghannoum, Jack Moehle, Richard Sause, Wesley Keller, Zeynep Tuna (U.S. Research Team). June 2011.

PEER 2011/103 *In-Situ Monitoring of the Force Output of Fluid Dampers: Experimental Investigation.* Dimitrios Konstantinidis, James M. Kelly, and Nicos Makris. April 2011.

PEER 2011/102 *Ground-Motion Prediction Equations 1964–2010.* John Douglas. April 2011.

PEER 2011/101 *Report of the Eighth Planning Meeting of NEES/E-Defense Collaborative Research on Earthquake Engineering.* Convened by the Hyogo Earthquake Engineering Research Center (NIED), NEES Consortium, Inc. February 2011.

PEER 2010/111 *Modeling and Acceptance Criteria for Seismic Design and Analysis of Tall Buildings.* Task 7 Report for the Tall Buildings Initiative - Published jointly by the Applied Technology Council. October 2010.

PEER 2010/110 *Seismic Performance Assessment and Probabilistic Repair Cost Analysis of Precast Concrete Cladding Systems for Multistory Buildlings.* Jeffrey P. Hunt and Božidar Stojadinovic. November 2010.

PEER 2010/109 *Report of the Seventh Joint Planning Meeting of NEES/E-Defense Collaboration on Earthquake Engineering. Held at the E-Defense, Miki, and Shin-Kobe, Japan, September 18–19, 2009.* August 2010.

PEER 2010/108 *Probabilistic Tsunami Hazard in California.* Hong Kie Thio, Paul Somerville, and Jascha Polet, preparers. October 2010.

PEER 2010/107 *Performance and Reliability of Exposed Column Base Plate Connections for Steel Moment-Resisting Frames.* Ady Aviram, Božidar Stojadinovic, and Armen Der Kiureghian. August 2010.

PEER 2010/106 *Verification of Probabilistic Seismic Hazard Analysis Computer Programs.* Patricia Thomas, Ivan Wong, and Norman Abrahamson. May 2010.

PEER 2010/105 *Structural Engineering Reconnaissance of the April 6, 2009, Abruzzo, Italy, Earthquake, and Lessons Learned.* M. Selim Günay and Khalid M. Mosalam. April 2010.

PEER 2010/104 *Simulating the Inelastic Seismic Behavior of Steel Braced Frames, Including the Effects of Low-Cycle Fatigue.* Yuli Huang and Stephen A. Mahin. April 2010.

PEER 2010/103 *Post-Earthquake Traffic Capacity of Modern Bridges in California.* Vesna Terzic and Božidar Stojadinović. March 2010.

PEER 2010/102 *Analysis of Cumulative Absolute Velocity (CAV) and JMA Instrumental Seismic Intensity (I_{JMA}) Using the PEER–NGA Strong Motion Database.* Kenneth W. Campbell and Yousef Bozorgnia. February 2010.

PEER 2010/101 *Rocking Response of Bridges on Shallow Foundations.* Jose A. Ugalde, Bruce L. Kutter, and Boris Jeremic. April 2010.

PEER 2009/109 *Simulation and Performance-Based Earthquake Engineering Assessment of Self-Centering Post-Tensioned Concrete Bridge Systems.* Won K. Lee and Sarah L. Billington. December 2009.

PEER 2009/108 *PEER Lifelines Geotechnical Virtual Data Center.* J. Carl Stepp, Daniel J. Ponti, Loren L. Turner, Jennifer N. Swift, Sean Devlin, Yang Zhu, Jean Benoit, and John Bobbitt. September 2009.

PEER 2009/107 *Experimental and Computational Evaluation of Current and Innovative In-Span Hinge Details in Reinforced Concrete Box-Girder Bridges: Part 2: Post-Test Analysis and Design Recommendations.* Matias A. Hube and Khalid M. Mosalam. December 2009.

PEER 2009/106 *Shear Strength Models of Exterior Beam-Column Joints without Transverse Reinforcement.* Sangjoon Park and Khalid M. Mosalam. November 2009.

PEER 2009/105 *Reduced Uncertainty of Ground Motion Prediction Equations through Bayesian Variance Analysis.* Robb Eric S. Moss. November 2009.

PEER 2009/104 *Advanced Implementation of Hybrid Simulation.* Andreas H. Schellenberg, Stephen A. Mahin, Gregory L. Fenves. November 2009.

PEER 2009/103 *Performance Evaluation of Innovative Steel Braced Frames.* T. Y. Yang, Jack P. Moehle, and Božidar Stojadinovic. August 2009.

PEER 2009/102 *Reinvestigation of Liquefaction and Nonliquefaction Case Histories from the 1976 Tangshan Earthquake.* Robb Eric Moss, Robert E. Kayen, Liyuan Tong, Songyu Liu, Guojun Cai, and Jiaer Wu. August 2009.

PEER 2009/101 *Report of the First Joint Planning Meeting for the Second Phase of NEES/E-Defense Collaborative Research on Earthquake Engineering.* Stephen A. Mahin et al. July 2009.

PEER 2008/104 *Experimental and Analytical Study of the Seismic Performance of Retaining Structures.* Linda Al Atik and Nicholas Sitar. January 2009.

PEER 2008/103 *Experimental and Computational Evaluation of Current and Innovative In-Span Hinge Details in Reinforced Concrete Box-Girder Bridges. Part 1: Experimental Findings and Pre-Test Analysis.* Matias A. Hube and Khalid M. Mosalam. January 2009.

PEER 2008/102 *Modeling of Unreinforced Masonry Infill Walls Considering In-Plane and Out-of-Plane Interaction.* Stephen Kadysiewski and Khalid M. Mosalam. January 2009.

PEER 2008/101 *Seismic Performance Objectives for Tall Buildings.* William T. Holmes, Charles Kircher, William Petak, and Nabih Youssef. August 2008.

PEER 2007/101 *Generalized Hybrid Simulation Framework for Structural Systems Subjected to Seismic Loading*. Tarek Elkhoraibi and Khalid M. Mosalam. July 2007.

PEER 2007/100 *Seismic Evaluation of Reinforced Concrete Buildings Including Effects of Masonry Infill Walls*. Alidad Hashemi and Khalid M. Mosalam. July 2007.

The Pacifi c Earthquake Engineering Research Center (PEER) is a multi-institutional research and education center with headquarters at the University of California, Berkeley. Investigators from over 20 universities, several consulting companies, and researchers at various state and federal government agencies contribute to research programs focused on performance-based earthquake engineering.

These research programs aim to identify and reduce the risks from major earthquakes to life safety and to the economy by including research in a wide variety of disciplines including structural and geotechnical engineering, geology/seismology, lifelines, transportation, architecture, economics, risk management, and public policy.

PEER is supported by federal, state, local, and regional agencies, together with industry partners.

PEER Core Institutions

University of California, Berkeley (Lead Institution)
California Institute of Technology
Oregon State University
Stanford University
University of California, Davis
University of California, Irvine
University of California, Los Angeles
University of California, San Diego
University of Nevada, Reno
University of Southern California
University of Washington

PEER reports can be ordered at https://peer.berkeley.edu/peer-reports or by contacting

Pacific Earthquake Engineering Research Center
University of California, Berkeley
325 Davis Hall, Mail Code 1792
Berkeley, CA 94720-1792
Tel: 510-642-3437
Email: peer_center@berkeley.edu

ISSN 2770-8314
https://doi.org/10.55461/WRZV8692